SISSA - SCUOLA
INTERNAZIONALE
SUPERIORE
DI STUDI AVANZATI
TRIESTE
Strada Costiera 11

ISAS - INTERNATIONAL SCHOOL FOR ADVANCED STUDIES

Radial and Non-radial Pulsation Modelling in Early-Type Stars

Thesis submitted for the degree of "Doctor Philosophiae"

Candidate
Antonella Porri

Supervisor
Prof. Roberto Stalio

1988

TRIESTE

CONTENTS

Preface

This work treats a particular subject in the field of the modern stellar astrophysics: pulsation in early-type stars.

Our understanding of the physics of stars and of their dynamics has been greatly advanced during the past 10-15 years, with the advent of observations from orbiting instruments and of high-resolution, high-sensitivity observations from ground-based telescopes. The observations have shown that a star is not a closed thermodynamic system and the stellar atmosphere is not a thermal (in radiative and hydrostatic equilibria) boundary region of the star isolated from its enviroment, as the *classical* interior and atmosphere models assumed, but instead that a star is a *complicated machine* where the mechanisms which are operative in the different stellar regions strongly interplay.

The distinction between different stellar regions is mostly a matter for useful, although arbitrary, definitions. The usual convention is that the interior consists of the *core* and the *envelope* bounded at the surface by the *photosphere.* The photosphere is the innermost part of the *atmosphere*, which may be greatly extended, but which is assumed to consist of material gravitationally bound to the star. The *expanding atmosphere* or *stellar wind* is not gravitationally bound to the star and interacts at great distance with the *interstellar medium* or with a star produced medium, the *circumstellar medium.*

The interaction with the inter/circumstellar medium shows that the star is not isolated from its enviroment. The characteristics of the stellar environment may be a consequence of the properties of the central star. For example, for the cool, luminous Mira variables, pulsation leads to shock waves that extend the atmosphere, enhancing dust formation; radiation pressure on the dust drives the wind away. Similarly for the Be stars, both pulsation (in this case, non-radial), and radiation pressure are expected to be important in the mass ejection process. The Be-star case is more difficult to model in detail, because the relevant pulsation is non-radial,

because rotation may play an important role, and because the efficiency of the radiative driving of the lines depends on the velocity field, and the velocity field is not known a priori. From recent investigations it is becoming increasingly clear that it is when mechanical driving (i.e. by pulsation) combines with another mechanism such as rotation or radiation pressure that the effects become very important.

Vice versa, it is sometimes the environment which affects the stellar properties, as in the case of pre-main sequence objects. At a certain phase in its evolution, a low-mass protostar loses its embedding nebulosity and becomes an optically visible stellar-like object. During this phase there is a delicate balance between outflowing and infalling material, and the star displays both equatorial infall and bipolar outflow. This is probably the phase in which the future star is acquiring its physical characteristics.

Another example of possible interplay between stellar regions comes from the observation that all the stars in the upper part of the H-R diagram ($M_{bol} \leq -6$) are variable in light, spectrum and radial velocity. These variations are not strictly periodic, though cyclic variations are often present with characteristic times which are short-term (some hours) or intermediate terms (some days). The intermediate-term variations are fully consistent with a pulsation mechanism. The same limit in bolometric magnitude marks the transition from easily detected (from UV spectroscopy) stellar winds ($\dot{M} \geq 10^{-9} M_{\odot}/yr$) to undetected winds ($\dot{M} < 10^{-9} M_{\odot}/yr$).

In addition, early-type stars near this limit and below (i.e. $M_{bol} \geq -6$) can have strong winds only if there is some effect that can initiate an outflow. Examples of the effects which appear to be important are: enhanced metal abundances, which allow radiation to initiate wind from lower luminosity stars; pulsation, either radial or non-radial; rotation and pulsation, as in Be stars; open magnetic field regions of chemically peculiar stars.

The recent suggestion that non-radial pulsation and stellar mass loss may be linked in some O stars, B supergiants and Be stars has changed our perceptions of the stellar winds from early-type stars. In particular, the mechanism of non-radial pulsation provides the possibility of understanding unexplained observations showing that the winds from hot stars exhibit a time-variable three dimensional

structure. Further progress in this area requires, on the theoretical side, realistic models, in order to verify if pulsation and pulsation-induced shocks may play a fundamental role in the mass loss processes in early-type stars and particularly in Be stars, which are, among the B-type stars, those with the highest and most variable mass loss rate; it also requires, on the observational side, the regular monitoring of selected stars, both spectroscopically and photometrically.

The interaction between rotation and pulsation velocity fields is treated in this thesis, in order to predict line profiles broadened by these two velocity fields. High-resolution line profile observations, in the visual, of Be stars are modeled through their possible pulsation cycle. The possible links between the stellar atmosphere dynamics and extended atmosphere are explored.

In Chapter I we present a brief summary of the properties and evolutionary status of most known classes of pulsating variables, of the basic properties and classification of non-radial pulsations and of the related formalism. The observational evidence of the connection between stellar pulsation and mass loss is also reported and discussed.

The model atmospheres that will be used in this study, in order to analyze the observational data, are described in Chapter II. The assumptions and the basic equations on which the *classical* atmosphere models are based are presented, their limits are discussed, and non-stationary models are introduced. We conclude that the *classical* models provide only a simplified representation of the physical processes occurring in a real stellar photosphere, but the *classical* atmosphere predictions can be used for the pulsating star energy distribution and line-profile studies.

In Chapter III we describe the algorithm developed in this work in order to compute line profiles of radial and non-radial pulsating stars. We discuss the advantages of the assumptions made when compared with previous works, and a comparison is made with published results. In order to compute line profiles broadened by rotation and pulsation we must calculate the intrinsic profile appropriate to the star of interest. The line profiles used are HeIλ-4471, -5876, -6678 and MgIIλ-4481. A study is made of the reliability of the adopted intrinsic profiles, computed by the available *classical* model atmosphere codes. In the same chapter the question is

raised about the identification of the non-radial pulsation free parameters based on the proposed procedure. In addition, the *k problem*, that is the disagreement between the observed and the theoretical values of the ratio of horizontal to vertical oscillation velocities, is extensively discussed.

The recent growth of interest in the short-term photometric and/or spectroscopic variability of Be stars and its possible explanation in terms of non-radial pulsation is due to the possible link between non-radial pulsation and the *Be phenomenon.* In Chapter IV the short term variability in three Be stars, α Eri, P Car, and ϵ Cap is studied. The three Be stars are in three different phases: α Eri shows a normal B spectrum, P Car shows a typical Be spectrum, ϵ Cap is in a Be-shell phase. The non-radial pulsation models provide reasonably good fits of many of the observed spectra in two of the stars studied. The observations are also discussed in the light of the rotational modulation and the binary hypothesis.

In Chapter V another aspect of stellar pulsation is treated: that is pulsation as seen from space observations in the ultraviolet wavelengths'. Only a few UV observations covering the whole pulsation cycle of a β Cephei star, exist so far. We have analyzed Voyager ultraviolet spectrometer (500−1700 A), low resolution, observations of the large amplitude β Cephei variable, ν Eri (B2III). The observations, covering approximately 6 pulsation cycles of the star, allow us to derive the UV light as well as the intensity variations of high excitation lines and to infer on new aspects of the pulsation characteristics of ν Eri.

CHAPTER I

Stellar Pulsation

§1.1 - *Introduction*

Pulsating stars are a subset of the wider class of *intrinsic variable stars*, that is stars whose variability arises from causes entirely within themselves, and not from geometric effects such as eclipses in binary stars.

In pulsating stars, large-scale, periodic or quasi-periodic motions, usually including the entire star, are present. The simplest kind of such motions is a purely radial pulsation: the star maintains a spherical shape at all times, but changes its radius. In a non-radial pulsation, the stellar form periodically deviates from the spherical shape. Non-radial pulsations are less prominent observationally because a portion of the star has opposite phase in brightness and velocity at different positions on the same star. The astrophysical importance of non-radial pulsations is, however, not less than that of radial pulsations.

The discovery of periodic variables came relatively late in the history of astronomy. The first authentic discovery of such a variable star was that of o Ceti (Mira), a Long Period Variable star (see §1.2), by Fabricius in 1596 (Ledoux and Waldraven, 1958) and before the end of the eighteenth century only two pulsating stars had been discovered: the Classical Cepheids (see §1.2), δ Cephei and η Aquilae (Campbell and Jacchia, 1941).

The idea that certain types of variable stars owe their variability to radial pulsations dates from the work of Shapley (1914), and the theoretical bases of stellar pulsation were laid in 1918 by Eddington (the early history of studies on stellar pulsation is described by Rosseland (1949) in Chapter I of his book "The Pulsation Theory of Variable Stars"). Since then, the study of pulsating stars has

provided a powerful tool in the study of stellar structure and in other branches of astrophysics.

The study of non-radial pulsation may be regarded to have started from the recognition of double periodicity in the light curves of some β Cephei stars. Since it seemed unlikely that purely radial oscillations were responsible for these phenomena, Ledoux (1951) proposed that these stars undergo non-radial oscillations in the presence of rotation. The theoretical study of non-radial stellar pulsations received a great boost with the publication of the Handbuch articles by Ledoux and Waldraven (1958). But the impetus to the study of non-radial pulsations came from the discovery of the solar five-minute oscillations by Leighton, Noyes and Simon (1962) and the interpretation of this in terms of non-radial oscillations of the Sun. From 1970, when the pulsation of some β Cephei stars and the solar five-minute oscillation were the only cases in which non-radial pulsations were suspected as a possible cause, the situation has changed drastically. Non-radial oscillations have been detected in many stars, like δ *Scuti* stars, some white dwarfs, and early supergiants. Especially the recent observational development has been very rapid. Numerous non-radial pulsating stars have been found near the upper main sequence (stars of spectral types from 08 to B5), surrounding the β Cephei domain without being included in it; they are the so called *line profile variable B stars*, or *53 Persei stars* (Smith, 1978). Non-radial pulsators have been found also among the Be stars, main sequence B stars that have, at some time, shown emission in their optical line spectrum. Near the main sequence, non radial pulsation probably continues to about B6 on the cool side and to 06 in the hot side (Smith and Penrod, 1985). The development of high-precision and high-speed spectroscopy is opening a new era for the observations of stellar variability.

The importance of pulsation is due to the fact that it provides information on stellar properties and structure, often during interesting stages in the star's evolution: i.e., during the approach to the main sequence, near the tip of the red giant branch, during the core He burning. In addition, in some stars, episodes of stellar pulsation are very closely linked to epochs of mass loss, and there are good physical reasons to expect that pulsation plays a key role in the mass loss

mechanism.

This chapter includes a brief summary of the properties and evolutionary status of most known classes of pulsating variables (§1.2), and of the basic properties and classification of non-radial pulsations (§1.3). The observational evidence for non-radial oscillations in early-type stars is reported in §1.4, and the connection between stellar pulsation and stellar mass loss, with particular reference to early-type stars, is discussed in §1.5.

§1.2 - *Pulsation in the H-R Diagram*

Throughout the domain of the Hertzsprung-Russel (H-R) diagram lie groupings of variable stars whose variability mechanism is known or believed to be due to pulsation. Figure 1.1 shows the approximate location of the various types of pulsational variable stars on a luminosity vs. effective temperature H-R diagram. Detailed definitions of the various classes of pulsating variable stars can be found in Hoffmeister et al. (1985), and a recent survey of the evolutionary state of the pulsating star classes is given in Willson (1988). A brief summary of the properties and evolutionary state of most classes of these stars is given in this paragraph.

Large amplitude radial pulsation occurs in three regions of the H-R diagram (Figure 1.1): the Long Period Variable (LPV) region, the Cepheid strip, and the β Cephei or β CMa strip.

The *Long Period Variables* are in the extreme right edge of the H-R diagram. All population I and II stars which reach this region are almost certain to be variable (Willson, 1988). The general class of LPV includes the very large amplitude, relatively regular *Mira* variables and the heterogeneous class of *Semi-Regular Variables.* Both Population I and II Miras are found to occupy the tip of the asymptotic giant branch. The shortest period Miras have P $\sim$ 200 days. The light range of Mira variables is very large, over two and a half magnitudes. Wheareas the Mira stars

are clearly pulsating, almost certainly in the fundamental radial mode (Willson, 1982), different mechanisms have been proposed in order to explain the variability of the Semi-Regular variables. Besides the radial and/or non-radial pulsations, single convection cells covering a large fraction of the stellar disc, as well as magnetic activity have been suggested. The class of Semi-Regular variables includes giant and supergiant stars with lower amplitude pulsation with respect to the Miras; stars that show regular variation superimposed on long term changes in magnitude; and stars whose variation can be characterized by typical timescales, but which are not regular.

In the Cepheid strip, in addition to the *Classical Cepheids* (Population I) , there are the population II Cepheids and related objects: the *W Vir, RV Tau, BL Her* and *RR Lyrae* stars. The R CrB stars are located near or possibly within the Cepheid strip (Cox et al., 1980). Population I stars with (progenitor) masses between about 3 and 15 $M_{\odot}$ cross the instability Cepheid strip three or more times during their post-main sequence evolution. Classical Cepheid periods are nearly all confined to the range $1-50$ days. The light curves are highly periodic, and the total visual magnitude range is about 1 magnitude. The radial velocity curves of Classical Cepheids are roughly mirror images of the light curves, when the astronomical sign convetion of the radial velocities is used. The velocity amplitudes typically lie in the range $30-40$ km/sec. The RR Lyrae stars are pulsating horizontal branch stars, i.e. in the core He-burning stage. Their periods range from 0.2 to 1 day and their amplitude is ≥ 1 magnitude. The BL Her stars are stars moving back towards the red giant region from the horizontal branch (Hodson et al., 1980). The W Vir and RV Taur stars are probably slightly more massive stars that are making blue loops or moving for the last time across the H-R diagram from the red to the blue (Harris, 1985). The periods of WVir variables range from 1 to 50 days and those of RV Tauri stars range from 50 to 100 days.

The β *Cephei* stars are found on and above the main sequence in a narrow domain, within the range of spectral types BO.5-B2. The β Cephei instability strip coincides with the "turn-around " region of the evolutionary track of massive stars ($M = 10 - 20\ M_{\odot}$) (Lesh and Aizenman, 1973), where the stellar structure changes

from core hydrogen burning to overall contraction and then to shell hydrogen burning. The pulsation periods of β Cephei stars range from about 3.5 to 6.5 hours. The amplitude of light variations are rather small in the visual (typical amplitudes are Δm=0.01−0.08 magnitude). They radiate most of their energy in the far ultraviolet, peaking shortward of about 1200 A, having effective temperatures from approximately 20,000 to 27,000 K. UV light variations are observed with amplitudes ranging from about 2 to 8 times the values in the visible. Such amplitudes increase as one goes to shorter wavelengths. The radial velocity variations are also small. Typical values of the full amplitude in the radial velocity curve are 10−50 km/sec. Almost certainly the β Cephei stars are pulsating in the fundamental radial mode (Stamford and Watson 1978a) but also non-radial pulsations are involved in the oscillations of some of the stars of this class (Unno et al., 1979). The observational characteristics of this class of pulsating stars will be presented with more details in section 1.4.1.

Non-radially pulsating stars are located in different regions of the H-R diagram.

Near the main sequence, surrounding the β Cephei region, without being included in it (spectral types 08 to B5), are the non-radial pulsating *53 Persei* variables and some *rapid-rotator pulsating B and Be stars.* These early-type non-radial pulsating stars will be presented in section 1.4.2. Non-radial pulsating stars are also found within the extensions of the Cepheid and Mira strips to lower luminosity. In the confluence of the Cepheid instability strip with the main sequence (spectral type range from early A to mid F) are the δ *Scuti* stars. These population I stars are observed to vary with a pulsation period of less than 0.3 days, and with typical visual amplitudes of 0.02 magnitude. Similar small amplitude variability is seen in the pre-main sequence or young main sequence *Herbig Ae* stars, starting around spectral type A0 (Finkenzeller and Mundt, 1984). At lower luminosity, in the confluence of the Cepheid instability strip with the white dwarf sequence, another class of non-radial pulsating stars is found: the *ZZ Ceti* variables. These are extremely short-period light variable stars. Their periods range from 200 sec to about 1000 sec, and the amplitude of their light curves from 0.01 to 0.3 magnitude. There is a correlation between the amplitude of the luminosity variations and the morphology

of the power spectra of the ZZ Ceti light curves: low-amplitude variables have relatively simple and stable power spectra and their periods are short; large-amplitude variables have complex and unstable power spectra and their periods are long (Unno et al., 1979).

Some overlap in the domains of the various classes of variables may exist. In addition, some stars which reside in a given region of variability may not be observed to be variable (see e.g. Bidelman, 1985). This behaviour is due to other factors, besides luminosity and temperature (such as composition and mass), playing a role in whether a given star is pulsationally unstable.

Our understanding of what excitation mechanism drives the observed pulsations of variable stars ranges from "fairly well understood" in the case of Cepheid variables to "still being investigated" as in the case of β Cephei stars.

Ionization zone instabilities are responsible for most of the large amplitude radial pulsators as well as a number of smaller amplitude radial and/or non-radial pulsators (Cox, 1980). When the star undergoes a gravity-induced compression, the temperature and pressure of the atmosphere increase and the hydrogen and helium, by their ionization, stock potential energy. When the recombinations occur, the radiation pressure increases and exerts pressure on the outer layers of the star. This mechanism, in which the energy dissipated by the pulsating motion is replenished by the effect of changing the opacity due to the ionization, counterbalances the dumming processes and perpetuates the pulsations. The combined HI and HeI ionization zones account for the pulsation in the Mira strip, including at least the Mira variables, perhaps some Semi-Regular variables, and the ZZ Ceti variables (Wood, 1982; Winget, 1986). Driving in the HeII ionization zone gives rise to pulsation in the Cepheid strip, that is in Classical and Population II Cepheids, RR Lyrae stars, and δ Scuti variables.

The pulsation mechanism, or mechanisms, for the β Cephei stars and the non-radially pulsating near mean sequence early-type stars are still unknown. An excitation mechanism of β Cephei non-radial pulsations has been suggested by Osaki (1974). It involves resonances between an eigenmode of non-radial oscillations of the whole star with the oscillatory convective motions of a rapidly rotating core.

This mechanism has been reexamined by Lee and Saio (1986) with the intention of extending it to the other early-type pulsating stars. The same authors have recently (1987a, 1987b) calculated non-radial pulsation eigenmodes in a rotating star having a convective core, and have shown that eigenfunctions of overstable non-radial modes have large amplitude both in the core and in the outer layers. The problem of the β Cephei and early-type pulsating star instability mechanisms has been reviewed recently by A.N. Cox (1986) and by Osaki (1987).

§1.3 - *Basic Properties and Classification of Stellar Pulsation: Radial and Non-Radial*

In this section we summarze the basic properties of non-radial pulsations, and introduce the related formalism. The development of the detailed equations for non-radial pulsations are given in two books: Unno, Osaki, Ando and Shibahashi (1979) and Cox (1980). The recent theoretical research work on this field can be found in the numerous proocedings of meetings on this argument edited by Belvedere and Paterno' (1984), Ulrich et al. (1984), Gough (1986), and Christensen-Dalsgaard and Frandsen (1987).

The basic equations used are the mass continuity, the momentum and the energy, together with the equation of state and constitutive relations. The simplest theoretical treatment of non-radial pulsations is under the assumption of the linear and adiabatic approximations. The assumption of adiabatic oscillations is correct if the wave period is much shorter than the heat loss time. In this case the problem is simplified considerably, as the energy equation is reduced to the adiabatic condition which implies the constancy of $p\rho^{-\gamma}$ following the motion. The system of equations which describes the linear, adiabatic, non-radial oscillations forms a boundary-value problem of fourth-order ordinary differential equations in the radial coordinate, r, and, for a given stellar equilibrium model, eigenvalues and eigenfunctions are to be calculated numerically.

In order to solve this system of equations, the assumption is that the perturbations of the physical variables can be separated into two terms: a term which is function of the radius alone, and a tangential term which is a spherical harmonic, consisting of the associated Legendre polynomial and an m-fold longitudinal sinusoidal variation. In a spherically symmetric star, which represents the equilibrium configuration, the perturbations of the physical variables take on the following form, in the spherical polar co-ordinates (r, Θ, Φ):

$$\Xi_{n,l,m}(r,\Theta,\Phi,t) = \xi_{n,l}(r)Y_l^m(\Theta,\Phi)e^{i\sigma_{n,l}t}, \tag{1.1}$$

where $\Xi_{n,l,m}$ is, for instance, the radial displacement ($= r - r_0$, the subscript $_0$ denotes the unperturbed state), $\xi_{n,l}$ is the eigenfunction, $\sigma_{n,l}$ the eigenfrequency, and Y_m^l the spherical harmonic, which is expressed explicitly by

$$Y_l^m(\Theta,\Phi) = P_l^m(cos\Theta)e^{im\Phi}, \tag{1.2}$$

where $P_l^m(x)$ denotes the associated Legendre polinomial. In expressions 1.1 and 1.2 n is the radial order of modes, $l(= 0,1,2,...)$ is the degree of harmonic, and $m(= -l,-l+1,..,0,...,l-1,l)$ is the azimuthal order. The order n indicates the number of nodes of the eigenfunctions in the radial direction. The degree l represents the number of border lines (lines of zero motion) by which the stellar surface is divided so that they oscillate in the opposite phase.The radial modes correspond to the special cases of l=0. Among them, the mode with $n = 0$ is called the fundamental radial mode, while those with $n > 0$ are called overtones. The other harmonics are called the dipole (l=1), the quadrupole (l=2), the octapole (l=3) oscillations, etc.. Modes with $l > 0$ and $n = 0$ are called fundamental or f-modes. The azimuthal order, m, represents the number of nodes on the stellar surface in Φ direction; m takes integer values from $-l$ to $+l$; the eigenfrequencies and the eigenfunctions of these $(2l+1)$ modes are degenerate in a spherically symmetric non-rotating, non magnetic star. The degeneracy is removed if preferred symmetry axes are introduced, as rotation, or magnetic field. In such a case the eigenfrequencies are split into pairs for each possible value of m, giving rise to multiplets:

$$\sigma_{n,l,m} = \sigma_{n,l} \pm |m|\Omega C_{n,l}, \tag{1.3}$$

where, in the more realistic case of rotation, $\sigma_{n,l}$ is the frequency (angular) of the nonrotating mode, $C_{n.l}$ a constant which depends on the non-rotating structure of the mode, and Ω the angular velocity of the star. The mode with $m = 0$ corresponds to standing oscillations symmetrical to the axis of rotation, while a mode with $m \neq 0$ represents a traveling wave mode with phase velocity around the equator

$$(\frac{d\Phi}{dt})_{phase} = -\frac{\Omega}{m}.$$

Thus, positive m modes represent retrograde modes with respect to stellar rotation, while those with negative m represent prograde modes.

We can adequately study the adiabatic oscillations to a first approximation, by neglecting non-adiabatic effects and viscosity. It is obvious that, since the oscillations are assumed to be adiabatic (no net heat gains or losses by the oscillating mass elements), this case can not tell us how the luminosity of a pulsating star changes during pulsation. It is clear, moreover, that this theory cannot yield information regarding the *pulsational stability* of a star. Oscillations assumed to be present initially will maintain the same amplitude for all time. In the case of non-adiabatic radial oscillations, since the system is no longer conservative, we can expect to find solutions with complex frequencies. In this case the solutions are characterized by secularly increasing or decreasing pulsation amplitudes. Only in this case is it possible to investigate the question of pulsation instability and the causes of pulsation in stars.

Nevertheless, the simple adiabatic theory gives, in most cases, a good description of several features, such as the periods of the pulsating stars, and the relative pulsation amplitude. The main reason for this is that the dynamical time scale is much shorter than the thermal time scale (by a factor 10^{10} for the Sun).

The richness of non-radial pulsation compared to radial pulsation is only due to the degree of freedom in the horizontal wave number represented by the quantum number l. Besides that, two different kinds of restoring force, the pressure force and

the buoyancy force, operate in non-radial pulsations. Since the gravitational force increases inward in the compression phase, and decreases outward in the expansion phase, gravity cannot be the restoring force for radial pulsation. On the other hand, gravity can act through buoyancy as the restoring force for non-radial oscillations. So two different kinds of modes exist in non-radial oscillations: pressure (acustic) modes and gravity modes. The pressure modes (p-modes) form a sequence of increasing eigenfrequency with the order of the modes specified by the number of nodes, i.e.,

$$\sigma_{p_1} < \sigma_{p_2} < \sigma_{p_3} < ... \longmapsto \infty$$

The gravity modes (g-modes) form a sequence of decreasing frequency, i.e.,

$$\sigma_{g_1} > \sigma_{g_2} > \sigma_{g_3} > ... \longmapsto 0$$

There are two characteristic frequencies governing the oscillatory property of the medium. One of them is the Lamb frequency, L_l, given by

$$L_l^2 = \frac{l(l+1)}{r^2} c_s^2,$$

where c_s denotes the speed of sound. The other characteristic frequency is the Brunt-Väisälä frequency denotated by N

$$N^2 = g(\frac{1}{\gamma}\frac{d\ln p_0}{dr} - \frac{d\ln \rho_0}{dr})$$

where g is the gravitational acceleration ($=GM_r/r^2$), p_0 and ρ_0 the pressure and the density of the imperturbed state respectively. A sound wave travels a wavelength $2\pi r/l$ horizontally in the period $2\pi/L_l$ and a blob of gas oscillates vertically, with positive or negative buoyancy under the local pressure balance with frequency N.

For high frequencies ($\sigma^2 > L_l^2, N^2$), the relative Eulerian pressure perturbation, p'/p_0, dominates the relative radial displacement ξ_r/H, where H denotes the pressure scale of height ($\mathrm{H}=p_0/\rho_0 g$). These large Eulerian pressure variations are responsible for most of the restoring forces which act during the oscillations. For low frequencies ($\sigma^2 < L_l^2, N^2$), p'/p_0 is less than ξ_r/H, and the restoring force is

due to the force of gravity. In the other regions ($L_l^2 > \sigma^2 > N^2$ or $L_l^2 < \sigma^2 < N^2$), the eigenfunction does not show spatial oscillation, but decreases exponentially with the distance from the wave propagation; these are called evanescent regions. The region in which both $\sigma^2 < L_l^2$ and $\sigma^2 > N^2$ is called the p-wave propagation zone, and the region in which both $\sigma^2 < L_l^2$ and $\sigma^2 < N^2$ is called the g-wave propagation zone. The energy of oscillation is mainly trapped in the propagation zone. The two propagation regions, separated by the so called evanescent zone, are coupled with a sort of *tunnel effect.*

Figure 1.2 shows the propagation diagram given by Sculfaire (1974) for a polytrope (index 3) model. This diagram shows in what part of the stellar interior a wave with a given frequency has, locally, a propagating or non-propagating character. Generally, non-radial p-modes are oscillations trapped near the surface and g-modes are those trapped deep in the interior.

According to Unno et al. (1979), the propagation diagram may be comparable to the potential energy function of the one-dimensional Schrödinger equation of quantum mechanics in such a way that a propagation zone corresponds to a potential well and an evanescent zone to a potential wall. Since eigenmodes are standing waves, they occur in a region of a potential well, that is enclosed by potential walls at both ends. The most important difference lies in the fact that in the case of non-radial oscillations there are two different kinds of potential wells: one is opened upward (p-wave zone) and the other is opened downward (g-wave zone).

Since we are interested in those oscillations that may produce observable motions in the stellar atmosphere, the most important modes are those of non-radial p-mode oscillations. Furthermore oscillations of non-radial p-modes are more heavily concentrated near the surface as the spherical harmonics index l is increased. This can be seen in the propagation diagram, because the Lamb frequency, L_l, moves upward with an increase of l. In reality, however, the classification of modes is not so simple as outlined above. If a convective zone ($N^2 < 0$) exists within a star, the spectra of unstable modes appear. These convective modes are often designated by the g^--modes. For the g^--modes, $\sigma^2 < 0$ and $|\sigma|$ decreases as n increases. Therefore a complication arises when $N^2(r)$ changes in a complicated

way, especially because of the evolutionary inhomogeneity in the mean molecular weight distribution.

In this thesis (Chapter III) results obtained with the adiabatic oscillation approximation will be used. Also, p-modes will be more frequently considered.

§1.4 - *Observational Evidence for Pulsation in Early-Type Stars: Radial and Non-Radial.*

The first observational evidence of non-radial pulsations was presented by Ledoux (1951) for an early-type star of the β Cephei type. In recent years, many early-type stars (with spectral type O and B) have been found to be variable. The length of the observed periods and the character of the light and line-profile variations indicate that variabilities are most likely caused by non-radial pulsations.

There are two ways to infer non-radial pulsations in OB stars: visual photometry and high resolution spectroscopy. Visual magnitude variations are generally small. Even the β Cephei variables do not show a large amplitude of visual light variations. This is partly due to the fact that they radiate most of their energy in the far ultraviolet', thus ultraviolet light variations are observed with a much larger amplitude. The small visual photometric amplitudes are often variable and superimposed on longer-term variability. A large amount of data is required in order to establish periodicities. In addition, the light curves are usually non-sinusoidal and this complicates the process of period determination using Fourier methods, which assume that the light curve is sinusoidal.

Under non-radial oscillations, the different parts of the surface of a star move in different ways, and this kind of motion must naturally affect spectral line profiles. Direct observations of the velocity fields characteristic of non-radial pulsations are possible, but very high spectral resolution ($\geq$ 20,000) and very high signal-to-noise ratio ($\geq$ 200) are needed. Spectrograph-detector systems which give this high resolution and signal-to-noise ratio data are limited in their wavelength coverage.

Problems linked to the use of line profiles in the analysis arise principally from the lack of uniqueness of mode identification, particularly when the mode has a low order degree.

Figure 1.3 reports the H-R diagram containing a representative sample of the OB stars in which observed variations are explained by non-radial pulsations. We see that the pulsation may range from as early as O4 (Baade, 1986) to as late as B8 (McNamara, 1986). The majority of early-type stars that exhibit non-radial pulsations have a luminosity class III-V (Smith, 1986).

Following A.N. Cox (1986) and Smith (1986, 1988), we divide the pulsating early-type stars into four classes. One class includes the stars that show at least one radial mode, and three classes that include stars with only non-radial modes. Members of the first class are the β Cephei stars. The other three classes are formed of the slow rotators 53 Per variables, the intermediate rotators and the fast rotators. These last include both normal B and Be stars. Previously identified classes of variable B stars can be included in this scheme. The early proposed Maia variables (Struve, 1955) can be regarded as 53 Per variables (McNamara, 1986) with both luminosity and line profile variations. Abt's (1957) supergiants would be either 53 Per or rapid rotator variables, but not β Cephei variables; they are known from their radial velocity and light variations with periods typical of non-radial modes. The ultrashort B star variables (Jakate, 1979) and the 53 Psc variables (Sareyan et al. 1980) would be 53 Per variables (Cox A.N., 1986). The 53 Per class may include also the slow variables found photometrically by Burki (1983) and by Waelkens and Rufener (1985), as suggested by the same authors.

1.4.1 - *β Cephei Stars.*

The β Cephei variables are a small group of early B stars that exhibit light and radial-velocity variations having the same short period. There is a phase lag of 90° of the light curve with respect to the radial velocity curve, that is maximum light occurs at the phase of "maximum compression".

In addition to a well-known list of 16 β Cephei variables that are slowly rotating and a list of 6 that are rapidly rotating (Lesh and Aizenman, 1973), there are dozens of other candidates that have recently been proposed (Balona and Shobbrook, 1983, and Balona and Englebrecht, 1985).

The larger amplitude of the β Cephei light variations at short wavelenghts (see §1.2) is well suited to the confirmation of suspected variables whose light variation is marginal at visible wavelengths. The UV side of the spectrum, and especially the region just above the Lyman discontinuity at 912 A, is important also because it provides a rather sensitive indicator of photospheric temperature changes; a significant fraction of the total stellar flux is, in fact, irradiated at these shorter wavelengths.

It is now well established that variations in β Cephei stars are caused by pulsations. A radial mode is always excited, but recent works on β Cephei pulsation suggest a more complex interpretation of the phenomenon. The light curves do not always display simple sinusoidal patterns (Furenlid et al., 1987; this thesis, Chapter V); these patterns may be different at different wavelengths, suggesting the presence of optical depth effects. The radial velocity curves often display similar complexity as that of the light curves (Furelind et al., 1986; 1987)

1.4.2 - *53 Persei Stars*

These stars are slow rotators; they range from luminosity classes V to II and spectral type from O9 to B5. There is some evidence that they are clustered near type B3-B5 (Waelkens and Rufener, 1985). Their variability was discovered by Smith (1978) in a survey of sharp-lined B stars. Periods range from a few hours to 3 days in the observer's frame. The observed non-radial modes in these stars have been interpreted in terms of spherical harmonics, with the quantum numbers l and m giving the surface structure of the modes (see §1.3). All modes observed are prograde ($m < 0$) with, generally, $-m = l = 2$. But it is not possible to exclude higher l modes, owing to the slow rotation velocity (see §4.4.3). Mode-switching and changes in mode amplitude have been reported by Smith (1978). Balona (1985) has photometrically observed some 53 Per variables, but only in a few cases was he

able to detect the periods that are used to model the line profile variations. On the contrary, for ϵ Per, recent observations by Smith et al. (1987) have shown that a period af 3.85 hours, identified as $-m = l = 4$, is seen in both light and line profile fitting.

1.4.3 - *Intermediate Rotators*

These stars are analogous to 53 Per variables, but their projected rotation velocity is higher ($75 \leq V sini \leq 175$ km/sec). Also for these stars the modes are prograde with $-m = l$, but their modal degree is higher, generally l=4 to 8. The higher projected rotational velocity with respect to the 53 Per stars allows one to take advantage of Doppler imaging principles (see Chapetr III) in modeling higher degree l modes. Typical periods are 2 to 8 hours in the observer's frame. Amplitudes are variable on timescales of weeks to months (Smith, 1988).

1.4.4 - *Rapid Rotators*

This fourth group of variable early-type stars includes both normal B and Be stars. Be stars are on or near the main sequence B stars which have at some time shown emission in their optical line spectrum. Transitions from a Be spectrum (H emission lines with a more or less central reversal) to a shell spectrum (H absorption lines with very narrow and deep cores which may or may not be bordered by emission wings), and to a normal B spectrum may occur in any direction. The time scales of these variations are of the order of decades.

Numerous Be stars are photometrically and spectroscopically variable on time scales of hours. The long-term variability seems to depend on the amount of emitting material around the star, and on the geometry of this material relative to the star and to the observer. The short-term variability has been tentatively ascribed to non-radial pulsation, and it is possible that this pulsation contributes to the Be phenomenon (§1.5).

Historically, short-term photometric variability was the first evidence that non-radial pulsation might be present in Be stars, though it was initially ascribed to the

effects of rotation or orbital motion. The amplitudes of the variations in the visual are typically a few 0.01 magnitudes, but may occasionally exceed 0.1 magnitude. The period determination is severely hampered by the periods being in the range between 0.3 and 2 days, by underlying long term variations, and by variable light curves. Amplitudes and shapes of light curves can change substantially on time scales between one day (e.g. EW Lac (Be 3IV), Stagg, 1986; λ Eri (Be 2 III), Percy, 1986) and years. These changes do not follow any systematic pattern.

The belief that the short-term variability of Be stars is due to non-radial pulsation comes principally from spectroscopic observations. Periodic line profile variations have been detected in the line profiles of quite a few Be stars (Walker et al., 1979; Baade, 1979, 1984a,b; Bolton, 1982; Vogt and Penrod, 1983; Smith and Penrod, 1985; Penrod 1986, 1988; Smith et al. 1986)

A large survey of short-term spectroscopic variability in rapidly rotating B stars is found in Penrod (1988). He obtained high signal-to-noise ratio spectra of about 25 stars of this type, and found that all but two of the program stars show obvious line-profile variations due to non-radial pulsation. Baade (1987) arrived at the same conclusion from a sample of southern Be stars. The pulsational mode structure of these stars is the following: the modes are probably retrograde in the corotating frame, but they are still prograde in the observer's inertial frame (Smith, 1988); in the great majority of cases at least one high degree mode ($4 \leq l \leq 10$) is present; in addition an l=2 mode is observed in some Be stars. Typical periods are 5 to 40 hours in the observer's frame. The high degree modes show irregular variations in amplitude, while the l=2 modes are far more stable.

Some authors maintain that short term variability in Be stars is due to rotational effects such as rotation of spots or spokes, rather than to non-radial pulsation, and they adduce the following reasons (e.g. Balona and Engelbrecht, 1986): (1) the periods are consistent with rotation periods: (2) the light amplitude can sometimes be as large as 0.1 magnitude, which may be too large to be produced by non-radial pulsation; (3) variability is seen in stars with spectral types from B0 to B8, which seems difficult to reconcile with any pulsation mechanism. One may dispute the last reason by pointing out that large amplitude light variations in non-radial pulsation

are not excluded, and that short-term variability is more common in Be stars of early spectral type (Baade, 1986), i.e. of the same spectral types of the 53 Persei and the β Cephei stars. Vogt and Penrod (1983) discarded rotation of spots or spokes as an explanation of the short-term variability of ζ Oph.

In order to explain the short term variability in Be stars, also the binary hypothesis is suggested. The fact that, generally, disproves this hypothesis is that many Be stars show a changing light amplitude.

The strength of the non-radial pulsation hypotesis is that it is physically plausible and it can explain a large number of observations of the line profile and short term light variations.

§1.5 - *Pulsation and Mass Loss*

Mass loss from stars to the interstellar medium is ubiquitous. In some cases the mass loss can be very large and affect stellar evolution. Mass loss processes, i.e. mechanisms and consequences in star evolution, are poorly understood.

Stellar pulsation is linked to those evolutionary phases in which substantial mass loss occurs, thus there are good reasons to expect that pulsation plays an important role in the mechanism of mass loss.

In a series of recent papers, Willson and Bowen (1984, 1986, 1988) have discussed the possible role of pulsation in driving mass loss in stars. Particular reference to Mira variables was given. The reason why pulsation can be effective in assisting mass loss is that it can provide a large fraction of the gravitational potential energy that is needed to lift the material from the star. Detailed modeling calculations for the atmospheres of the Mira variables, which exhibit radial pulsations of long-period and large-amplitude (see §1.2), and are known to have high mass loss rates (10^{-7} to 10^{-6} $M_{\odot} yr^{-1}$), are carried out by Willson and Hill (1979) and by Bowen (1988a, b). In these stars mass loss is shown to result from interactions between pulsation-induced shocks, which greatly extend the atmosphere, and

radiation pressure, which acts on dust grains in the atmosphere. Even moderately large-amplitude radial pulsation and vertical amplitude non-radial pulsation generates shock waves. Pulsating-induced shocks cause a great extension of the stellar atmosphere, and other mechanisms, such as radiation pressure, but also rotation, provide the terminal momentum.

Willson (1986) has applied to hot stars some results obtained by the models previously developed for the outer atmosphere of Mira variables. She has discussed the general role that pulsation might play in driving mass loss in early-type stars, and particularly in Be stars.

We restrict our attention to the possible link between radial and non-radial pulsation and mass loss in early-type stars, even if reference to analogies with large-amplitude and long-period radial pulsating stars will be made. In this paragraph observational evidence of the link between pulsation and mass loss are presented, and the role which pulsation might play in driving mass loss in early-type stars is reported.

There are at least two observational features in favour of shock waves in the atmosphere of a pulsating star. The first is the presence of discontinuities within the radial velocity curve and the second, is the existence of emission/absorption components in the spectral lines. Secondary effects can be seen as a temporary increase in line strength. The shock effects are enhanced in the UV lines. However, these facts are not compelling, as other mechanisms are possible. Observational evidence for shock waves is found in the major classes of radial pulsating stars. Figure 1.4 gives a few examples of emission features interpreted as the consequence of a shock propagating through the atmospheres of stars belonging to different classes of pulsating stars. Large amplitude shock waves are observed to be present in the atmospheres of the large-amplitude and long-period Mira variables; spectral line doubling with $\Delta V \geq 30$ km/sec is present in infrared spectra (Hinkle et al. 1981) and even the visible spectra contains evidence for such shocks (Willson et al., 1982; Gillet et al., 1984). RV Tauri, W Virginis and RR Lyrae stars clearly show hydrogen emission, interpreted as shock wave effects. Concerning the radial pulsating early-type stars, also the β Cephei stars show rapidly changing emission

absorption components in the line wings. Goldberg and Walker (1974) have detected in the spectra of β Cep an asymmetric sharpening in the red wing of the Hα line. Le Contel and Morel (1982) have observed a small emission component in SiIII (see Figure 1.4b) and MgII in γ Peg. These emissions are interpreted as the consequence of a shock propagating through the atmosphere. Stamford and Watson (1978b) have shown that the line-doubling episodes exhibited by the β Cephei star, BW Vulpeculae, can be roughly accounted for by shock models. Smith (1986 b) noted that even small pulsations can cause strong shocks. For example, the pulsational amplitude in the photosphere of γ Peg is 5 km/sec, yet a shock component develops at -55 km/sec in the blue wing, and the line strength changes by 25 percent during the pulsation cycle. The strength and Doppler shift of the shock features is expected to be only a slowly increasing function of pulsation amplitude (Willson and Bowen, 1986).

Concerning the non-radial pulsating early-type stars, shocks are expected to develop for sufficient amplitude of the vertical wave velocity. There are observational problems in finding shock signatures in the line profiles of a non-radial pulsating star. Features due to pulsation can mask the shock emission/absorption, and if the projected rotation velocity is large, as in the case of Be stars, the shock emission/absorption is masked by the underlying broad protospheric profile. Shock wave interpretation has been proposed by Smith (1986 a) for the existence of transient extended wings in ϵ Per (a non-radial pulsating B star). Of course, as noted by the same author, there are other mechanisms that can cause transient extended line wings, for example a horizontal wave velocity causing shifts of material near the stellar limb. Also Penrod (1988) reported that transient extended wings are common in the line profiles of large amplitude non-radial pulsating Be stars. Variations in line strength of 53 Persei stars (Smith, 1978) may be an indirect indication of shock, but they can also explained by temperature variations as well.

The recent growth of interest in the short-term variability of Be stars and their explanation in term of non-radial pulsation is due to the possible link between non-radial pulsation and mass loss. The Be star are, among the main sequence B stars, those with the largest amplitude of mass loss and variability of it. The

outstanding problem of the Be stars is that of the driving mechanism of mass loss and its variability. An important characteristic of these stars seems to be their rapid rotation. Rotation and radiation pressure are important in driving steady mass loss, but they are not necessarily sufficient, and they do not explain the phase changes of these stars, that is the transitions from a Be to a shell and to a normal B spectrum (§1.3). Bolton (1982) was the first to draw attention to the possibility of a correlation between the observed amplitude of the short-term variability of a pulsating Be star, λ Eri and the Hα emission in this star. More recently Penrod (1988) has found that the amplitude of the line profile variability in λ Eri decreased from 20 km/sec to nearly zero within a few days of the beginning of an emission episode in this star. Baade (1983) proposed, on the basis of observations of η Cen, that short-term spectroscopic variability might be a precursor of shell episodes in Be stars. Vogt and Penrod (1983) reported strong evidence for a correlation between short-term variability and emission in ζOph. Harmanec (1984) pointed out that there was a correlation between the amplitude of the short-term variability of o And and its mean brightness, which is believed to depend on the amount of emitting material in its circumstellar disc.

Willson (1986) investigated the effects in the outer atmosphere of early-type stars of periodic isothermal shocks caused by the vertical component of the pulsation, assumed to act like a piston. If shocks deposit energy in high-density regions of the atmosphere, this energy may not be completely radiated away, and the structure of the atmosphere may change if shocks convey sufficient energy. In determining the structure of the star's outer atmosphere, the relation between the two following quantities assumes importance: the values of the radius, r_{ad}, where the induced pulsation shocks became adiabatic and the radius, r_P, of the *sonic point*, that is the point in which the Parker wind becomes supersonic. The term *Parker wind* is used to refer to the critical, transonic solution of the momentum equation, for an arbitrary temperature distribution (see Parker, 1965). If $r_{ad} \geq r_P$ the shocked gas can cool, it can do work against gravity by expansion, and finally it can produce a "cool wind". If $r_{ad} < r_P$ the material at r_{ad} is tightly bound by gravity and it does not expand as freely, the temperature rises, producing a "hot corona" and ther-

mally driven wind. r_{ad} increases with the pulsational period and with the pulsation amplitude, because they increase the density at each position in the atmosphere. The radiation pressure acts on r_P, bringing the sonic point close to the star. Also rapid rotation has an effect on r_P, moving the sonic point inward at the star's equatorial plane. For large amplitudes and long periods it is possible to have $r_{ad} \geq r_P$ and hence a cool wind. For moderate pulsation amplitudes, we expect $r_{ad} < r_P$ and hence the formation of a hot corona. The effect of rotation will lead to some dependence of hot corona and wind flux on latitude. This dependence is increased by pulsation with larger amplitude near the equator, as is the pulsation of most of the Be stars. This provides a very natural mechanism for outward material in the equatorial plane of a Be star, with the possible simultaneous existence of a hot corona in the polar regions. A given star may switch from one of the two states, hot corona and cool wind, by a change in the pulsation amplitude and/or by a change of period. Variability in mass loss may be so explained.

Castor (1987) and Castor et al. (1988) have discussed the possibility of mass loss associated with pulsation-induced shocks in early-type stars, and they have pointed out that two factors can make the pulsation ineffective to play a fundamental role in early-type star winds: the cooling efficiency of the early-type star atmospheres, and the fact that the observed pulsation periods in these stars are much longer than their wind flow times (1-2 hours), so that the wind should relatively easily adapt to the motion at its base. Concerning the Be stars, this comparison ignores the important fact that the flow time in the equatorial plane of a Be star is more than one order of magnitude longer respect to that of the other early-type stars (Baade, 1986).

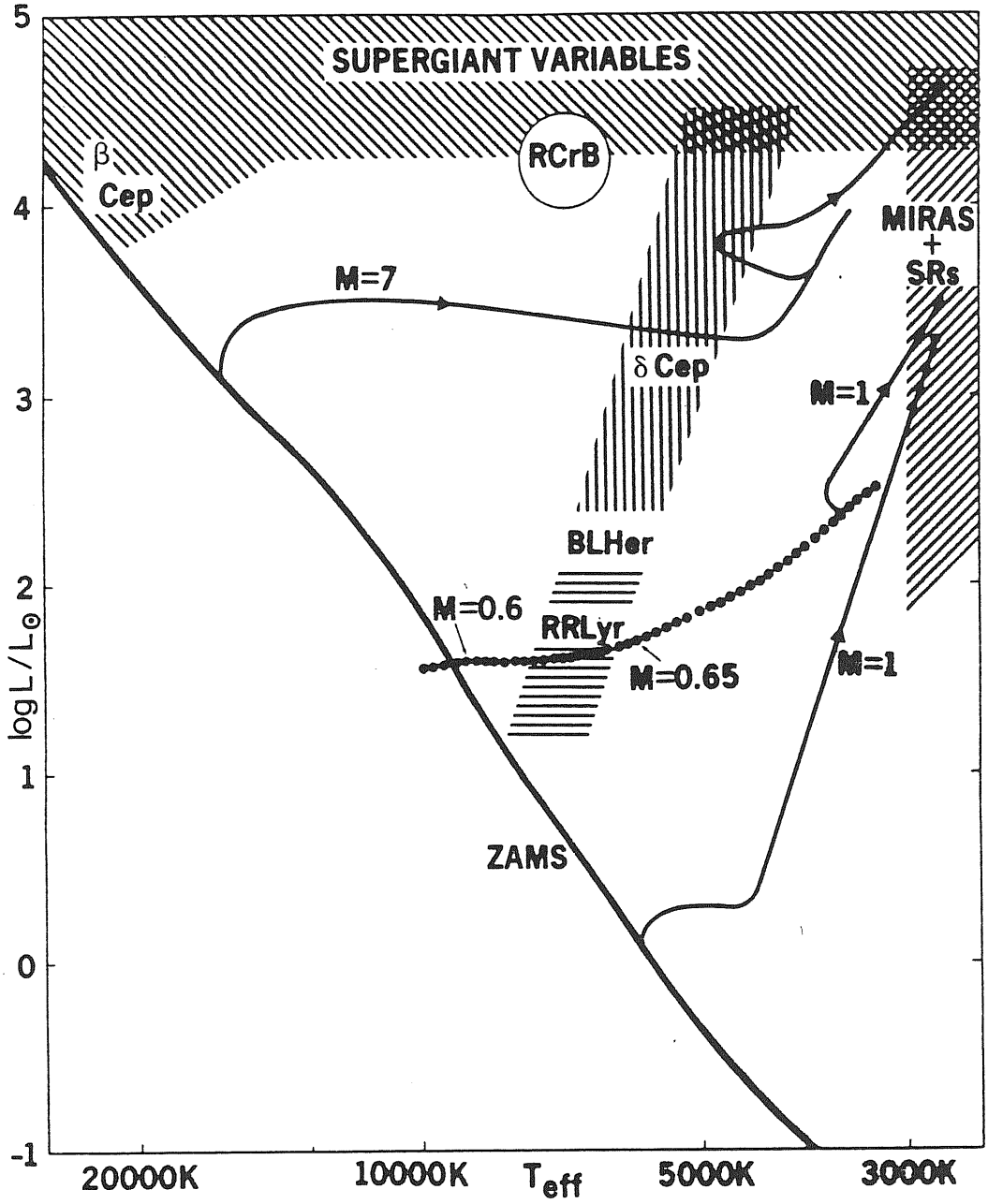

Figure 1.1 – Pulsational instability regions on the HR diagram. Standard zero-mass loss evolutionary tracks of mass equal to 1 $M_\odot$ and 7 $M_\odot$ stars of solar composition are reported for reference (Figure from Willson and Bowen, 1984)

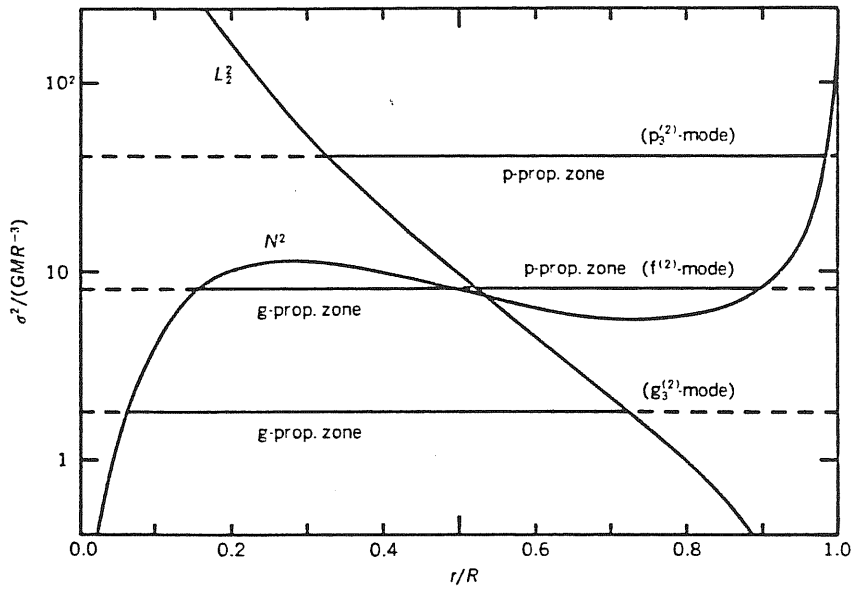

Figure 1.2 – Variations of N^2 and L_l^2 for a polytrope (index n=3) model. Three horizontal lines show the wave propagation zones. (Figure from Unno et al., 1979)

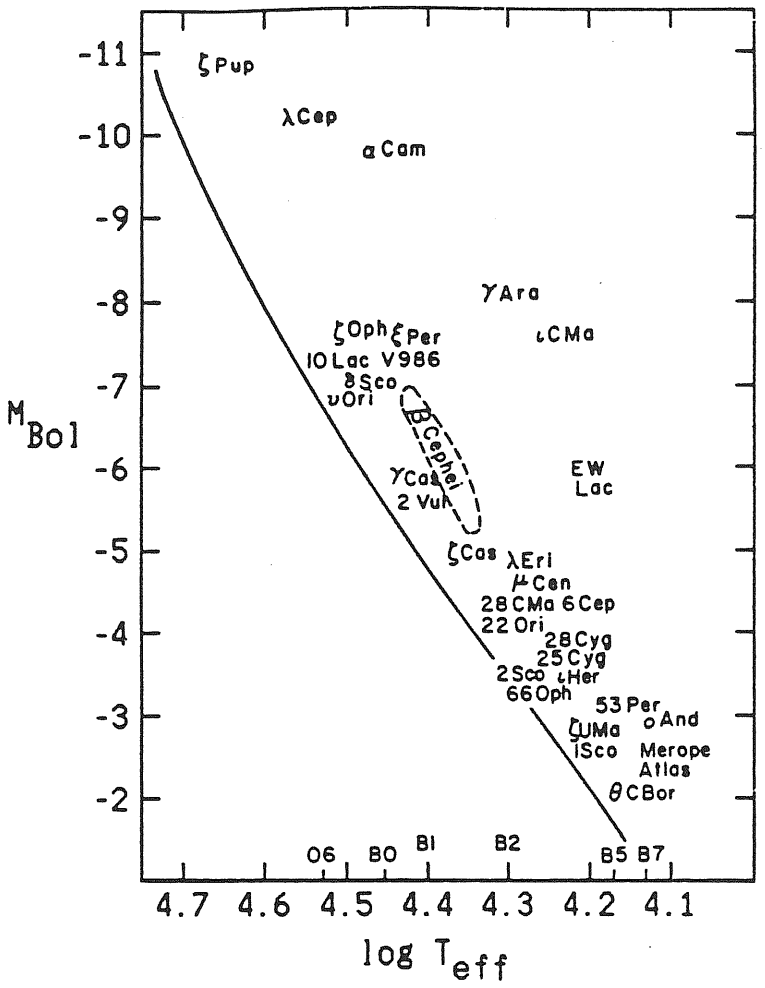

Figure 1.3 – HR diagram for non-radial pulsating early-type stars (Figure from Smith, 1986 b)

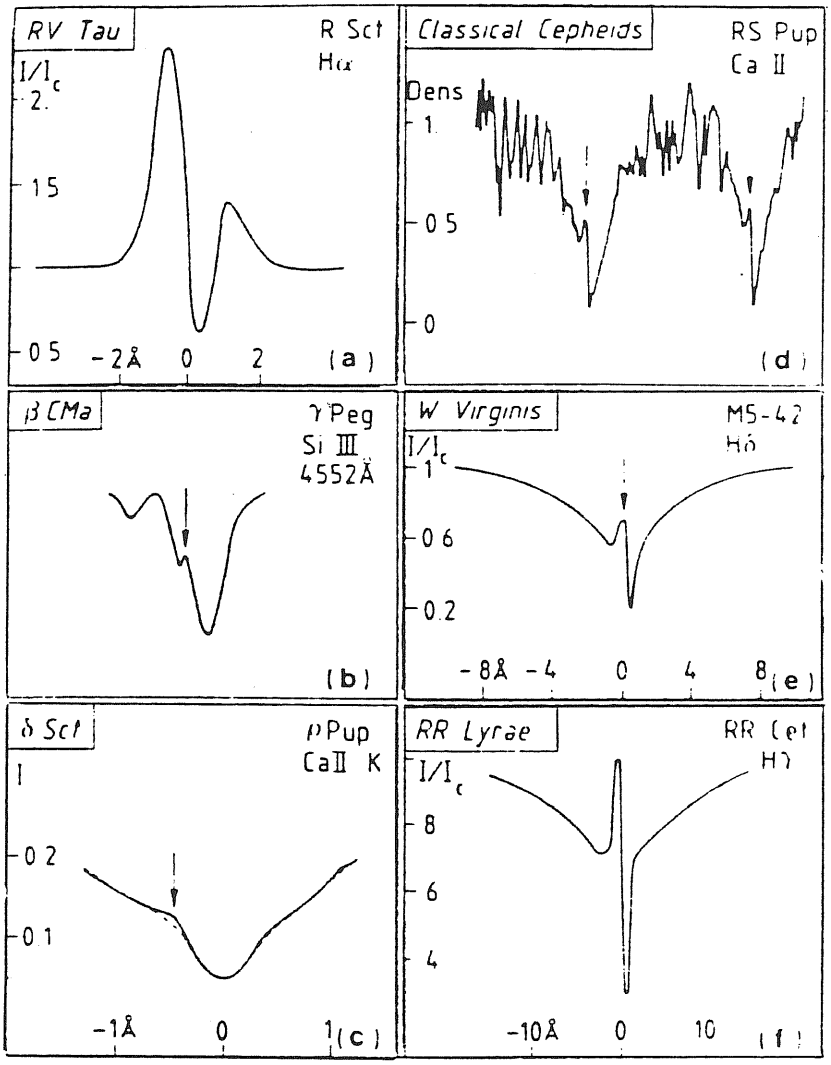

Figure 1.4 – A few examples of emission/absorption features supposed to be produced by shock waves propagating through the atmosphere of pulsating stars. (Figure from Gillet et al., 1984).

References

Abt, H.A.: 1957, Ap. J., 126, 138.

Baade, D.: 1979, The Messenger (ESO), 19, 4.

Baade, D.: 1983, Astr. Ap., 124, 283.

Baade, D.: 1984a, Astr. Ap., 134, 105.

Baade, D.: 1984b, Astr. Ap., 135, 101.

Baade, D.: 1986, in "Highlights of Astronomy", J. P. Swings, ed. 7, 255.

Baade, D.: 1987, in "The Physics of Be Stars", A. Slettebak and T. Snow eds, Cambridge Univ. Press, p. 361.

Campbell, L., and Jacchia, L.: 1941, "The Story of Variable Stars", (Philadelphia: The Bakiston Company.)

Balona, L.A.: 1985, M.N.R.A.S., 203, 1041.

Balona, L.A. and Shobbrok, R.R.: 1983, M.N.R.A.S., 205, 309.

Balona, L.A., and Englebrecht, C.A.: 1985, M.N.R.A.S., 212, 889.

Balona, L.A., and Engelbrecht, C.A.: 1986, M.N.R.A.S., 219, 131.

Belvedere, G., and Paterno', L. (eds.): 1984, "Oscillations as a Probe of the Sun's Interior", Mem. Soc. Astron. Ital., 55, No. 1,2.

Bidelman, W.P.: 1985, in "Cepheids: Theory and Observations" IAU Coll. No. 82, B. Madore ed., Cambridge University Press, p. 126.

Bolton, C.T.: 1982, in "Be and Shell Stars", IAU Symp. No. 98, M. Jaschek and H.G. Groth eds., Dordrecht: D. Reidel, p. 181.

Bowen, G.H.: 1988 a, in "Pulsation and Mass Loss in Stars", R. Stalio and L.A. Willson eds., p. 3.

Bowen, G.H.: 1988 b, Ap. J., 329, 299.

Burki, G.: 1983, Astr. Ap., 121, 211.

Castor, J.I.: 1987, in "Instabilities in Luminous Early Type Stars", H.J.G.L.M. Lamers and C.W.H. de Loore, (Dordrecht Reidel), p. 159.

Castor, J.I., Osaki, S.P., Rybicki, G.B.: 1988, in "Pulsation and Mass Loss in Stars", R. Stalio and L.A. Willson eds., Dordrecht: Reidel, p. 229.

Christensen-Dalsgaard, J., and Frandsen, S. (eds.): 1987, "Advances in Helio and Astereosismology", Reidel, Dordrecht.

Cox, J.P.: 1980, "Theory of Stellar Pulsation", Princeton Univ. Press.

Cox, J.P., King, D.S., Cox A.N., Wheeler, J.C., Hansen, C.J., Hodson, S.W.: 1980, Sp. Sci. Rev., 27, 529.

Cox, A.N.: 1986, in "Stellar Pulsation", A.N. Cox, W.N. Sparks, and S.G. Starrfield eds., (Springer-Verlag), p. 36.

Eddington, A.S.: 1918a, M.N.R.A.S., 792.

Eddington, A.S.: 1918b, M.N.R.A.S., 79, 177.

Finkenzeller, U. and Mundt, R.: 1984, Astr. Ap. Suppl., 55, 109.

Furenlid, I., Meylan, T., and Young A.: 1986, in "Stellar Pulsation", A.N. Cox, W.M. Sparks, S.G. Starrfield eds. (Springer-Verlag), p. 62.

Furenlid, I., Young A., Meylan, T., Haag, C., Crinklaw, G.: 1987, Ap. J., 319, 264.

Gillet, D., Bouchet, P., and Maurice E.: 1984, The Messanger, 39, 38.

Goldberg, B.A., Waelker, G.A.H.: 1974, Astr. Ap., 32, 355.

Gough, D.O. (ed.): 1986, "Sismology of the Sun and the Distant Stars", Reidel, Dordrecht.

Jakate, S.: 1979, Ap. J., 126, 138.

Harmanec, P.: 1984, I.A.U. Inf. Bull. Var. Stars., No. 2506.

Harris, H.: 1985, in "Cepheids: Theory and Observations", B.F. Madore ed., Cambridge U Press., p. 232.

Hinkle, K., Hall, D.N.B., and Ridgway, S.T.: 1981, private communication to L.A. Willson.

Hodson, S.W., Cox, A.N., and King, D.S.: 1980, Sp. Sci. Rev., 27, 503.

Hoffmeister, C., Richter, G., Wenzel, W.: 1985, "Variable stars" (Berlin: Springer-Verlag).

Le Contel, J.M., Morel, P.-J.: 1982, Astron. Ap., 107, 406.

Ledoux, P.: 1951, Ap. J., 114, 373.

Ledoux, P., and Waldraven, Th.: 1958,in "Handbuch der Physik", ed. S. Flugge (Berlin: Springer-Verlag), p. 353.

Lesh, J.R., Aizenman, M.L.: 1973, Astr. Ap., 22, 229.

Lesh, J.R., and Aizenman, M.L.: 1978, Ann. Rev. Astron. Ap., 16, 215.

Lee, U., and Saio, H.: 1986, M.N.R.A.S., 221, 365.

Lee, U., and Saio, H.: 1987a, M.N.R.A.S., 224, 513.

Lee, U., and Saio, H.: 1987b, M.N.R.A.S., 225, 643.

Leighton, R.B., Noyes, R.W., and Simon, G.W.: 1962, Ap. J., 135, 474.

McNamara, B.J.: 1986, in "Stellar Pulsations" A.N. Cox, W.N. Sparks, and S.G. Starrfield eds., (Springer-Verlag), p. 92.

Osaki, Y.: 1974, Ap. J., 189, 469.

Osaki, Y.: 1987 in "Instabilities in Luminous Early Type Stars", H.J.G.L.M. Lamers and W.H. de Loore eds., Reidel Publishing Company, p. 39.

Parker, E.N.: 1965, Sp. Sci. Revs., 4, 666.

Penrod, G.D.: 1986, P.A.S.P., 98, 35.

Penrod, G.D.: 1988, Ph.D. thesis, University of California, Santa Cruz.

Percy, J.R.: 1986, P.A.S.P., 98, 342.

Sareyan, J.P., Le Contel, J.M., Valtier J.C. and Ducatel, D.: 1980, in IAU Colloquium n. 58, A.N. Cox and D.S. King eds., p. 353.

Shapley, H.: 1914, Ap. J., 40, 448.

Sculfaire, R.: 1974, Astr. Ap., 36, 107.

Smith, M.A.: 1978, Ap. J., 224, 927.

Smith, M.A.: 1986a, Ap. J., 307, 213.

Smith, M.A.: 1986b, in "Hydrodynamic and Magnetohydrodynamic Problems in the Sun and Stars", Y. Osaki ed., Tokyo, p. 145.

Smith, M.A.: 1988, in "Pulsation and mass loss in Stars", R. Stalio and L.A. Willson eds., p. 251.

Smith, M.A., and Penrod, G.D.: 1985, in "Relations between Chromospheric-Coronal Heating and Mass Loss in Stars", R. Stalio and J. Zirker eds., Trieste, p. 394.

Smith, M.A., Gries, D., and Penrod, G.D.: 1986 in "Physics of Be Stars", IAU coll. 92, p. 464.

Smith, M.A., Fullerton, A.W., and Percy, J.R.: 1987, in "Stellar Pulsation", A.N. Cox, W.M. Sparks and S.G. Starrfield eds. (Springer-Verlag), p. 79.

Stamford, P.A., and Watson, R.D.: 1978a, in "Changing Trends in Variable Star Research", Bateson F. ed., (Dordrecht: Reidel), p. 504.

Stamford, P.A., and Watson, R.D.: 1978b, Proc. Ast. Soc. Australia, 3, 273.

Stagg, C.R.: 1986, in "Phisics of Be Stars", IAU Coll., 92 p. 90.

Struve, O.: 1955 Sky and Tele., 14, 461.

Ulrich, R.K., Harvey, J., Rhodes, E.J. jr., Toomre, J. (eds.): 1984, "Solar Seismology from Space", NASA, JPL Publ. 84-84.

Unno, W., Osaki, Y., Ando, H. Shibahashi, H.: 1979, "Non-radial Oscillations of Stars", University of Tokio press.

Vogt, S.S., and Penrod, G.D.: 1983, Ap. J., 275, 661.

Waelkens, C., and Rufener, F.: 1985, Astr. Ap., 152, 6.

Walker, G.A.H., Yang, S., and Fahlmann, G.G.: 1979, Ap. J., 233, 199.

Willson, L.A.: 1982, in "Pulsations in Classical and Cataclysmic variable Stars", J.P. Cox and C.J. Hansen, eds., 269.

Willson, L.A.: 1986, Pub. Astr. Soc. Pacific, 98, 37.

Willson, L.A.: 1988, in "Pulsation and Mass Loss in Stars", R. Stalio and L.A. Willson eds., p. 285.

Willson, L.A., and Hill, S.J.: 1979, Ap. J., 228, 854.

Willson, L.A., Wallerstein, G., and Pilachowski, C.: 1982, M.N.R.A.S., 198, 483.

Willson, L.A., and Bowen, G.H.: 1984, Nature, 312, 429.

Willson, L.A., and Bowen, G.H.: 1986 in "Relations Between Chromospheric-Coronal Heating and Mass Loss in Stars", R. Stalio and J. Zirker, eds., (Tabographis, Italy), p. 129.

Willson, L.A., and Bowen, G.H.: 1988, in "Proceedings of the Vatican Workshop on Circumstellar polarization", G. Coyne ed., in press.

Winget, D.E., 1986, Higlights of Astronomy, 7, 221.

Wood, P.R.: 1982, in "Pulsations of Classical and Cataclysmic Variable Stars" J.P. Cox and C.J. Hanson. eds., p. 284.

CHAPTER II

Model Atmospheres

§2.1 - *Introduction*

By the term stellar atmosphere we intend the transition region from the stellar interior to the interstellar medium. It is the astronomer, not the the star, that draws the boundary between a stellar atmosphere and the interior. The outer layers merge smoothly with the interior regions, and the same physical principles must operate in both, but only the atmosphere is susceptible to direct observation. So the stellar atmosphere is the connecting link between the observations and the stellar interior: radiation coming from it can be detected and interpreted in order to give information on the physical state of the star as a whole.

A model atmosphere is a mathematical construction that provides a representation of an actual atmosphere in the form of a tabulation of various quantities, such as temperature, particle densities, degrees of ionization and excitation of the various atmosphere costituents (atoms, ions, molecules), as a function of the atmosphere geometrical depth. This description of the physical structure of an atmosphere is a prerequisite for calculating the emergent spectrum, which can then be compared with the observations. If the observed spectrum is the same as the predicted spectrum, in its most significant characteristics, the model is said to be representative of the star and it is concluded that the parameters and physical processes used to construct the model are similar to what actually occurs in the stellar atmosphere.

Stellar model atmospheres have been calculated since the mid 1940's. The pioneering works on this subject are summarized in Pecker (1965), with a presentation of the equations which are needed to find the model atmosphere temperature

and density structure and to predict the spectrum. Subsequently with the development of numerical analysis techniques and the availability of large computers, many other models have been computed. The conceptually simplest model atmospheres are those which are based on the hypotheses that the star is a close thermodynamic system (it exchanges only radiative energy with the surrounding medium, but no mass or non-thermal energy), and its atmosphere is formed by plane-parallel homogeneous layers in radiative and hydrostatic equilibrium. It is usually assumed that, at the microscopic level, the detailed balance (LTE) holds. In more advanced models the star atmosphere is considered to be in statistical steady state (non-LTE).

In the early 1970's, with the development of the non-LTE models, it was thought that the stellar atmosphere theory had reached its maximum development and that the future would consist of only small improvements of the non-LTE theory. But the concomitant advent of observations from space demonstrated that this was not true. When satellite spectra extending to $\approx$ 1000A became available, it became evident that the *classical* models, even the non-LTE ones, were inadequate to explain some of the new observations. In particular, model atmospheres were unable to predict the presence in OB stars of the resonance lines of ions such as OVI, NV, CIV and SiIV, indicating the presence of gas heated to higher electron temperatures than the star's effective temperature, nor did they predict the shapes and displacements of these resonance lines, indicating outflow of matter at speeds often exceeding the velocity of escape from the photosphere. Mass loss signatures were subsequently discovered in the radio and infrared ranges, and the presence of high temperature regions were also inferred from X-ray observations. The outer atmosphere conditions: high ionization, production of X-rays, and rapid flow violate the assumptions on which the *classical* atmosphere models are based. So we can conclude that the *classical* model atmospheres provide only a simplified representation of the physical processes occurring in a real stellar photosphere. This is, in principle, true not only for early-type stars, but for all stars covering the different parts of the H-R diagram.

In the following section (§2.2) we introduce the assumption and the basic equations on which the *classical* atmosphere models are based. In section 2.3 we make a

comparison between the spectra predicted from the *classical* model atmospheres and the observed early-type star spectra. In section 2.4 we introduce the non-stationary stellar atmosphere models.

§2.2 - *Classical Atmosphere Models*

The problem of building an atmosphere model in its greatest generality is very complex. While it is relatively easy to formulate the equations describing the physical state of the material in a stellar atmosphere, by considering the microprocesses occuring in each element of the gas, their solution presents a hard non-linear mathematical problem. This is so because each variable at any depth of the atmoshere is coupled with each variable at every other depth. It is therefore necessary to make a number of simplifications in order to solve it.

The assumptions in a classical model atmosphere are:

Homogeneous plane parellel layers- The atmosphere is assumed to be stratified in plane parallel layers. The planar geometry is valid when the thickness of the atmosphere is small compared with the radius of the star. This assumption simplifies the transfer problems, because it reduces the spatial variables of the problem to only one: the depth of the atmosphere.

Hydrostatic equilibrium- The condition that the atmosphere is in hydrostatic equilibrium is used to define the variation of gas pressure with geometric height. It is assumed that the total pressure evenly balances the gravitational force.

Radiative equilibrium- The variation of temperature with depth is given by this condition. It may be expressed by requiring that no energy is generated or lost in the atmosphere. This hypothesis then implies that the frequency-integrated total flux at each depth in the atmosphere is constant.

Steady state- The presence of velocity fields can affect the stellar atmosphere problem in many ways. In some cases the phenomena may be explicitly time-dependent,

as in the case of radial and non-radial pulsations. In the classical models, a completely static atmosphere is assumed; that is, all the atmosphere properties are assumed to be time-independent. So not only stellar pulsations, but all time-dependent phenomena, such as variable magnetic fields, shocks, expanding envelopes, etc., are neglected.

Also either detailed balance (LTE) or statistical steady-state equilibrium (non-LTE) is considered. In the former case, the rate at which each atomic process occurs is exactly balanced out by the rate at which its inverse occurs. In the second case, the atomic level occupation numbers are time-independent, i.e. the total rate at which atoms leave a given level must be exactly balanced out by the total rate at which atoms enter that level, when all relevent atomic processes are taken into account.

With these assumptions, we define the basic quantities and construct the equations necessary in order to solve the problem of model atmospheres.

The radiation passes through the atmospheric gas (assumed to be perfect) and interacts with the material. The interaction counts on a wide variety of physical processes that can be described from a macroscopic point of view. In order to describe the removal of energy by matter from the radiation field and the emission of radiation from stellar material, we define the total absorption coefficient or opacity, $K(\nu)$, and the emission coefficient or emissivity $\gamma(\nu)$ respectively. We define $K(\nu)$ such that an element of material of cross section dA and length ds, removes from a beam with specific intensity $I(r,\nu)$, incident normal to dA and propagating into a solid angle $d\omega$ an amount of energy

$$dE_\nu = K(\nu)I(\nu)dAdsd\omega d\nu dt \tag{2.1}$$

within a frequency interval $d\nu$ in a time interval dt. The total absorption coefficient is the product of an atomic cross-section and the number of density of absorbing atoms (molecules) distributed over all the excitation states that can interact with photons of frequency ν. The mean free path, $1/K(\nu)$, gives a measure of the distance over which a photon can propagate before it is removed from the beam. In a similar way we define the emissivity, $\gamma(\nu)$, such that the amount of energy relased by an

element of material of cross section dA and length ds, into a solid angle $d\omega$, within a frequency interval $d\nu$, in a direction normal to dA, in a time interval dt is

$$dE_\nu = \gamma(\nu) dA ds d\omega d\nu dt. \tag{2.2}$$

Let us consider the energy passing througth a fixed volume element. We shall find an energy change due to absorption and emission within the volume

$$\delta E = [I(r + dr, \nu + d\nu, t + dt) - I(r, \nu, t)] dA d\omega d\nu dt$$

$$= dI_\nu dA d\omega d\nu dt = (\gamma(r, \nu) - K(\nu) I(r, \nu, t)) dA d\omega d\nu dt ds. \tag{2.3}$$

Under the hypothesis of a plane-parallel layer atmosphere, the only linear dimension entering into the description of it is the depth, z. If θ is the angle between the direction normal to dA and z, so that

$$ds = dz / cos\theta,$$

from 2.3 we get

$$cos\theta \frac{dI(z, \nu)}{dz} = \gamma(\nu) - K(\nu) I(z, \nu), \tag{2.4}$$

the time-independent transfer equation for plane parallel model atmosphere calculations. The coordinate z increases upward in the atmosphere, i.e. toward the observer. This equation can be written in a more standard form by defining two new quantities: the optical depth and the source function. The optical depth:

$$\tau(z, \nu) = - \int_z^{z_{max}} K(\nu) dz$$

gives the integrated absorptivity of the material along the line of sight. We define the source function to be the ratio of total emissivity to total opacity

$$S(\nu) = \frac{\gamma(\nu)}{K(\nu)}.$$

The transfer equation can be written as

$$cos\theta \frac{dI_\nu}{d\tau_\nu} = I_\nu - S_\nu \tag{2.5}$$

It is clear that we can determine the radiation field in the gas, which constitutes the stellar atmosphere, if we specify the values of K_ν and S_ν as functions of position and frequency. K_ν and S_ν depend on the details of the macroscopic interactions between radiation and materia and also on the state of the gas. Since the stellar atmospheres are regions of high temperature and low density, the gas consists mainly of single atoms, ions, free electrons and, in cool stars, also molecules. The state of the gas is specified when the occupation number of all available bound and free energy levels are known. In order to specify the occupation numbers, there are two main approaches: local thermodynamic equilibrium, LTE, or non-local thermodynamic equilibrium, non-LTE.

In LTE the distribution of atoms over bound and free levels can be uniquely specified by two thermodynamic variables: temperature and density, for instance. The equilibrium among excited states is assumed to be given by Boltzman' s equation, the ionization equilibrium is assumed to be given by Saha's equation and the electron velocity distribution is assumed to be maxwellian.

In the non-LTE approach, assumptions on the relative populations of states of atoms, ions and electrons are not made a priori; the level populations are computed self-consistently, recognizing that the intensity of radiation in the gas is controlled by the atomic populations, but it in turn controls these populations by influencing the transition rates between the states. In non-LTE a self consistent simultaneous solution of the radiative transfer and statistical equilibrium equations is sought. The rate of change of the population of the states is given by

$$\frac{\partial n_i}{\partial t} = \sum_{j \neq i} n_j P_{ij} - n_i \sum_{j \neq i} P_{ij} = 0, \tag{2.6}$$

where P_{ij} denotes the total rate from level i to j. For each state one such equation exists. In general the rates P_{ij} and P_{ji} will contain both radiative and collisional terms.

The hydrostatic equilibrium assumption leads to a particularly simple form for the pressure balance equation. In a one-dimensional planar static atmosphere the hydrostatic equilibrium equation is

$$\frac{dP}{dz} = \rho g, \tag{2.7}$$

where P is the total pressure, sum of the gas pressure, radiation pressure, and turbulence pressure,

$$P = P_{gas} + P_{rad} + P_{tur},$$

g the surface gravity and ρ the mass density.

For the radiative equilibrium assumption, the total energy absorbed by the material must be equal to that emitted and hence

$$\frac{1}{4\pi}\int_0^\infty \int \gamma_\nu I_\nu d\omega = \frac{1}{4\pi}\int_0^\infty d\nu \oint k_\nu d\omega. \tag{2.8}$$

We can express the condition of radiative equilibrium in another way, by integrating in $d\omega$ and in $d\nu$ the transfer equation (2.4), and taking into account the relation 2. 7. This implies that the total flux for unit surface (F) is constant, and it is given by the following relation:

$$F = \sigma T_{eff}^4, \tag{2.9}$$

where σ is the Stefan-Boltzman constant and T_{eff} is another fundamental parameter characterizing the model, defined as the temperature of a black body that emits the actual stellar flux.

A LTE steady-state stellar atmosphere model is obtained by solving simultaneously the equations of radiative transfer, hydrostatic and radiative equilibrium under the approximation that the distributions of atoms and ions over their various possible energy states (level population) are described by using the Boltzman and Saha laws. In the non-LTE hypothesis, the equations of statistical equilibrium fix the level population.

The first LTE modeling procedures were based on the *temperature correction* approach developed by Strömgren (1944). For determining the temperature structure the radiative and transfer equations are solved iteratively: first solving the

equation of transfer with an approximate temperature law, then solving the equation of radiative equilibrium to find improvements on the temperature law, and so on. If the temperature distribution is known, the equation of hydrostatic equilibrium can be integrated and the density structure of the atmosphere can be calculated. In the late 1960's a powerful technique was developed by Feautrier (1968). The equations of transfer and radiative equilibrium are solved simultaneously. This technique was subsequently the basis of Auer and Mihalas's (1969) *complete linearization method* for solving the non-LTE model atmosphere. In this method, the simultaneous treatment of the equations of radiative transfer, hydrostatic, radiative and statistical equilibria assures that the coupling among all the physical variables is fully accounted for, self-consistently, to the first order, at each stage of the calculations.

A set of classical LTE model atmospheres is given by Kurucz (1979 a, b). The models are computed by use of a statistical distribution-function representation of the line opacity of almost 10^6, transitions and continuous opacity for HI and HII, HeI-HeIII, CI-CIV, NII-NV, OII-OIV, NeI-NeVI, MgI, AlI, SiI, H^+, H^-, H Rayleigh and electron scattering. In these models the temperature in the outermost layers, for a given chemical composition and pressure, is lower than that computed by models which do not include the line opacity (Figure 2.1). In fact, the inclusion of the lines causes a redistribution of flux in the spectrum and the temperature distribution responds accordingly to bring this about under the flux costancy constraint. The blockage of the flux by the lines results in a heating of the deeper layers. For this reason the whole process is called *line blanketing.*

The Mihalas (1972a) models (LTE and non-LTE) do not include the effect of line blanketing. The chemical composition consists of hydrogen and helium in a ratio by number of 10 to 1 with a small admixture of a representative "fictitious light element" which has abundance and ionization stages so adjusted as to represent approximately the effect of the continuous absorption due to ions of C, N and O. An example of differences between LTE and non-LTE models is shown in Figure 2.2 for a model with $T_{eff} = 15000$K and $\log g = 2.5$. In the LTE case we see an initial plateau where the Paschen and Balmer continua become trasparent and then

a final drop due to the Lyman continuum. By contrast, in the non-LTE model, the Lyman continuum switches from a cooling continuum to a mild source of heating, owing to the relative underpopulation of the ground state (i.e. less opacity).

The differences between the temperature structure in the LTE and non-LTE models decrease rapidly as the gravity increases and increase as the effective temperature increases. Figure 2.2 also reports the temperature distribution in a LTE Kurucz model at the same T_{eff} and $\log g$. We should note the significant differences in the Mihalas LTE model compared to Kurucz models for $\tau \geq 10^{-2}$, because sufficient line opacity is not included.

Recently Anderson (1985) has computed a classical non-LTE model atmosphere at $T_{eff} = 35000$K and $\log g = 4$ with contributions of 93 b-f transitions and 128 b-b transitions of 29 ions of H, He, C, N, O, Ne, Mg, Si and S included. A comparison of this model with both the Mihalas and Kurucz models, at the same effective temperature and gravity, show that the depth dependence of the temperature better fits Kurucz' s temperature structure over the whole atmosphere, while it is considerable lower than Mihalas temperatures in the outer layers (see Figure 2.3). The reason for this is that in the non-LTE calculations of Anderson the addition of line opacity increases the opportunity for electrons to cascade into the first orbital level, where they can absorb Lyman continuum photons more effectively and in practice make the outer atmospheric layers cooler than predicted by non-LTE models with only H and He opacities. In Figure 2.3 the differences of the temperature profiles of the Kurucz's LTE and Anderson's LTE models are due to the different opacities that are considered in the two models.

The line blanketing has a significant effect on the temperature-pressure structure of a model atmosphere and the inclusion in the model atmosphere calculations of realistic opacities is , at present, object of intensive efforts.

§2.3 - *Classical Model-Atmosphere Predictions and Early-Type Star Spectra*

There are several criteria for selecting an appropriate model to represent the atmosphere of a star. The energy distribution is one of the major spectroscopic outputs from the model atmosphere calculations, so often a star is identified with a model by fitting the observed and predicted energy distributions. A model atmosphere can also be selected by using the synthetic spectrum approach. The fitting of the observed absorption-line spectrum with the theoretical ones gives information on the star atmosphere parameters, when high resolution spectra are available.

Spectral energy distributions of main sequence early-type stars can be fitted sufficiently well by the calculations. We need data covering an extended λ-range: if possible the Balmer, Paschen and Brackett continua, and to have the Lyman continuum would be optimal. Low resolution data can be used, even if they do not allow us to see the details of the spectrum (individual lines). For early-type stars, which are the object of the present research, the important wavelength range for this type of analysis is the FUV region (912-2000 A) where much of their energy is radiated.

The comparison of the observations with the model atmosphere calculations is essentially limited by the difficulty in obtaining an "accurate" model, that is a non-LTE model atmosphere which includes the opacity sources due to atomic transitions. We have available only non-LTE unblanketed models (Mihalas, 1972 a) or the Kurucz (1979 a, b) grid of LTE blanketed models (§2.2). The question of the choice between the two atmosphere models, line-blanketed LTE or unblanketed non-LTE, for representing the energy distribution of early-type stars is much debated. Recently Longo et al. (1988) have discussed this problem and, using their data and published results by Massa and Savage (1985), Anderson (1985), Torres (1988), have concluded that Kurucz's models are more reliable for predicting the fluxes of early-type stars.

An automatic procedure has been developed by Morossi and Malagnini (1985) for selecting a model to represent the atmosphere of a star. The method consists

of a numerical comparison between observed and theoretical data. The atmosphere parameters are determined by the best fit, in the least-square sense, of the observed energy distribution with the theoretical ones. The fitting functions are derived from a theoretical grid consisting of energy distributions computed from the LTE blanketed models of Kurucz (1979 a) at equally spaced values of T_{eff} and $\log g$.

As we have already said, we can obtain information on the atmosphere parameters also by fitting the observed and theoretical absorption line spectra. Individual line profiles can be easily calculated under the LTE hypothesis. It is just a question of computing the ratio of line and continuum fluxes: F_λ/F_{con}. To do this, one must have a suitable expression for the line absorption coefficient in terms of the number of atoms/ions in the levels from which the line is formed, the oscillatory strength value for the line, *gf*, and the damping constants. The level populations are fixed by the Saha and Boltzman laws at the local temperature and density.

To calculate non-LTE line profiles, one must adopt a model of the atom. The number of ionization states and levels to be dealt with is limited by the speed and by the memory storage capacity of the available computer. Generally, model atoms are adopted which have one or two stages of ionization and 10 to 15 levels explicitly described by their excitation energies and statistical weights. It is necessary to have information on all the required radiative and collisional cross sections which affect the populations of the levels involved in the lines. The non-LTE level can be obtained from the simultaneous solution of the equations of radiative transfer and statistical equilibrium by the complete linearization method developed by Auer and Mihalas. The final step is to use these level populations with a detailed expression for the depth-dependent line-absorption coefficient, to solve the equation of radiative transfer and predict the line profiles.

Comparison of line profiles obtained from LTE and non-LTE calculations shows that the differences are complex. It is not easy to generalize, but we can say that the cores of lines which have well-developed wings in the visible spectral region become deeper when non-LTE physics is used, while the wings change very little. This is well illustrated by the Hα and Hγ lines in Figure 2.4, where the theoretical Hα and Hγ profiles calculated by Mihalas using LTE and non-LTE models (T_{eff}=19000 K

and $\log g = 4$) and observed ones in ι Her (B4V) are compared. At Hγ the effects of departures from LTE are very small. The wings and the equivalent width of Hγ are little changed. The fitting of the Hγ wings is an important way of estimating gravity and the present result indicates that essentially the same value of $\log g$ will be obtained by either LTE or non-LTE analysis. More striking are the changes due to non-LTE at Hα. As can be seen in Figure 2.4, the non-LTE calculation is in excellent agreement with the Hα observed profile, even into the line core, where the LTE predictions fail. The effects of departures from LTE in the hydrogen lines increase for O stars and low-gravity early B stars (Mihalas, 1972b); they are stronger for the line seen longward of 5000A (this may be seen also by comparing Hα and Hγ profiles in Figure 2.4).

The most characteristic spectroscopic feature of the B stars is the presence of a well-developed spectrum of HeI. The helium lines offer many important possibilities for diagnostics of the atmospheric structure. Results of an extensive set of computations of the HeI spectrum in B stars using LTE and non-LTE model atmospheres are presented and discussed in Auer and Mihalas (1973 a). Over a wide range of effective temperature and gravity, departures from LTE do not have much impact on the equivalent widths in the blue violet region. The differences, in most cases, are smaller than the typical errors in measurement and the errors inherent in the broadening theory (see Figure 2.5). As we proceed toward the red, these effects become larger. This trend can be explained by noting that the red and infrared lines have weak wings; thus the equivalent width is dominated by the depth of the line core, which in turn depends very much on the details of the mechanism of line-formation. For HeIλ-5876 and -6678 lines, the use of non-LTE physics results in a strong, deep core, which increases the equivalent width. Much improved agreement between the observed and predicted HeIλ-5876 and -6678 line profiles is obtained when departures from LTE are taken into account (Auer and Mihalas, 1973 a) (see Figure 2.6).

We can select an appropriate model to represent the atmosphere of a star by comparing observed spectral regions, containing several line profiles, with model calculations by the spectrum synthesis method (Faraggiana et al., 1986 and refer-

ences therein). This method can be used even if the observed image is crowded with blended lines, and it enables us to draw abundance values. The method consists in using as input data a model atmosphere; usually Kurucz's LTE models are used. Element abundances and a line list with excitation potentials and gf values are given as input in a given spectral range. The lines which contribute to the stellar spectrum are selected and the computed theoretical spectrum is convolved with functions representing the instrumental profile and possible macroscopic motions. Finally the observations are compared with the calculations, and the abundances of the elements are adjusted until the calculated profiles match the observed ones reasonably well.

The above described criteria for interpreting stellar spectra are successful in modeling the photospheric layers of many early-type stars. For main-sequence stars, determinations of effective temperature and $\log g$ by different methods are in agreement. For B-type supergiants the agreement is less satisfactory because non-LTE effects are more important, owing to the low gravity, and the inadequancy of the plane-parallel geometry assumption.

The classical model atmospheres, as we have already said (§2.1), are unable to predict the spectrum formed in the presence of velocity fields: rotation, pulsation, expansion in the photospheric and/or outer atmospheric layers. In addition, the classical methods are inadequate for modeling the characteristics of outer atmospheres of early-type stars: electron temperatures larger than the stellar effective temperature, variability on time scales that range from minutes to years, etc..

§2.4 - *Non Stationary Models*

2.4.1 - *Rotation*

Many of the characteristic features of the spectra of early-type stars indicate the presence of velocity fields. Among these, rotation plays a very important role, in particular for B stars, where many rapid rotators are found, some of them close to the "break-up" velocity (gravitational acceleration at the equator equal to the centrifugal acceleration).

The effects of rotation on the spectral energy distribution are small except for very rapid rotation, i.e. near the break-up velocity. The shape of the spectral lines, however, is considerably changed, owing to the relative Doppler shifts of the light coming from different parts of the stellar disc. The basic problem of diagnosing the rotational status of a star from its spectral line profiles has been extensively studied. The first approach was to convolve an intrinsic flux profile (either computed or observed) with a rotation-broadening function and to compare it with observed profiles. Allowance is usually made for limb-darkening in the continuum; only in Stoeckley and Mihalas (1973) were rotationally broadened profiles calculated by taking into account also the limb-darkening in the lines. This approach implies that the star is spherically symmetrical and in solid-body rotation. This means that for a given projected rotation velocity the line profiles do not change even if the inclination angle changes.

In the presence of very rapid rotation, the shape of a star is distorted and the effective temperature changes as a function of the gravity on the stellar surface (hence of the latitude) according to the von Zeipel (1924) law. Continuum energy distribution and rotation-broadened profiles for rotationally distorted stars have been computed by Collins and Sonnerborn (1977 and references therein) including the variations of surface gravity and effective temperature. The procedure that they followed is to use a different model atmosphere at different places on the stellar surface. The choice of model is based on predictions of the surface gravity and temperature from the theory of the stellar interior, in the case of stars that

rotate rigidly or nearly so. The amount of radiation crossing each unit of area and its spectral distribution change as a function of the position. The specific intensity is calculated at each point on the surface and it is integrated over the visible hemisphere of the star. The general result of these calculations is that rapid rotation tends to make the predicted energy distribution redder than it would be if it rotated slowly.

With regard to the spectral lines, Collins and Sonnerborn (1977) showed that, in a distorted star, the profiles vary with the inclination of the star, even if the projected rotation velocity is held constant. In addition, these rotationally broadened profiles are often narrower than those calculated by the convolution approach, for the same projected rotation velocity, primarily because of gravity darkening (lower surface-brightness near the equator than at the poles).

2.4.2 - *Turbulence*

Motions of the photospheric gas, which are on a large scale compared to atomic dimensions, but on a small scale compared to the size of the star, are called turbulence (this term was introduced by Rosseland in 1928). The Sun is the only star for which some idea of the geometry of these motions can be formulated. In dealing with the star we simply distinguish between microturbulence, where the size of the turbulent element is small compared to the mean free path of the photon, and macroturbulence, where the size of the turbulent element is large compared to the mean free path of the photon.

Turbulence alters the line profiles in a stellar spectrum through the irregular Doppler shifts due to motion. The effect of microturbulence is to increase the width of the Doppler core of the line absorption coefficient, with the result that the equivalent widths of the lines, at which saturation effects occur, are also enhanced. This broadening affects the relation between the equivalent widths and abundances (the flat part of the curve of growth is raised). Macroturbulence causes only an increase in the Doppler width of the core of the observed line, without influencing the total equivalent width.

Since 1934, when Struve and Elvey introduced the concept of microturbulence

for spectral line broadening, this mechanism has frequently been used in the analyses of stellar spectra. Also non-LTE analysis of line spectra in early-type stars have demonstrated that the best fit with the observations is obtained with an additional broadening of the atomic absorption coefficient. That this broadening is due to macroscopic velocity fields is an assumption; however, it is strongly supported by empirical findings as well as by theoretical arguments. For example, to the observation of solar photosphere granulation reveals the existence of irregular non-stationary motions. Theoretically we expect stellar atmosphere turbulence, in all high Reynolds number velocity fields, driven by convection or by expansion. We must say that also acuostic, shock waves or finally gravity waves , in their superposition with random phases, can act spectroscopically as turbulence, though they are not turbulence in the hydrodynamic meaning of this word.

Microturbulence has been measured for many stars from the fit of measured equivalent widths to theoretical ones (Smith, 1971; Andersen, 1973). Also the line half widths can give information on microturbulent motions (Smith, 1973, Day et al., 1973). Non-LTE analysis of the light-ion-spectra in early-type stars by Mihalas (1972 c), Mihalas and Hummer (1973), Kamp (1973) and by Auer and Mihalas (1973 b) demonstrated that, in the presence of turbulent motions, the best fit with the observations was obtained with an additional broadening of the atomic absorption coefficient corresponding to microturbulent velocities from 4 km/sec to 15 km/sec.

The only way macroturbulence can be detected is from the line profiles. The Fourier technique can be used for obtaining reliable estimates of macroturbulent motions by the convolution between the macroturbulence velocity distribution and the intrinsic flux profile, and comparison with the observations (Gray, 1976). In addition, only in the Fourier domain it is possible to distinguish macroturbulent from rotation broadening (Gray, 1976). Evidence of macroturbulence in stars has been found mainly in supergiants. Macroturbulence often of the order of 50 km/sec are implied by the line shapes of the early-type supergiants (Ebbets, 1979). The ratio of macroturbulence to rotation increases with the luminosity and possibly with temperature (Slettebak, 1956).

2.4.3 - *Extended Atmosphere*

The winds of early-type luminous stars are known to be very strong, with mass loss rates ranging from 10^{-7} to 10^{-4} $M_{\odot}$/yr, and with terminal speeds ranging from 1000 to 3000 km/sec. The existence of acceleration of the outer atmosphere material implies the action of a propulsion mechanism. Theories of winds based on a radiation pressure origin have been developed by Lucy and Solomon (1970) and by Castor, Abbott and Klein (1975). These theories have been successful in matching many of the observed properties of early-type star winds, but there are a number of observations that are not explained by them. Among these is the variability of early-type star winds on a variety of time scales, from minutes to years. In 1979 Abbott showed that near-main-sequence early B stars are near the threshold luminosity for a radiation-driven wind. Some authors have looked for alternative acceleration mechanisms. Limber and Marlborough (1968) studied the possibility that magnetic fields provide outward acceleration on the flow of ions in B-type stars. Thomas (1973) and Cannon and Thomas (1977) concluded that the source of outward directed motions may be sought in mass flow from subphotospheric layers. As we have already said (Chapter I), recent theoretical and observational works have led to the suggestion that a combination of pulsation and other mechanisms may play an important role in the mass-loss process. In the presence of velocity fields, the classical model-atmosphere hydrostatic equilibrium constraint is no longer adequate for determining the variation of gas pressure with the geometric height.

No models of extended moving atmospheres of early-type stars fully consistent with the physical processes that appear to occur, have yet been developed. In order to obtain the temperature and pressure density structure, one should solve, simultaneously, the combined equations for conservation of mass , momentum and energy as well as the equations of radiative transfer in a three dimensional atmosphere, taking into account all the ways in which gas, radiation and magnetic field can interact and exchange energy. The boundary conditions are that the atmosphere is irradiated on the inner side by a flux of radiation and of mechanical or magnetic energy, generated in the interior of the star, and that on the other side it is open to interstellar space. The problem is difficult to solve and it will require very powerful

techniques of mathematical analysis. Less realistic models have been developed in which only the transfer equation is solved, assuming an *ad hoc* temperature distribution, specifying the outer atmosphere velocity field as a simple function of the distance from the photosphere of the star, and in which the conservation of mass gives the density distribution.

2.4.4 - *Pulsation*

As regards the stellar pulsation, we have indicators of its presence both from the spectral energy distribution and from the line profiles. From an atmospheric model of a pulsating star and from studies of the energy distribution we can obtain information on the temperature and gravity variations; from line profile studies, we can derive information on the velocity structure. In order to construct a pulsating star atmosphere model, one should solve the aerodynamic equations for a pulsating star and the radiative transfer equation. Two more realistic paths can be followed: 1) we can solve the aerodynamic equations for a pulsating star; 2) we can follow an "analytical" approach, applying the diagnostic methods developed in the study of static model atmospheres, of the type used by Collins and Sonnerborn (1977) (see §2.4.1) .

The first approach consists in a prediction of the whole star structure by applying the aerodynamic equations subject to boundary conditions. One of these conditions comes from the atmosphere itself, about which we have information from the observed spectrum. However, in most cases the atmosphere is not taken into account and the outer boundary condition is given by assuming that the pressure at the outer boundary is zero, which doesn't describe the *real* situation in the atmosphere.

The second approach consists in obtaining from the observations, by a diagnostic technique based on the radiation field produced by the classical models of a static atmosphere, the values of the thermodynamic parameters (T_{eff} and gravity) and of the velocity field. This approach is based on the assumption that the star atmosphere is "static" during the time of a single observation, i.e. the pulsation period must be long compared to the typical observation time.

From these two approaches another would follow: derive T_{eff} and gravity following path 2 and use these results on the atmospheric structure to establish a set of outer boundary conditions for the aerodynamic equations. Path 1 with these better constraints can be applied, and the iteration can be repeated several times.

The first approach is followed in Karp (1973, 1975). He investigated the effects of radial velocity gradients on line profiles, and other observable quantities of Cepheids, using simplified hydrodynamic model atmospheres. He included also the radiative transfer, but assumed that the source function was unperturbed by the motion, thus neglecting the possible interlocking effects of radiation at different frequencies, which result from the relative motion of different parts of the atmosphere. He did allow for the displacement of the line at each layer in the model as seen by a stationary observer. He did not consider line blanketing and non-LTE effects. Subsequently Lesh and Karp (1978) used this method for predicting line profiles in the presence of a combination of radial pulsation and stellar wind. They assumed a depth dependent velocity field of the following form:

$$v = -A \cdot \log \tau + v_p,$$

where τ is the continuum optical depth, A is an acceleration parameter, v_p is the pulsation velocity.

With particular reference to the long-period variable stars, such as the Mira variables, hydrodynamic calculations were carried out by Willson and Hill (1979) and recently by Bowen (1988 a, b), who updated the work of Willson and Hill by including the effects of radiation pressure on the dust. He did not consider the complete radiative transfer problems, but used the Eddington approximation for a gray spherical atmosphere to calculate a local equilibrium temperature.

The second approach is followed in the study of the energy distribution of β Cephei stars (see Kubiak, 1972, and Stamford and Watson, 1977), and in the studies of line profiles affected by radial and non-radial velocity fields, of which Osaki (1971) is the precursor (see the following Chapter).

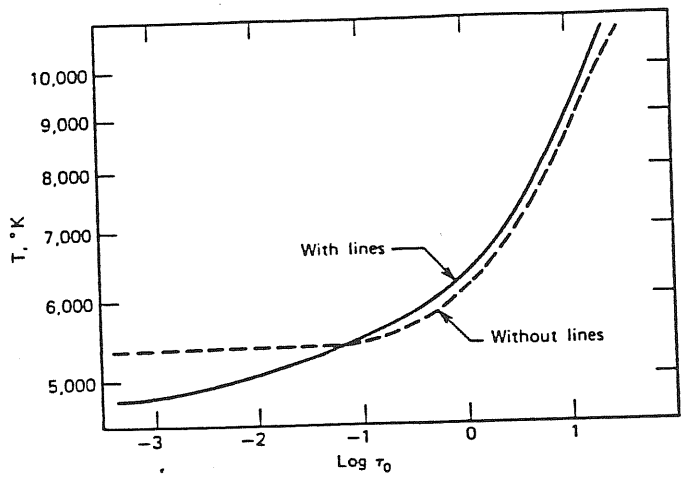

Figure 2.1– Line blanketing effect on the temperature distribution. T_{eff}=6500 K, log g=4 and solar abundance models (Figure from Gray, 1976).

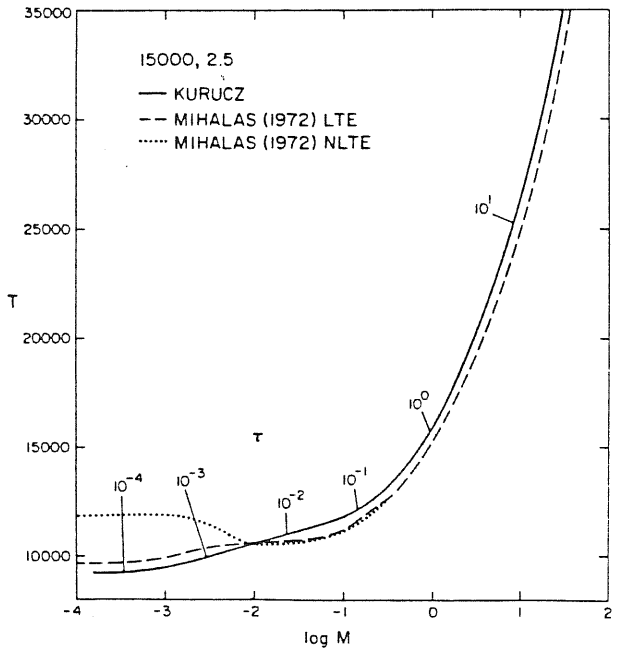

Figure 2.2– Temperature column mass of atomic nuclei in LTE and non-LTE 15000, 2.5 models by Mihalas and LTE model by Kurucz (Figure from Kurucz 1979 a).

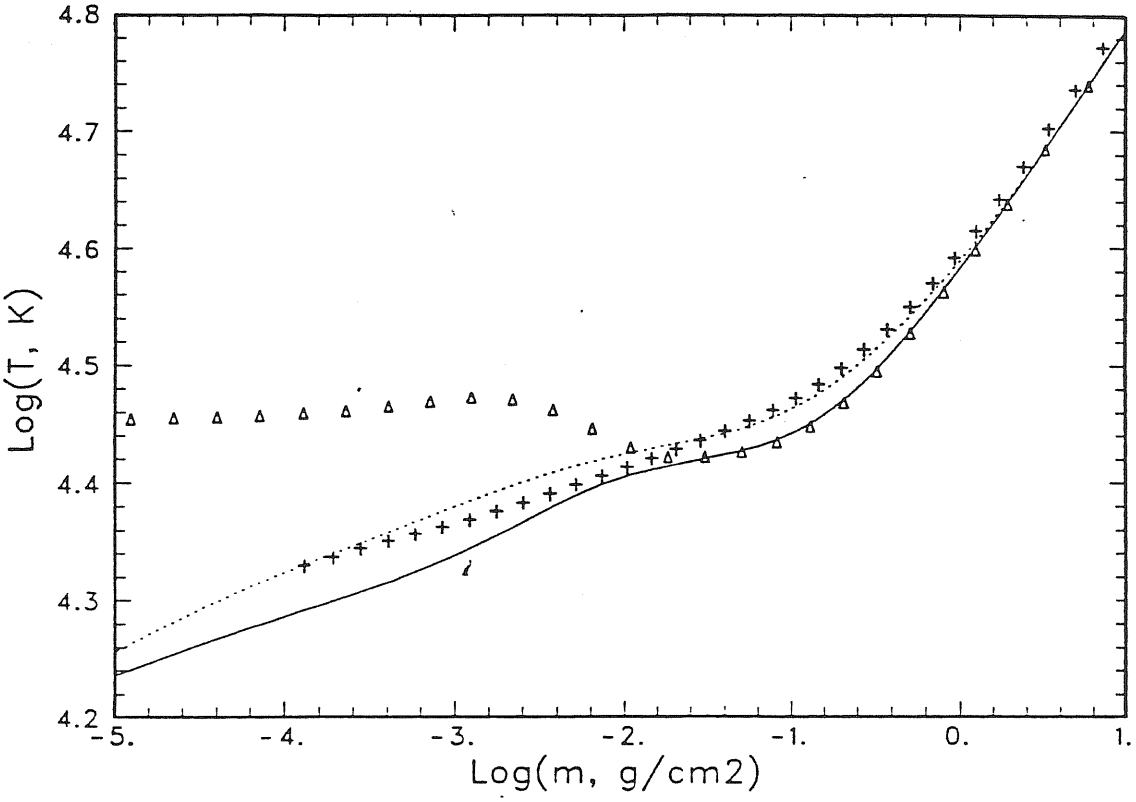

Figure 2.3– Electron temperature vs. column mass of atomic nuclei in $T_{eff} = 35000$ $\log g = 4$ models. Solid line: non-LTE blanketed model by Anderson. Dashed line: LTE blanketed model by Kurucz. Triangles: unblanketed non-LTE model by Mihalas (Figure from Anderson, 1985).

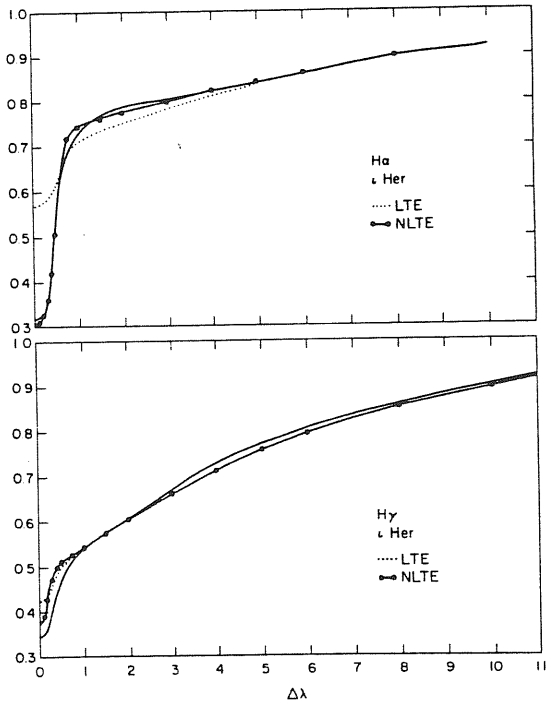

Figure 2.4– Hα and Hγ profiles observed in ιHer (solid lines) and predicted from LTE (dotted curve) and non-LTE (filled circles) models with T_{eff}=19000K and log g=4. (Figure from Mihalas, 1972 b)

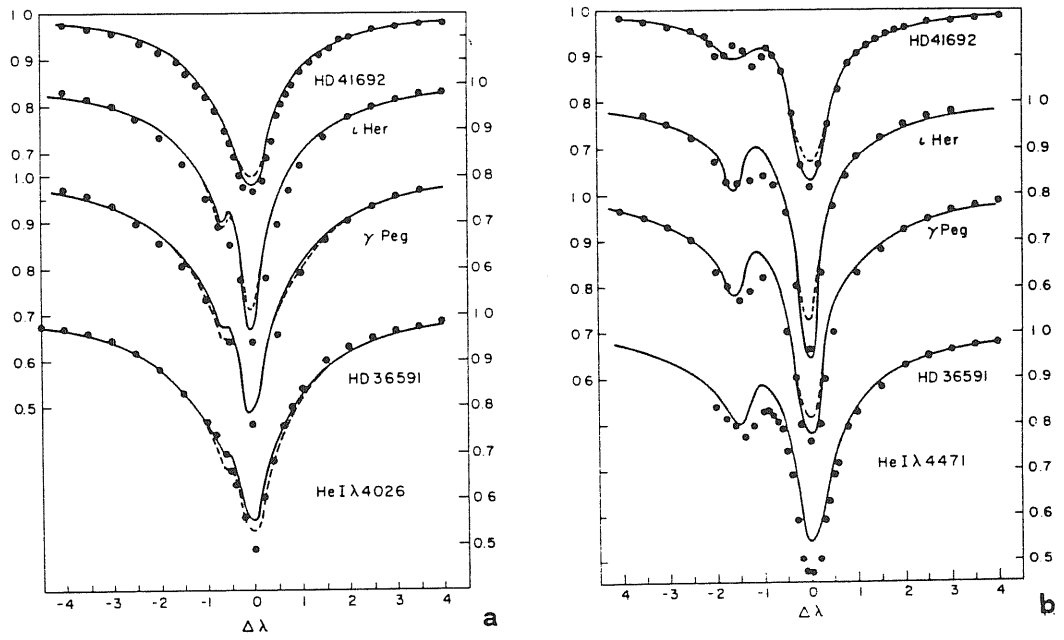

Figure 2.5– (a) Comparison of observed HeIλ-4026 profiles (•) with the theoretical non-LTE predictions (solid curve) and LTE predictions (dashed curve). (b) Same as (a) for HeIλ-4471 (Figure from Auer and Mihalas, 1973 b).

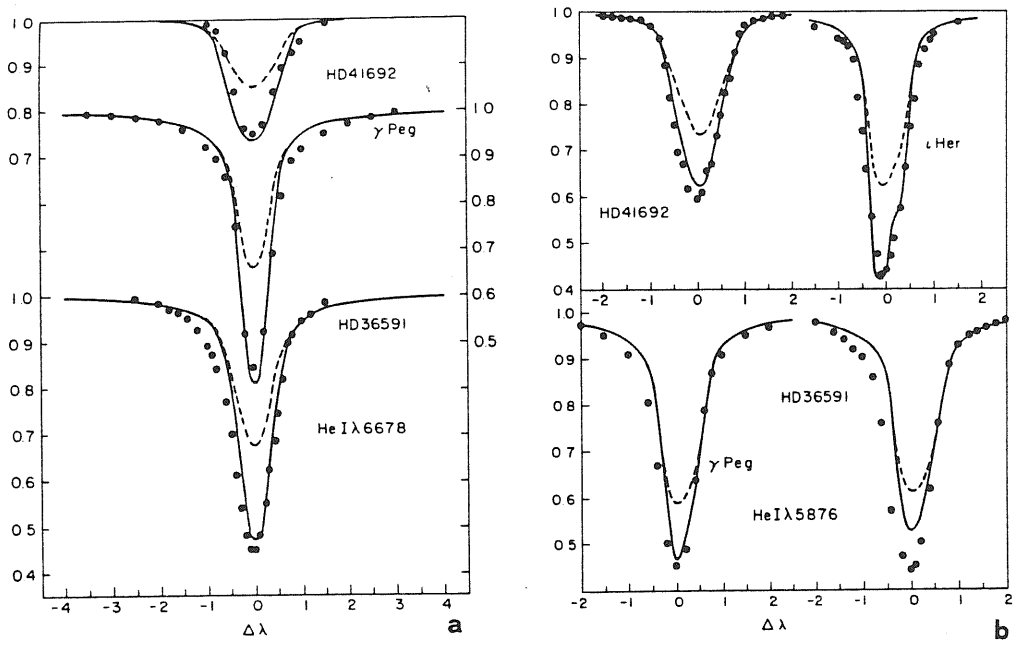

Figure 2.6– (a) Comparison of observed HeIλ-6678 profiles (•) with the theoretical non-LTE predictions (solid curve) and LTE predictions (dashed curve). (b) Same as (a) for HeIλ-5876 (Figure from Auer and Mihalas, 1973 b).

References

Abbot, D. C.: 1979, in "Mass Loss and Evolution at O Type Stars", eds. P. Conti and C. de Loore (Dordrecht: Reidel), p. 237.

Anderson., L. S.: 1985, Ap. J, 298, 848.

Andersen, P.H.: 1973, Publ. Astron. Soc. Pac., 85, 666.

Auer, L. H., and Mihalas, D.: 1969, Ap. J., 158, 641.

Auer, L. H., and Mihalas, D.: 1973 a, Ap. J., 184, 151.

Auer, L. M., and Mihalas, D.: 1973 b, Ap. J. Suppl., 25, 433.

Bowen, G. H.: 1988 a, in "Pulsation and Mass Loss in Stars", R. Stalio and L.A. Willson eds., p. 3.

Bowen, G. H.: 1988 b, Ap. J., 329, 299.

Cannon, C. J., Thomas, R. N.: 1977, Ap. J., 211, 910.

Castor, J. I., Abbot, D. C., Klein, R. I.: 1975, Ap. J., 195, 157.

Collins, G.W.,Sonneborn, G.H.: 1977, Ap. J. Suppl., 34, 41.

Day, R.W., Lambert, D.L.,and Sneden, C.: 1973, Ap. J., 185, 213.

Ebbets, D.: 1979, in "stellar Turbulence", D.F. Gray and J.L. Linsky, eds., Springer-Verlag, p. 113.

Ebbets, D.: 1979, in "Stellar Turbulence", D.F. Gray and J.L. Linsky eds., Springer-Verlag, p.113.

Faraggiana, R., Castelli, F., Morossi, C., Kondo, Y.,and van der Hucht, K., A.: 1986, Ap. J. Suppl., 61, 719.

Feautrier, P.: 1968, Ann. Astrophys.,31,257.

Gray, D. F.: 1976, "The Observation and Analysis of Stellar Photospheres", Wiley, New York.

Kamp, L.W.: 1973 Ap. J., 180, 447.

Karp, A. H.: 1973, Ap. J., 180, 895.

Karp, A. H.: 1975, Ap. J., 201, 641.

Kubiak, M.: 1972, Acta Astron., 22, 11.

Kurucz, R. L.: 1979 a, Ap. J. Suppl., 40, 1.

Kurucz, R. L.: 1979 b, Dudley Obs. Rept. No. 14, p.271.

Kurucz, R. L., Peytremann, E., and Avrett, E. H.: 1974, "Line Blanketed Model Atmospheres for Early-Type Stars", Washington, Smithsonian Inst..

Lesh, J. R., Karp, A. H.: 1977, Veroff Remeis Stenw. Bamberg, 11, 625.

Limber, D. N., and Marlborough, J. M.: 1968, Ap. J., 152, 181.

Longo, R., Stalio, R., Polidan, R. S., Rossi, L.: 1988, Ap. J., in press.

Lucy,. L. B., and Solomon, P. M.: 1970, Ap. J., 159, 879.

Massa, D., and Savage, B. D.: 1985, Ap. J.,299, 905.

Mihalas, D.: 1972a "Non-LTE Model Atmospheres for B and O Stars", NCAR-TN/STR-76.

Mihalas, D.: 1972b, Ap. J., 176, 139.

Mihalas, D.: 1972c, Ap. J., 177, 115.

Mihalas, D.: 1973, Ap. J., 179, 208

Mihalas, D., Hummer, D.G.: 1973, Ap. J., 179, 827.

Morossi, C., Malagnini, M. L.: 1985, Astron. Ap. Suppl., 60, 365.

Osaki, Y.: 1971, Publ. Astr., Soc., Japan, 23, 485.

Pecker, J. C.: 1965, Ann. Rev. Astron. Ap., 3, 135.

Rosseland, S.: 1928, M. N. R. A. S., 89,49.

Slettebak, A.: 1956, Ap. J., 124, 173.

Smith, M. A.: 1971, Astr. Ap.,11, 325.

Smith, M. A.: 1973, Ap. J., 182, 159.

Stamford, P. A., and Watson, R. D.: 1977, M. N. R. A. S., 180, 551.

Stoeckley, T. R., and Mihalas, D.: 1973,"Limb Darkening and Rotation Broadening of Neutral Helium and Ionized Magnesium Line Profiles in Early Type Stars", NCAR-TN/STR-84.

Strömgren, B.: 1944, Pub. mind, medd. Kobenhavens, Obs., No. 144.

Struve, O.,and Elvey C.T.: 1934, Ap. J., 79, 409.

Thomas, R. N.: 1973, Astron. Ap., 29, 297.

Torres, A. V.: 1988, Ap. J., in press.

Von Zeipel, H.: 1924, M. N. R. A. S., 84, 665.

Willson, L. A., and Hill, S. J. :1979, Ap. J. ,228, 854.

CHAPTER III

Radial and Non-radial Pulsation Effects on Line Profiles

§3.1 - *Introduction*

Pulsation affects the absorption lines of the star in two different ways. First, the surface motion of the star causes variations in the velocities and therefore in the profile of the lines; second, the temperature and gravity of a pulsating star change with time, and, as they change, they cause variations in the equivalent width and profile of lines.

These effects are very clearly seen in radial pulsating β Cephei stars: radial velocity curve amplitudes from 2.2 (β Cru, B0.5 III) to 80 km/sec (BW Vul, B2 III) are observed (Lesh and Aizenman, 1978); light and color variations suggest that temperature variations are associated with the pulsation. As we have already said, the magnitude variations of β Cephei stars at visual wavelengths are very small, rarely more than 0.1 mag and often only a few thousandths of magnitude (Lesh and Aizenman, 1978), but the light amplitude increases steadily with decreasing wavelength (see §1.3) Model atmosphere energy distributions fitted to ultraviolet observations indicate effective temperature variations large enough to change noticeably the equivalent width of the line profiles.

The possibility of non-radial pulsation as an alternative cause of profile variations was first suggested by Ledoux (1951), in connection with the observed variations of line widths in some β Cephei stars. The pioneering study on the shapes of line profiles affected by non-radial velocity fields was published by Osaki (1971). The approach followed by Osaki consists in the calculation of non-radial pulsating star line profiles using the radiation field produced by a static atmosphere, i.e. it does not deal with line-formation processes or model atmosphere computation in

the presence of non-radial motions. Osaki assumes that during a time sufficiently short, compared to the pulsation period, the star can be considered in a *static* state, that is the kinematic phenomenon can be assumed to be a slow passage through a series of equilibrium states. Variations in surface area and in brightness due to oscillation are neglected.

Smith (1977, 1985), Stamford and Watson (1976), Kubiak (1978) and Baade (1984) have shown that observed profile variations in the B stars can be matched by model profiles produced by non-radial velocity fields similar to those developed by Osaki (1971).

Line profiles of radial and non-radial pulsating stars are computed in the present work. The approach developed is similar to that used by Osaki (1971). In the following section (3.2) the adopted line profile modeling algorithm is described. In §3.3 rotation effects on the line profiles are presented. In §3.4 radial and non-radial pulsation effects on the line profiles are presented and discussed, and a comparison is made with published results. In §3.5 the question is raised regarding the mode identification of non-radial pulsation based on the proposed procedure. In §3.6 the *k problem*, that is the disagreement between the observed and the theoretical values of the ratio of horizontal to vertical oscillation velocities, is discussed. A comment section on the limits of the present approach, due to the assumption of a single model atmosphere (i.e. a single temperature and pressure law) for representing pulsating stars, concludes Chapter III (§3.7).

§3.2 - *The Line-Profile-Modeling Algorithm*

The procedure of line profile modeling by pulsation and rotation is as follows: we divide the stellar visible disc into many surface elements and calculate the velocity of each element due to the combined effect of rotation and oscillation. We then choose a certain stellar absorption line and calculate its intrinsic profile for a given effective temperature and surface gravity, appropriate to the star of interest,

by using the classical atmosphere computer code. The line profile is then formed by adding up the intensities from each element taking into due account the Doppler shift corresponding to the line of sight velocity and of the limb-darkening law. We neglect surface brightness and area variations due to oscillation. Thus, line profile variations are assumed to be generated solely by Doppler effects.

In order to compute line profiles broadened by radial or non-radial pulsation and rotation, we must specify the surface geometry and choose a model atmosphere. In addition, the following parameters must be specified: the pulsation mode, identified by the integers l and m, the pulsation amplitude, the phase, and the ratio of horizontal to vertical velocity amplitude, k. We must remember that k is not a free parameter, but its value is related to the frequency of oscillation and to the stellar mass and radius. We also must choose the inclination, i, of the axis of rotation relative to the line of sight, and the equatorial rotation velocity. Sometimes the effect of broadening due to macroturbulence is included.

3.2.1-*The Basic Surface Geometry*

By defining a *surface geometry* we intend to define the way of dividing the surface of the star into pieces which are easy to work with and allow for integration. Generally the visible stellar disc is divided into a rectangular grid (Vogt and Penrod, 1983 a; Smith, 1987), by drawing chords parallel and perpendicular to the star's projected rotation axis. All the surface elements that are on the same strip parallel to the star's projected rotation axis have the same rotation velocity.

The approach followed in this work is different. The surface of the star, assumed to be spherical, is divided into *zones*, similar to geographical zones of latitude (see Figure 3.1). The centre of the observed disc is taken as the *zone pole*. The zones are separated by circles at a constant distance from the *zone pole*, polar distance. Each zone is divided into *sectors* such that the area (and approximate shape) of each sector is the same over the whole sphere.

We have followed this approach because (1) in this geometry the system of sectors is oriented on the surface of the star according to the line of sight; thus the

surface elements of each zone have the same polar angle, p, that coincides with the limb-darkening angle, so that the same intrinsic profile can be computed, by the model atmosphere, in each zone (note that all the sectors for which $p < \pi/2$ are visible); and (2) this geometry permits us to include envelopes or shells surrounding the star, to simulate a non-spherical body quite well, and to simulate the effects of eclipses of one star by another (see Hutchings, 1977).

The number and the size of the sectors into which the star is divided are freely changeable. Let this number be S (this is an important input parameter to the program). The number of zones on the sphere and the polar angle of each zone depend on S. The polar angle of the first zone boundary is $\sqrt{\pi/S}$. The total number of zones over the sphere, Z, is given by

$$Z = integral\ part(\frac{1}{2} + \frac{\pi}{2 \cdot \sqrt{\pi/S}})$$

$$= integral\ part(\frac{1}{2} + \frac{1}{2}\sqrt{\pi S}). \tag{3.1}$$

The polar angle of the upper boundary of n^{th} zone is $2n\sqrt{\pi/S}$, so that the polar angle, p, of the centre is

$$p = (2n - 1) \cdot \sqrt{\frac{\pi}{S}}, \tag{3.2}$$

$\sqrt{\pi/S}$ being the angular distance between the upper boundary and the centre.

The number of sectors in a zone, SZ, depends on the surface of the zone. The area of each sector must be the same over the whole sphere. So that SZ is given by:

$$SZ = \frac{4\pi \sin p\sqrt{\pi/S}}{4\pi/S}$$

$$= \sin p \cdot \sqrt{\pi S}. \tag{3.3}$$

In each zone the sectors are placed so the last one lies on a great semicircle passing through the rotation pole and the centre of the zone pole. Thus the angle

α, in the plane of the zone centre, between the centres of the mth sector and the last sector, measured at the centre of the cross section (see Figure 3.1), is

$$\alpha = \frac{2\pi m}{SZ},$$

and substituting equation (3.3) we obtain

$$\alpha = \frac{2\pi m}{integral\ part(\sqrt{\pi S}\sin p)}. \tag{3.4}$$

None of these relations is exact, since there must be a whole number of sectors in each zone. Thus the total number of sectors on the star surface is not exactly S and the shapes of the sectors are not all the same. However, the accuracy of the quantities is improved by increasing the value of S. Table 3.1 gives an idea of the approximations made.

The number of sectors into which the star surface must be divided depends (1) on the rate of change of the physical parameters in the model, and (2) on the accuracy of the observations to be matched. For example, in the case of non-radial pulsation characterized by high l-mode ($l \geq 6$), more sectors on the star surface are needed in order to obtain reliable profiles. In addition, the number of sectors needed will depend on the equatorial rotation velocity of the star. Only by trials can we find the number of sectors needed to obtain a reliable profile. The accuracy must also be traded off against computing time.

When a rotating star undergoes non-radial oscillation, the velocity over the surface is given by

$$\vec{V} = \vec{V}_{rot} + \vec{V}_{osc} \tag{3.5}$$

where $\vec{V}_{rot}$ is the velocity of rotation and $\vec{V}_{osc}$ is that of oscillation. If the angular velocity of the star is $\vec{\Omega}$, which may be also function of the spherical polar coordinate Θ, we have the well known relation

$$\vec{V}_{rot} = \vec{\Omega} \times \vec{r} \tag{3.6}$$

The velocity field for a single non-radial pulsation mode with spherical harmonic indices l and m can be written in the spherical polar coordinates (r, Θ, Φ) as (see §1.3)

$$\vec{V}_{osc} = a(r) \cdot (1, k\frac{\partial}{\partial\Theta}, k\frac{1}{sin\Theta}\frac{\partial}{\partial\Phi})Y_l^m(\Theta,\Phi)e^{i\sigma t}, \tag{3.7}$$

where *a(r)* is the velocity amplitude in the radial (vertical) direction, k is the constant of proportionality between the horizontal and vertical motions, and the other symbols are already specified in §1.3. The value of k is related to the frequency of oscillation such that

$$k = \frac{GM/R^3}{\sigma^2} = (\frac{Q}{0.116})^2, \tag{3.8}$$

where $\frac{\sigma}{(GM/R^3)^{1/2}}$ is the dimensionless frequency of oscillation, σ is the frequency of oscillation in the corotating frame of reference of the star, which is related to that of the inertial frame (see §1.3, equation 1.3); G is the gravitational constant, M and R are the stellar mass and radius, and Q is the pulsation constant.

We need an expression for the velocity, $\vec{V}$, of a surface element in the direction of the observer. With the usual convention on the sign of the radial velocity, if V_r, V_Θ and V_Φ are the spherical components of $\vec{V}$, the velocity in the direction of the observer is given by:

$$V_{obs} = -V_r(\cos i \cdot \cos\Theta + \sin i \cdot \sin\Theta \cdot \cos\Phi) - V_\Theta(\sin i \cdot \cos\Theta \cdot \cos\Phi - \cos i \cdot \sin\Theta) -$$

$$-V_\Phi(\sin i \cdot \sin\Phi). \tag{3.9}$$

Now we must find the relations between the coordinate system of the star (r, Θ, Φ) and the coordinate system of the observer (r, p, α) which we have previously defined. From Figure 3.2, and remembering the fundamental relations among the angles of a spherical triangle, we find that:

$$cos\Theta = cosi \cdot cosp + sini \cdot sinp \cdot cos\alpha, \tag{3.10}$$

$$\sin\Theta = (1 - \cos^2\Theta)^{1/2}, \tag{3.11}$$

$$cos\Phi = \frac{cosp - cosi \cdot cos\Theta}{sini \cdot sin\Theta}, \tag{3.12}$$

and

$$sin\Phi = \frac{sin\alpha \cdot sinp}{sin\Theta}. \tag{3.13}$$

Note that we cannot use $\cos\Phi = (1 - \sin^2\Phi)^{1/2}$ because Φ covers all four quadrants, and therefore this last relation has a sign ambiguity.

With relations (3.5) to (3.13) we can obtain the velocities over all the visible disc.

3.2.2 - *The HeI Intensity Profiles*

In order to compute line profiles broadened by rotation and pulsation we must calculate the intrinsic profile appropriate to the star of interest. The intensity profile, $I_\lambda(0,\mu)$, rather then the flux profile, is needed, so that the full limb darkening of the line is taken into account. As we have already said in Chapter II, available model atmospheres are Kurucz (1979 a, b), LTE and blanketed, and the non-LTE, unblanketed models of Mihalas (1972).

We are interested in B-type stars, in which one of the most characteristic spectroscopic features, besides the H spectrum, is a well-developed spectrum of HeI. An extensive set of computations of the HeI spectrum in B stars, based on LTE and non-LTE unblanketed model atmospheres, are presented and discussed by Auer and Mihalas (1973) and Stoeckley and Mihalas (1973). In addition, we have available the Kurucz line-profile code, WIDTH8 code (Castelli, 1987), which allows us to calculate LTE profiles from Kurucz's LTE blanketed model atmosphere grid.

Intensity profile calculations, as a function of the cosine of the limb-darkening angle, for the HeI triplets λ-4026,-4471,-4713 and -5876, and for the HeI singlet λ-4387 are tabulated in Stoeckley and Mihalas (1973). The forbidden components of HeIλ-4026, -4471 and -5876 are treated as overlapping lines. The adopted helium-hydrogen number ratio is 0.1. Profiles are calculated for six effective temperatures from 15000 K to 27500 K and for log g=4.0, 3.0, and 2.5.

The model helium atom adopted in these calculations is described in Auer and Mihalas (1973) (see Figure 3.3 for the Gotrian diagram). The populations obtained by the statistical equilibrium equations are used to calculate the line profiles using the available broadening theories. For isolated helium lines, the Stark widths and shifts of Griem et al. (1962) in Voigt profiles are used. For the diffuse triplet lines with overlapping forbidden components (HeIλ-4026 and 4471), the results of Barnard et al. (1969) and Shamey (1969) are used. All the calculations are performed assuming a pure thermal Doppler broadening with no turbulence.

Auer and Mihalas (1973) (see §3.4) found that, over a wide range of effective temperatures and gravities, departures from LTE do not have much impact on the line profiles in the blue-violet region, but they do affect the lines in the visual-red region (e.g. HeI λ-5876 and -6678). Departure from LTE introduces equivalent-width changes of the order of 25 percent at λ -5876 and 60 percent at λ -6678. The line wings of these two line profiles are essentially unaffected by departure from LTE; the primary effect is confined to the cores of the lines (see Figure 3.4 for HeIλ-5876).

A comparison is made between the HeIλ-4471,-5876, -6678 flux line profiles computed by Stoeckley and Mihalas with their LTE models, and by us using the grid of Kurucz LTE line-blanketed model atmospheres, the Kurucz code ATLAS8, and the Kurucz line profile code, WIDTH8. The grid of 1200 Kurucz models and the Kurucz codes, ATLAS8 and WIDTH8, are available on the DEC VAX 11/750 computer of the Astronet node of Trieste (Castelli, 1988). We have adopted the same helium-to-hydrogen number ratio as Stoeckley and Mihalas (1973), and used the Stark widths and shifts of Griem et al. (1962) in Voigt profiles.

Figure 3.5 reports the equivalent width of HeI λ-4471 -5876 and -6678 lines at $\log g = 4$ versus T_{eff}, taken from Auer and Mihalas (1973), and obtained by us using the Kurucz LTE blanketed model atmosphere and profile codes. We note that there are differences between the equivalent widths of the lines computed by Mihalas with LTE models and by us. We ascribe these differences to the different temperature and density distributions of the two LTE models, unblanketed and blanketed respectively (see §2.2 and Figures 2.2, 2.3). They concern the core and

the wings of the line profile (see Figure 3.4 for HeIλ-5876) and increase as the effective temperature increases. For the HeIλ-4471 line profiles, the disagreement with Auer and Mihalas' calculations is very high. This is principally due to a more correct treatment of the Stark broadening (including the forbidden component at 4469) by Mihalas.

Intensity profile calculations for these lines, as a function of the limb-darkening angle, were made by modifying the WIDTH8 program. The comparison of intensity profiles, obtained at different values of the cosine of the limb-darkening angle, for the HeIλ-4471 and -5876 lines by Stoeckley and Mihalas (1973), and by us using the Kurucz LTE blanketed model atmosphere and profile codes shows (1) that the differences in the equivalent width of the intensity profiles decrease as the limb-darkening angle decreases; (2) that the ratios of the equivalent widths of the intensity profiles obtained at different values of the limb-darkening angle in the two models are about the same.

3.2.3 - *The Mg II Intensity Profiles*

Magnesium flux and intensity profile calculations of the singly ionized line MgIIλ-4481 are computed and tabulated in Stoeckley and Mihalas (1973). The two components of this line are treated as overlapping lines. The adopted magnesium to hydrogen number ratio is 3.0 10^{-5}. like the helium lines, also these profiles are calculated for six effective temperature, from 15000 K to 27500 K and for $\log g = 4.0$, 3.0 and 2.5.

A comparison is made between MgIIλ-4481 flux and intensity profiles computed by Stoeckley and Mihalas, and by us using the grid of Kurucz LTE line-blanketed model atmospheres, the Kurucz code ATLAS8, and the Kurucz line profile code, WIDTH8. The adopted broadening theory is that of Griem et al. (1962), and the adopted magnesium hydrogen number ratio is 3.0 10^{-5}, which is currently the best estimate derived from the observations.

Figure 3.6 reports the equivalent width of MgII λ-4481 at $\log g = 4$ versus T_{eff} taken form Stoeckley and Mihalas (1973), and obtained by using the Kurucz LTE

blanketed model atmosphere and profile codes. Departure from LTE introduces equivalent width changes of the order of 20 percent. The comparison of intensity profiles, obtained at different values of the cosine of the limb-darkening angle for MgIIλ-4481 line by Stoeckley and Mihalas (1973) and by us using the Kurucz LTE blanketed model atmosphere and profile codes confirms the results obtained for helium lines (§3.4.2).

§3.3 - *Rotation Effects on the Line Profiles*

Rotationally broadened lines have been computed for several values of the projected equatorial rotational velocity $V_{rot}sini$, taking into account the variation of the intensity profile from center to limb by using the line-profile-modeling algorithm presented in the previous paragraph.

The visible disc of the star is divided into 5000 sectors; solid body rotation is assumed, and departures from spherical symmetry are neglected.

If the star is rotating with an angular velocity Ω, each sector has an observed radial velocity of

$$V_{obs} = \Omega R sini \cdot sin\Theta \cdot sin\alpha \cdot sinp, \qquad 3.14$$

where R is the radius of the spherical surface and the other symbols are as specified in the previous pragraph.

The specific intensities, at each *zone* on the star surface, are obtained by a cubic spline of the specific intensity computed in Stoeckley and Mihalas (1973). A comparison is also made with the rotationally broadened flux profile calculated by the same authors (see §2.4.1).

Figure 3.7 reports the HeIλ-5876 line profile, at T_{eff}=17500 and $\log g = 4$, broadened by rotation ($V_{rot} \sin i = 50$ km/sec). The comparison with the same line profile computed by Stoeckley and Mihalas (1973) shows that there are small differences (about 1 percent) in the line core.

For rapid rotation, i.e. projected equatorial rotation velocity > 100 km/sec, the computed line profile cores are not very smooth. This is true even if we increase the number of sectors in the visible disc to 8000, at the expense of computer time. The differences with Stoeckley and Mihalas' (1973) calculations, however, do not exceed 3 percent. We can obtain smooth profiles by adopting a "correction factor", using a procedure derived from the comparison with Stoeckley and Mihalas' computations.

Also in the case of a star rotating with differential rotation, i.e. with an angular velocity that is a function of the angle Θ, we can easily calculate the line profiles by introducing in equation 3.14

$$\Omega = \Omega(\Theta).$$

The geometry defined above may be used even if, owing to rapid rotation, the star surface is not strictly spherical. By introducing surface or atmospheric parameters which are functions of the angle Θ, it is possible to simulate a non-spherical body quite well. In the presence of very rapid rotation, i.e. near the break-up velocity, the shape of a star is distorted and departures from sphericity become important, thus a more complex geometry must be used. Figure 3.8 a reports the cross-sections of rotating stars for different values of the angular velocity. We must choose a model for the distorsion with the provise that the body must have at least two (orthogonal) planes of symmetry and be representable by ellipsoids, spheroids or Roche lobes. The method may be to use the zones and the sectors as described in the previous paragraph, but to centre the pole of the zones on a fixed point on the stellar surface, rather than on the observed center of the disc, which now is no longer circular (Hutchings, 1977). We must also consider that the effective temperature changes as a function of the gravity, and hence of the angle Θ on the stellar surface (see Figure 3.9), according to the von Zeipel (1924) law. So different model atmospheres must be used at different sectors (see §2.4.1).

§3.4 - *Radial and Non-Radial Pulsation Effects on Line Profiles*

Line profiles broadened by rotation and non-radial pulsation are computed and the effects of the pulsation amplitude and mode on the line shape are investigated and compared with published results.

We consider the radial pulsation, l=0, because it is the principal pulsation mode of β Cephei stars; the non-radial pulsation l=2, because it gives the typical example of line profile variations; and the higher harmonic pulsations, $l \geq 6$, because line profile variations observed in some Be stars are explained by these modes.

Concerning the other oscillation modes, it is found that the dipole oscillations, l=1, may yield variations similar to those of the l=0 mode and that l=3 with $m \neq 0$ oscillations may yield variations similar to the l=2 modes. The standing waves m=0 deserve particular attention because they have a totally different effect on the line profile with respect to the intermediate standing wave solutions which satisfy the condition $0 < |m| < l$ (tesseral modes). For the particular case l=1, m=0, and considering an observer looking down on the pole of the pulsating star, the axisymmetric oscillation will closely mimic a radial pulsation, because nearly the entire visible hemisphere is moving toward or away from the star's center at the same time. For various values of observer-inclinations, the amplitude and asymmetries will be considerably reduced, but the qualitative effect remains the same. Also for higher l, m=0 modes the profiles resemble closely those of a radially pulsating star, and at increasing l, the variations in the profiles decrease.

In sections 3.4.2 and 3.4.3 short-period oscillations are considered, for which , of the three terms that describe the non-radial velocity field, the radial term dominates at the stellar surface. In section 3.4.4 the effects of the horizontal oscillatory velocity on the line profiles are presented.

3.4.1 - *l=0 Mode*

In this case we may write the projected radial velocity of a point on the stellar disc as follows

$$V_{rp} = A_r \cos p \cos \phi,$$

where A_r is the radial pulsation velocity, and ϕ is the pulsation phase (reϕ = 0 at velocity maximum).

Figure 3.9 shows what happens to a representative profile at velocity maximum (reϕ=0) when the projected rotational velocity, V_{rot}sin i, is held constant (= 25 km/sec) and A_r is increased. The line full-width at half maximum remains essentially constant, but the measured radial-velocity amplitude and the ratio of the left to right half width at half-maximum, in units of full width at half-maximum (degree of asymmetry), increase. In addition the depth decreases. This is because the core is moved to longer wavelengths more than the wings are, and the cancellation of the two shifts is incomplete.

The relation between the centroid-radial-velocity line and the pulsation velocity in the atmosphere is (Campos and Smith, 1980):

$$2 \cdot K = coeff(\frac{V_{rot} sini}{10})^{0.06} \cdot A,$$

where *coeff* is the "classical geometrical coefficient", which gives the correction for the center-to-limb effects. The value commonly adopted for *coeff* is 24/17=1.41. We find *coeff*=1.43 for a T_{eff}=17500 log g=4 model and for different values of the projected rotation velocity, V_{rot} sin i, (from 5 to 50 km/s). Campos and Smith (1980) find for B star models *coeff*~ 1.5. Parson (1972) finds *coeff*=1.31 for the differentially expanding atmospheres of Cepheids.

Figure 3.10 shows what happens to a representative profile, at velocity maximum (reϕ=0), when the rotational velocity is changed and the amplitude A_r is held constant. When the projected rotation velocity increases, the line broadens and the radial velocity of the line, which becomes more difficult to measure, increases only very slightly. The important change is that the line becomes more

asymmetric (Campos and Smith, 1980). For V_{rot}sin i$\sim A_r$ the degree of asymmetry goes through a maximum.

We have seen (§2.4) that the Fourier technique gives reliable estimates of both stellar rotation velocities and turbulent velocities. The Fourier analysis of line profiles can be applied also in the case of expanding and rotating atmospheres (Duval and Karp, 1978). The line shape from a stationary model atmosphere is convolved with a function representing the displacement of the line profiles at various points on the stellar disc, due to the combined effects of rotation and expansion. It will be recalled that the convolution theorem holds only when the two broadening functions to be combined are independent of one another. The finding that an increased rotation can enhance asymmetries shows that the rotation and pulsational velocity fields are correlated across the disc. Thus these fields cannot be described by convolving functions. Applications of the convolution theorem to them gives incorrect results (Smith and Gray, 1976; Stamford and Watson, 1977).

The realization that it is the combined effect of rotation and pulsation velocities that produces asymmetry will enable us to understand how radial pulsation can produce virtually no profile variations in sharp-lined stars, as in γ Peg (B2IV) (Campos and Smith, 1980), and large asymmetries in more rapid rotators, as in σ Sco (B1III)(Campos and Smith, 1980).

3.4.2 - *l=2 Mode*

There exist five distinct modes m= -2, -1, 0, $+1$, and $+2$ belonging to the quadrupole modes (l=2), and their eigenfrequencies are degenerate in the case of no rotation (see Chapter I). Modes with negative and positive m represent traveling waves in the same and opposite directions as the rotation, while the mode with m=0 represents a standing oscillation symmetrical to the axis of rotation.

The modes with m=$\pm$2 are symmetrical with respect to the equator. The velocity of the second harmonic oscillation at the surface for m= $\pm$2, is obtained

from equation 3.7 as:

$$V_r = A \cdot sin^2\Theta \cdot cos\phi,$$

$$V_\Theta = A \cdot ksin^2\Theta \cdot cos\phi,$$

and

$$V_\Phi = \mp 2A \cdot ksin\Theta \cdot sin\phi$$

where

$$\phi = \sigma t \pm 2\Phi$$

and

$$A = 3a(R)$$

For both theoretical and observational reasons the l=2, m=-2 non-radial mode is preferred (Osaki, 1971, 1974). A typical result for the line profiles is shown in Figure 3.11 for A/V_{rot}sin i=0.7, V_{rot} sin i=50 km/sec, k = 0.1 and i=$\pi/2$. The algorithm very closely reproduces the published profiles of Osaki (1971) (his Figure 1). Our profiles, like those of Osaki, are very diffuse around phase ϕ=0.75, are sharp around ϕ=0.25, and have depressed red and blue wings at ϕ=0.0 and 0.5 respectively. The line broadening develops into line doubling at ϕ=0.75. The symmetry properties of equation 3.7, for l=2 and $m\pm$ 2, mean that profiles at ϕ=0.25 (or 0.75)$\pm\delta\phi$ are mirror images if $\delta\phi \leq 0.25$.

The previous results show that traveling waves cause modulations both in line width and in asymmetry. The measured radial velocity curve for different values of the ratio A/V_{rot}sin i, and V_{rot}sin i = 50 km/sec is reported in Figure 3.12. We see (Figures 3.11 and 3.12) that our l=2 m=-2 profiles have a line broadening phase on the descending branch of the radial velocity curve.

In Figure 3.13 we report the variations in line full-width half-maximum for different values of A. We find that an increase in A accentuates the profile distortions up to A$\sim$ V_{rot}sin i, a point not reached in most variables. Consistently with the results of Osaki (1971), we find that the sharpest lines arise when A/V_{rot} sin i$\sim$ 0.7.

In order to see the *aspect* effects on the line profiles, we have calculated profiles for different values of the inclination angle, i. In accordance with Osaki, we find that the observed radial velocities, measured in units of $V_{rot} \sin i$, and the line profile distortions are almost identical for different i. Smaller deviations, than those found for large values of i, are obtained for i=30°. Figure 3.14 shows the profiles obtained at ϕ=0.25 and at ϕ=0.75 (V_{rot} = 70km/sec, $A/V_{rot} \sin i$ = 0.49, and k = 0.1) for $sini$ = 0.5 and $sini$ = 1. This can be easily understood if one considers the dependence of the oscillation amplitude and that of the rotational velocity upon the co-latitude Θ, which are $V_{l=2\, m=\pm 2} \propto sin^2\Theta$ and $V_{rot} \propto sin\Theta$, respectively.

A wave traveling in the opposite direction to the rotation , with $m = +2$, has the same characteristics as that of $m= -2$, but the sharpest lines occur around phase ϕ=0.75, on the descending branch of the radial velocity curve, and the lines become broad around phase ϕ=0.25, on the ascending branch of the radial velocity curve.

Modes with $l = 2$ and $m = \pm 1$ are anti-symmetric with respect to the equator. Ledoux (1951) neglects this mode because of its asymmetry, but there is no firm basis for neglecting it (Osaki, 1971).

For l=2 and m=$\pm$1, from equation 3.7 we obtain

$$V_r = Asin2\theta \cdot cos\phi,$$

$$V_\Theta = 2Akcos2\Theta \cdot cos\phi,$$

and

$$V_\phi = \mp 2Akcos\theta \cdot sin\phi,$$

where

$$\phi = \sigma t \pm \phi$$

and

$$A = \frac{3}{2} a(R).$$

The line profile variations for m=-1 and m=-2 have quite similar characteristics for i=45°. Figure 3.15 reports the profiles obtained at ϕ=0.25 and 0.75 for

$V_{rot} \sin i$ = 70 km/sec, i=45°, A/V_{rot} sin i = 0.70, and k =0.1. It is seen that the profiles obtained are surprisingly similar to the profiles reported in Figure 3.9 at ϕ = 0.25 and 0.75. We find, in accordance with Osaki (1971), that this mode is more sensitive to the value of the inclination angle, i, with respect to the l=2, m=−2 mode. That is, the shape of the lines and the radial velocity curves depend rather strongly on the inclination used.

Although the observed line broadenings and radial velocity curves of some β Cephei stars may be explained by the l=2 m=−1 mode with i=45°, almost equally well as by the mode m=−2, we do not find any work in which the main oscillation of a β Cephei star is identified with this non-radial oscillation mode, for two reasons: this mode is less favoured theoretically (Ledoux, 1951) in respect to the symmetrical mode m=−2, and, in addition, as we have already said, it is very sensitive to the observer's aspect.

The relationships between the line profile variations for m=−1 and m=1 modes are the same as those between m=−2 and m=+2 modes.

The velocity of the second harmonic oscillation at the surface for m=0 is given by

$$V_r = a(R)(\frac{3}{2}cos^2\Theta - \frac{1}{2})cos\sigma t,$$
$$V_\Theta = -3a(R)sin\Theta \cdot cos\Theta \cdot cos\sigma t,$$

and

$$V_\Phi = 0.$$

The l=2 m=0 waves have a totally different effect on the line profile with respect to the other non-radial waves considered. Their effects on profiles are similar to radial pulsation, but the amplitude of the radial velocity and asymmetries will be considerably reduced. That is, at a random inclination the standing wave (l=2 m=0) amplitudes needed to produce the observed radial velocity amplitudes and asymmetries will usually be considerably larger than the radial ones. For this reason, and also for the fact that one would expect $m \neq 0$ modes to be excited along with m=0, observed β Cephei line profile variations are explained by radial pulsation, even if they may be explained as well by the m=0 mode (Campos and Smith, 1980).

3.4.3 - $l \geq 4$ *Modes*

It was originally thought that nonradial modes with high l could not be observed in stars because of the cancellation effects of high l modes over the visible disc. It was also thought that line-profile variations would not be observed in rapid rotators because of diffuse appearance their of absorption lines. However, it has turned out (Vogt and Penrod 1983 b) that rapid rotation helps to enhance the visibility of the high l non-radial mode because it tends to resolve the stellar disc into different parts within the absorption line profiles through the rotational Doppler shift. This phenomenon is called *Doppler imaging.* Rotationally broadened spectral lines are one-dimensional velocity maps of the stellar discs. Thus, observational manifestation of low l non-radial modes in 53 Per stars and high l modes in Be stars may simply reflect the different visibility of different modes depending on stellar rotational velocities, and it could be that these two sub-classes of stars have similar oscillations.

The value of l determines the degree of oscillation toward the stellar equator, while the value of m describes the number of wave crests along the equator. $l - |m|$ is equal to the number of mode lines with constant stellar latitude. The rotational Doppler effect does not provide information on any structure perpendicular to the equator. For high $l - |m|$ values, the effects on the observed profiles of adjacent bands (defined by the node lines of constant to stellar latitudes) tend to cancel each other out because they are one-half cycle out of phase. For lower $l - |m|$ values the effect of the high non-radial pulsation mode on the line profiles is the appearance of bumps that move on the profile. The number of traveling bumps on the profile (times two, to account for the invisible hemisphere) coincides with the spherical harmonic index m. For the $l = m$ modes the appearance of the distortions on the profile is greatest.

Figure 3.16 illustrates how bumps are formed in the line profiles for the l=8 and m=-8 mode with an amplitude of 20 km/sec, a k value of 0.1, and an inclination of 70°. The arrows represent the direction in which a local absorption line is shifted by the addition of nonradial pulsation.

Keeping the pulsation mode, l and m, fixed we find that a pronounced bump occurs when a blueshifted lobe on the left and a redshifted lobe on the right combine to produce a little absorption at the wavelength corresponding to a position half way between them. We find, in accordance with Vogt and Penrod (1983 a), a maximum in the visibility of these bumps in a rapidly rotating star for l $A/V_{rot} \sin i$ of about 1.

Line profiles obtained by fixing the amplitude and the pulsation mode, but at different values of the inclination angle i, show that the higher pulsation mode are not particularly sensitive to the values of the angle i.

3.4.4 - *Horizontal Motion Effects on the Line Profiles*

The line profile variations, presented in the previous section, arise almost entirely from vertical velocities. The value that has been assumed for the ratio of the horizontal to vertical velocity amplitudes, k, is 0.1 and we find negligible differences between profiles obtained assuming k values less than 1 and profiles obtained assuming k =0.

Transverse oscillatory velocity fields produce no Doppler effects near the disc center, being perpendicular to the line of sight. However, at the stellar limbs their effects coincide fully with those of rotation, producing strong line profile wings.

In Figure 3.17 are reported l=2, m=-2 line profiles obtained assumung k = 2, $V_{rot}sini$ = 50 km/sec, $A/V_{rot}sini$= 0.7, and $sini$ = 1, for different values of the phase. We must note that the profile asymmetry goes through a reversal, with respect to the case of low values of k (see Figure 3.11 for comparison, ϕ=0. and 0.5), but the centroid-radial velocity line does not change. At the symmetric phases, ϕ=0.25 and 0.75, the profiles have a "boxy" and "triangular" shape respectively, but exhibit little variation in half-width.

For high l modes we find that on increasing the values of k, the traveling bumps in the profile became less visible.

§3.5 - *The Choice of Free Parameters*

This section discusses how periods and the other free parameters must be chosen in order to model observed line profiles by the non-radial pulsation line-broadening algorithm.

The following parameters must be specified: the pulsation period, the pulsation mode, by l and m, the pulsation amplitude, the ratio of horizontal to vertical velocity amplitude, k, the inclination of the axis of rotation relative to the line of sight, the equatorial rotation velocity, and the macroturbolence velocity.

Often the length of periods of non-radial pulsating stars is such that is impossible to follow the star through a full cycle during a night. The procedure is to observe the star over a few hours during one night to calculate a rough period from the observed differences in phase predicted by a travelling-wave solution, and to require that the period satisfy the line profile modeling for successive nights of observation.

The other free parameters needed for the profile modeling fall into three general groups: static atmosphere parameters, non-radial mode designation, and pulsational velocities. Among the static atmosphere parameters, projected rotational velocity figures prominently, because the line profile variations result from the vectorial addition of the rotational and pulsational velocities. In addition, also the inclination of the rotation axis relative to the visual must be specified, because, as we have already said, the effects of non-radial pulsations on line profiles depend also on this. The average macroturbolence has to be determined, and sometimes for each run, since there is some evidence for variability of this parameter (Smith and Mc Call, 1978).

The most difficult free parameters to choose are the two non-radial mode numbers, l and m, which specify the surface distribution of velocities across the disc. Generally we first choose the value for the spherical harmonic index, m, which also gives also an upper limit to the value of l. If the line profile variations resemble those resulting from radial pulsation (section 3.4.1) we can be in the presence of

radial pulsation (l=0, m=0) or of standing non-radial oscillation (m=0). If traveling bumps are present in the profile, we are in the presence of traveling waves ($m\neq0$). In intermediate and rapid rotators the number of traveling bumps on the profile can give an indication of the value assumed by m (see section 3.4.3), and the "direction" of their motion across the profile gives an indication of the sign of m. The blue-to-red movement of a bump across the line profile sets the requirement that the modes be prograde, $m<0$. Line profile doublings can be explained by $|m|=2$ modes, and the asymmetry changes at the profile give an indication of the sign of m. β Cephei, 53 Persei and δ Scu observations show that when more than one mode is present the m's are of the same sign.

In order to specify the spherical harmonic order l, we must consider that, theoretically, there is evidence that the mode $|m| = l$ is preferred (Busse, 1970, Osaki, 1974). β Cephei and 53 Persei observations show that only $|m| = l$ modes produce profile variations large enough to match the observed one, and the choices l=2 and 3 work best (Smith and McCall, 1978). The periodic line profile variations observed in Be stars show that at least one high degree mode is present. In addition to a high degree mode sometimes an l=2 mode is observed in the mild Be stars for which non-radial pulsations are observed, with one exception, ςOph (Smith, 1986).

The third group of parameters that must be specified are the pulsational velocities: the radial (vertical) pulsation velocity amplitude, $a(R)$, and the ratio of the horizontal to vertical velocity amplitude, k.

The signatures of large values of k are strong wings in the line profiles. In addition, as we have seen (section 3.4.4), for l=2 pulsation modes, when $k \geq 1$ the line profiles at the symmetry phases (ϕ = 0.25 and 0.75) exhibit little variation in half-width. For high-degree modes, only with a low value of k we can model traveling bumps across the profile. It is known that the k-value is not a free parameter, but is theoretically related to the oscillation frequencies by equation (3.8). Often the values of k imposed from the observed line-profile modeling do not agree with the observed frequencies of oscillations, this the so-called *k problem* that will be analyzed in the following paragraph.

The value of $a(R)$ is influenced by the inclination of the rotational axis of

the star with respect to the observer. As we have already said, all line profile variations tend to increase with the inclination angle, i. Large profile change can suggest a large inclination angle or else large $a(R)$. We are not able to plan rigid constraints on the inclination and on radial pulsation amplitude. The problem of the non-uniqueness of the velocity field inferred form a single star may also be partly overcome by postuling that, statistically, the solutions obtained should not depend on inclination.

Osaki (1985) has given an example how a spheroidal and a toroidal mode can lead to indistingushable line profile variations in a rapidly rotating star. He considered sectorial Rossby mode with $m=-l$. The components of the pulsation velocity of the Rossby mode are described by

$$V_{Rossby} = B(0, \frac{1}{sin\Theta}\frac{\partial}{\partial\Phi}, -\frac{\partial}{\partial\Theta})P_l^m(cos\Theta)e^{i(\sigma t+m\Phi)}$$

where B stands for the velocity amplitude of the Rossby waves, and the angular frequency of oscillation, σ, is given by

$$\sigma = m\Omega(-1+\frac{2}{l(l+1)}).$$

These velocity fields have no vertical component. The theoretical basis of this idea is that spheroidal and toroidal eigenfunctions became mixed in rapidly rotating stars (Veugelen, 1983). Buoyancy and Coriolis forces coalesce and the result is a new family of non-radial modes which can be considered either as g-modes modified by rotation or as modified Rossby-modes. He shows that for l=8 sectorial toroidal mode-component produces, at i=30°, similar-looking profiles to the ones caused by k ~0, l=8 spheroidal modes at i=90°. As noted by Smith (1986), it is still too early to utilize this criterion in practice. The integrated line-of-sight velocity component of the spheroidally pulsating star considered by Osaki is maximized because it is viewed equator-on. By contrast, at an inclination of 30° the toroidal, purely horizontal velocity fields are small (not only their line-of sight component).

3.6 - *The k Problem*

In order to reproduce the observed line profile variations in 53 Persei, in some βCephei stars and in Be stars a very small k-value has to be chosen (i.e. $k \leq 1$) (see Smith and McCall, 1978; Smith, 1978a,b, 1980, 1982; Vogt and Penrod, 1983 a). From the theory we know that the k-value is not a free parameter, but it is theoretically related to the oscillation frequency by equation (3.8). Since the observed frequencies of oscillations are rather low, particularly in the corotating frame of the star, the k-value must be large (i.e., $k > 1$) for most cases, and we find negligible differences between profiles obtained assuming $k < 1$ and profiles obtained assuming k=0. For periods which occur in 53 Per, o Vel, and Spica, equation 3.8 predicts values of k from 10 to 50 (Smith, 1982). It contradicts the requirement imposed from the line-profile modeling, and this is the so-called *k-problem.*

The k-problem does not concern only pulsating early-type stars. In the ZZ Ceti stars, equation (3.8) leads to $k \sim 500$, but the observational evidence (Kepler, 1984) permits one to say only that $k \geq 1$.

Two suggestions have been made in order to resolve the k-problem in early-type stars. The first, advanced by Osaki (1985), is that spheroidal and toroidal eigenfunctions become mixed in rapidly rotating stars. This suggestion could solve the k-problem for rapidly rotating stars because the toroidal mode-component produces similar looking profiles to the ones caused by $k \sim 0$ (see §3.5). However, this is true only at a given inclination angle. The k-problem remains open for slow rotators, as the toroidal terms are very small for them. In addition, toroidal mode-motions are responsible for the gas moving in a horizontal, vortical path. A consequence of this is that no pressure or temperature variations result, at least to the first order in V^2 (Robinson et al., 1982). To the same approximation the star maintains its spherical shape and does not exhibit variations in light caused either by temperature or by geometrical effects. However, variations in light are clearly observed in many non-radial pulsating OB stars (See Chapter I). A similar argument has been used by Robinson et al. (1982) and by Kepler (1984) to show that most ZZ Ceti stars

exhibit spheroidal and not toroidal modes. Nonetheless, as pointed out by Smith (1986), the modes could have a substantial toroidal component.

Another suggestion for solving the k-problem has been made by Smith (1986). Lee and Saio (1986) indicated that in order to describe the surface behavior at a non-radial mode, one must include additional terms, such as Y_m^{l+2}, Y_m^{l+4}, etc. to the leading term Y_m^l. The profiles computed by Smith with the first additional term added resemble profiles computed with $k < 1$ sectorial modes.

Both of these suggestions can be tested further by theory and observations.

§3.7 - *Final Comments*

In all the calculations presented we neglect surface temperature variations due to oscillation; that is, line profile variations are assumed to be generated solely by Doppler effects of the motions.

Model atmosphere energy distributions fitted to ultraviolet observations indicate effective temperature variations of around 4000 K for BW Vulpeculae, the β Cephei star with largest known amplitude in brightness and velocity (Furenlid et al., 1987). In ν Eri, a β Cephei star of less amplitude temperature variations of the order of 2500 K are suggested (this thesis Chapter VI), i.e. large enough to change the equivalent width of the line profiles noticeably.

Variations in the strengths of temperature-sensitive lines and in colours suggest that temperature variations, from $\pm$500 to $\pm$1000 k, are associated with non-radial pulsation in 53 Persei stars (Waelkens and Rufener, 1985; Smith et al, 1984; Chappelier et al., 1986). There are also suggestions of temperature variations in Be stars linked to the presence of l=2 modes (Smith, 1986).

If temperature variations produce changes in the line shapes, their effects are different from those due to velocity changes. Temperature does not combine vectorially with the local rotational velocity, so that the temperature variations are less sensitive to varying geometrical factors across the disc (Smith, 1986). Temperature

effects are greatest on line profiles for an l=2 mode because the cancellation effects, which are important for high modes, are minimal in this case.

TABLE 3.1

Numerical accuracy of the integration.

S	No. of Zones	No. of Sectors	Sector Areas	
			Pole	Equator
20	4	19	0.6	0.7
50	6	47	0.25	0.26
100	9	96	0.125	0.133
1000	28	986	0.0127	0.0128
5000	63	4973	0.00251	0.00251

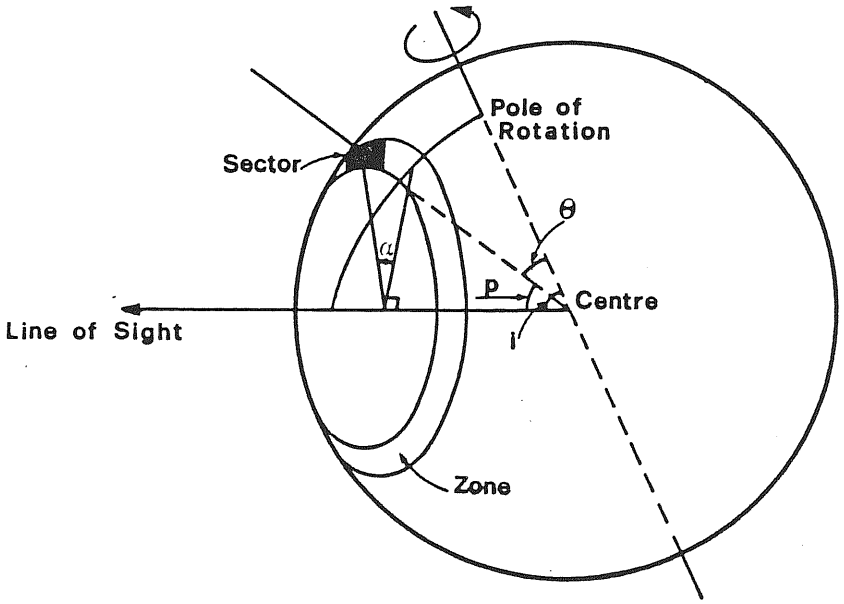

Figure 3.1 – Basic geometric definitions.

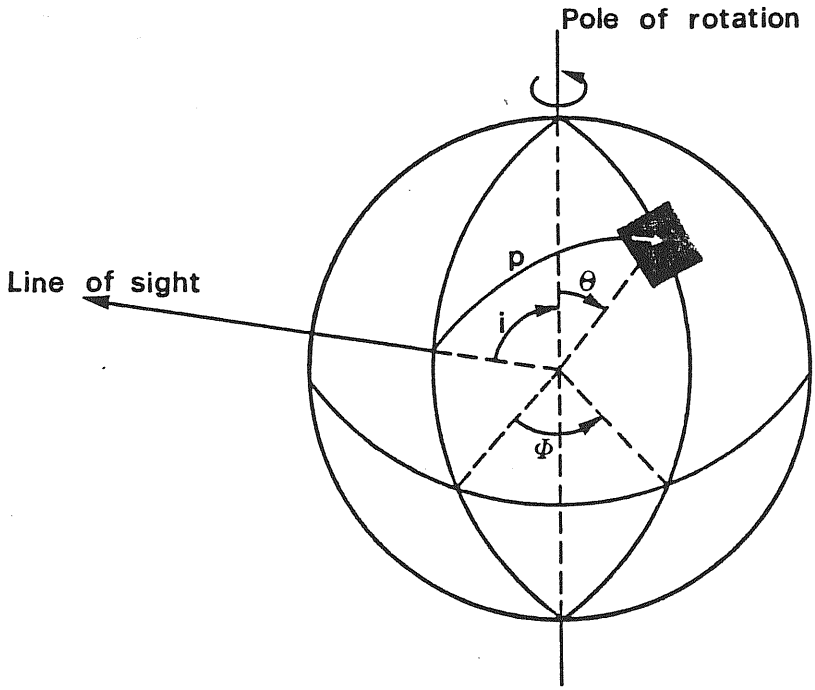

Figure 3.2 – The coordinate system of the star and the coordinate system of the observer.

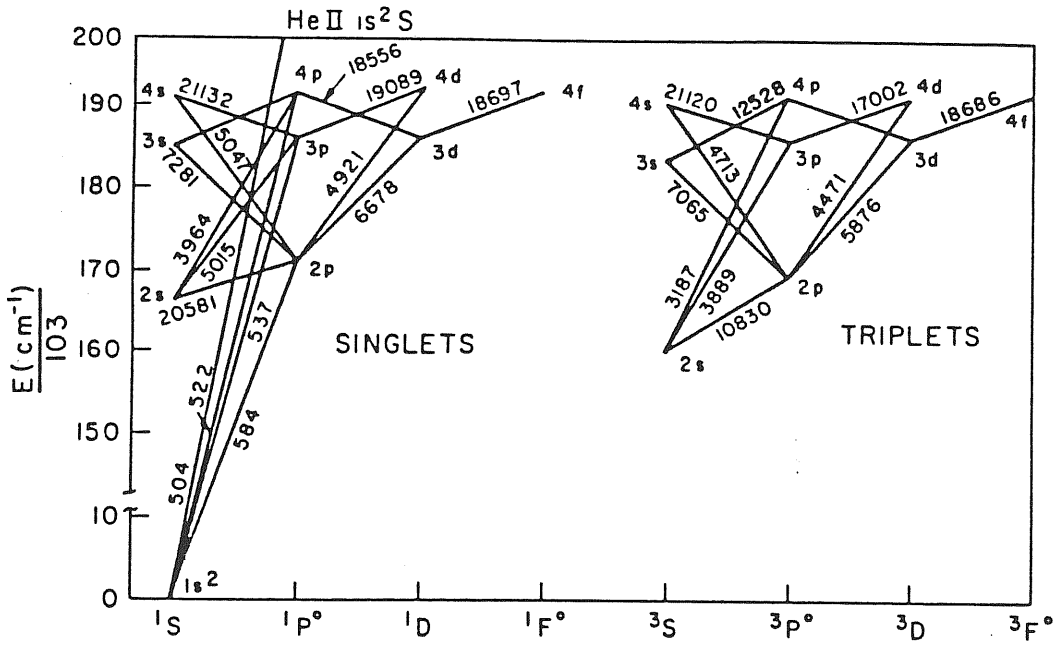

Figure 3.3 – Model helium atoms (Figure from Auer and Mihalas, 1973).

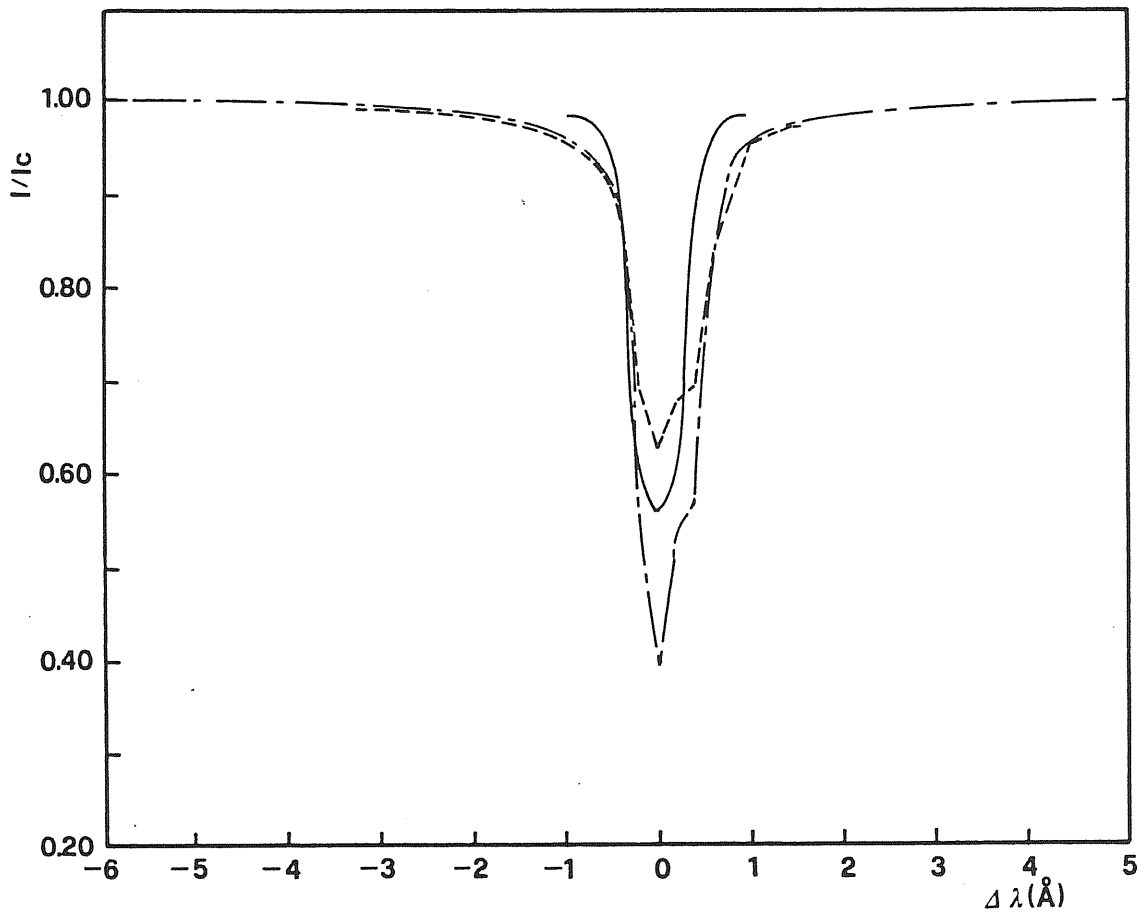

Figure 3.4 – Comparison of HeIλ-5876, T_{eff}=17500 log g=4 theoretical predictions: non-LTE prediction (long-dashed line), Mihalas LTE predictions (dashed line), Kurucz LTE predictions (continuum line).

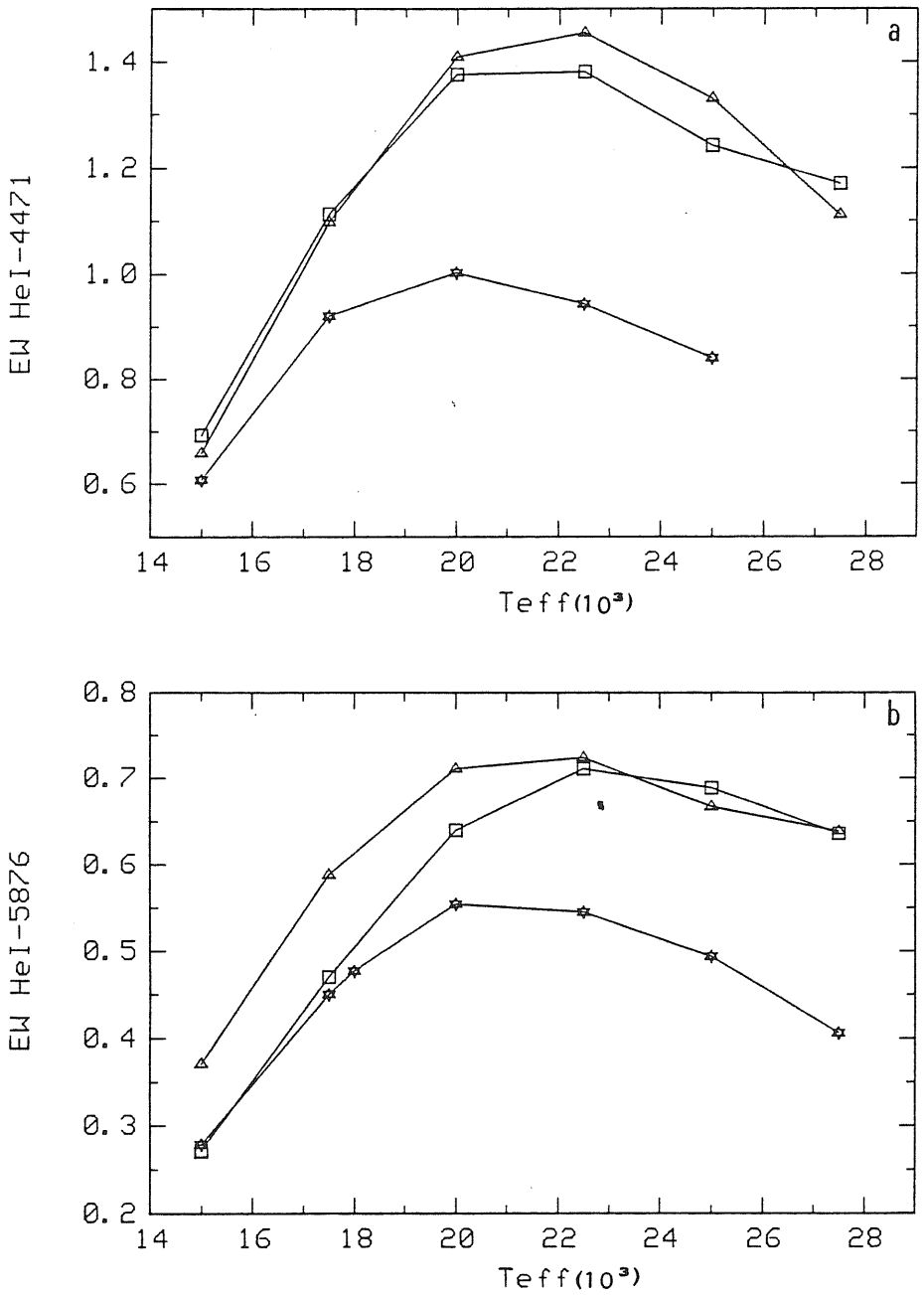

Figure 3.5 – (a) Equivalent width of HeIλ-4471 at log g=4, △ Mihalas non-LTE predictions, □ Mihalas LTE predictions, ⋆ Kurucz LTE predictions. (b) Same as (a) for HeIλ-5876.

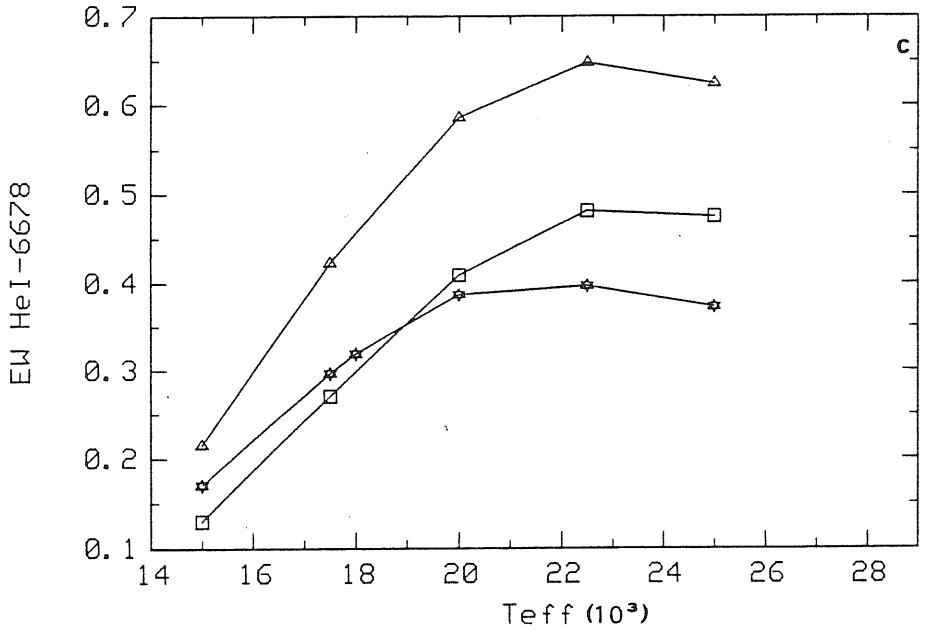

Figure 3.5 (c) – Same as 3.5 (a) for HeIλ-6678.

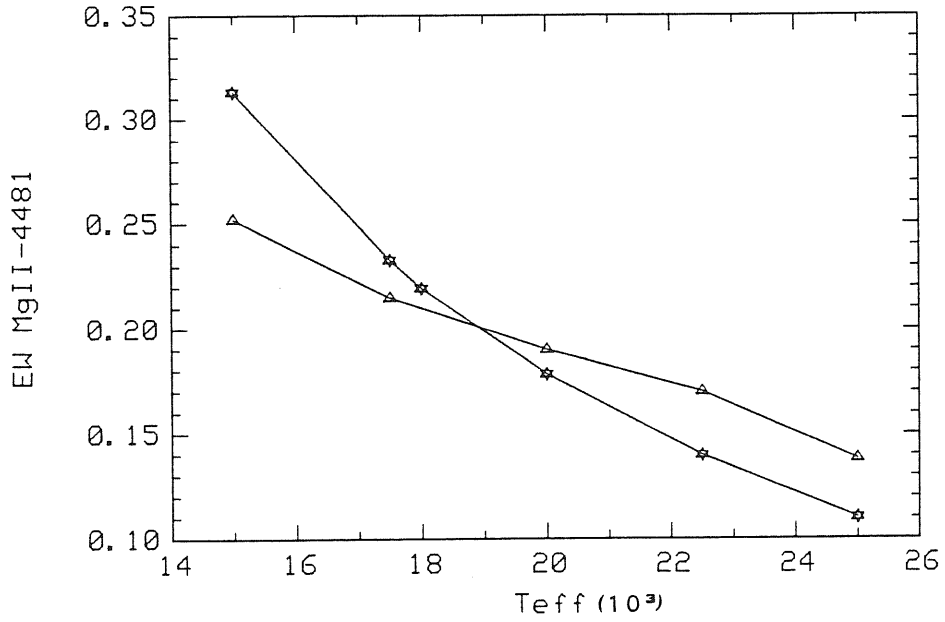

Figure 3.6 – Same as Figure 3.5 for MgIIλ-4481.

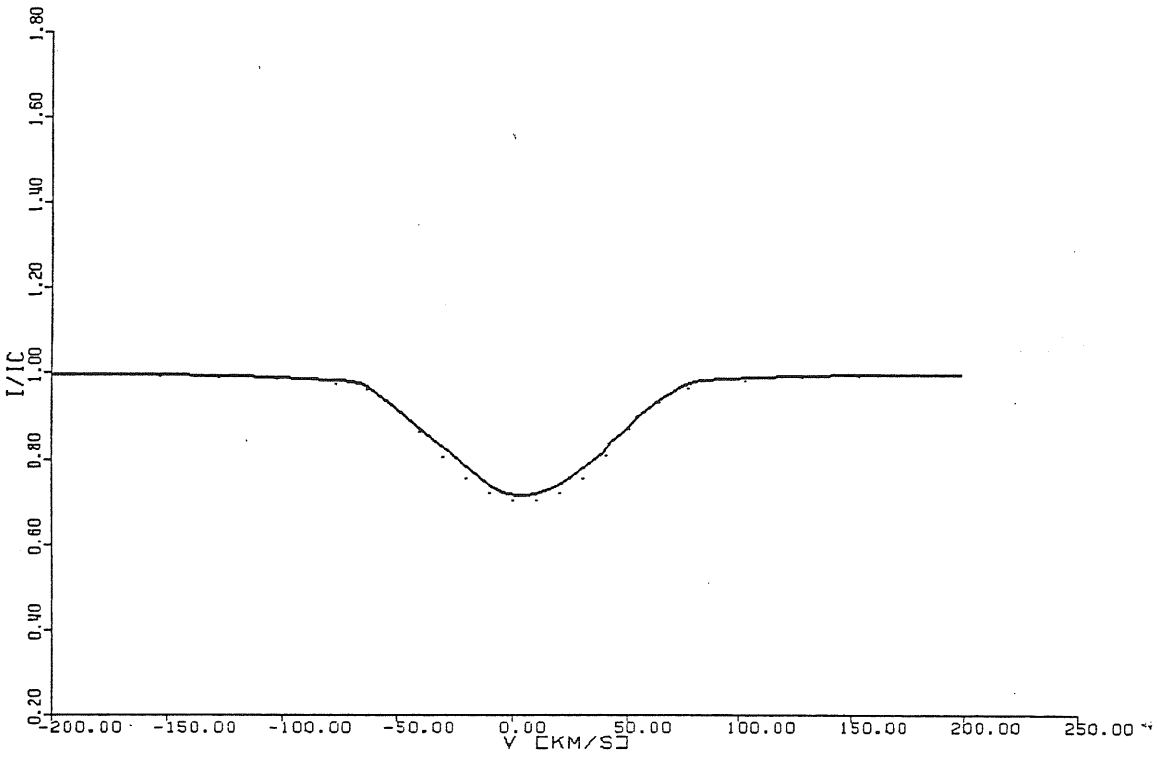

Figure 3.7 – HeIλ-5876 (T_{eff}=17500 and log g=4) rotationally broadened (V_{rot} sin i=50 km/sec) profiles: solid line, proposed modeling algorithm predictions, dotted line, Stoeckley and Mihalas (1973) predictions.

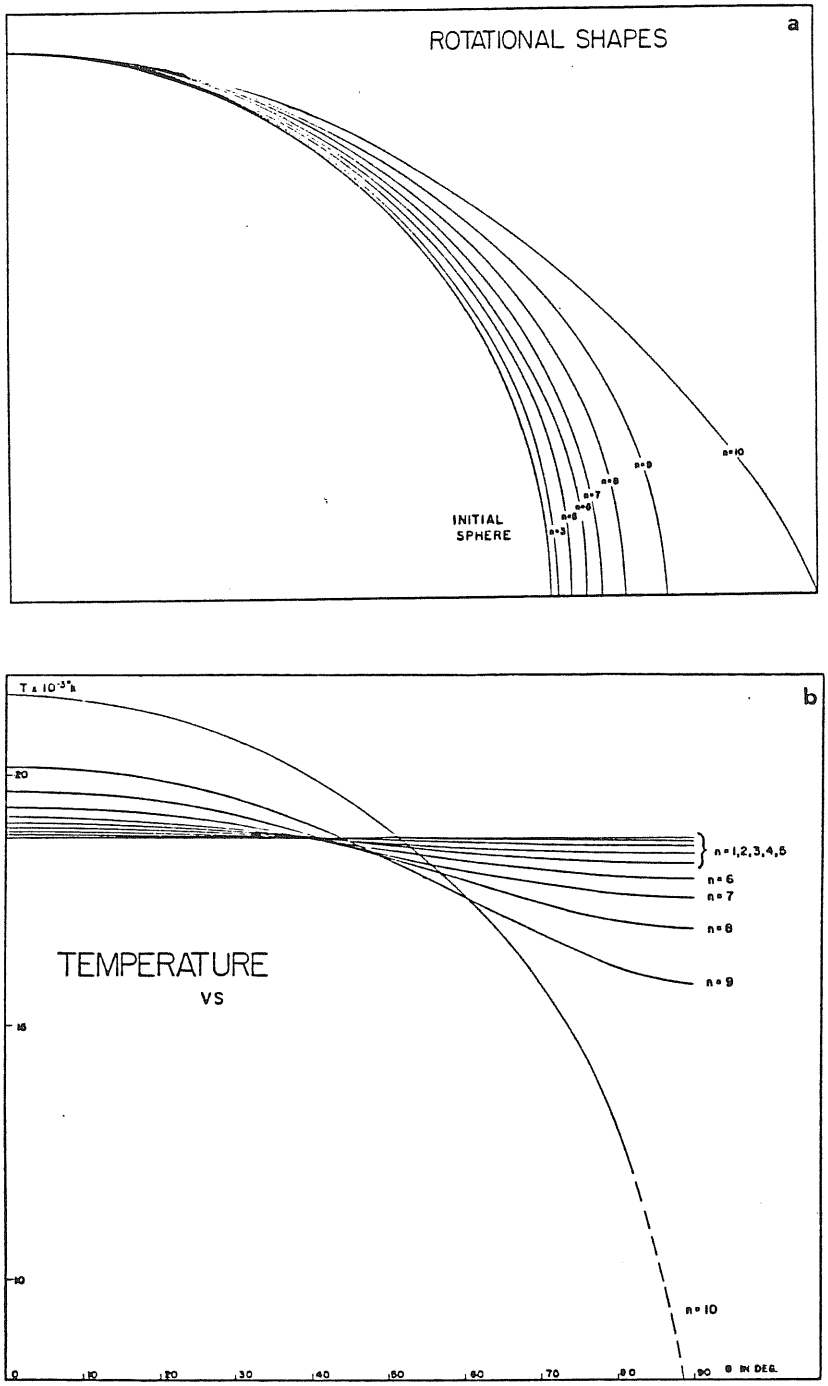

Figure 3.8 (a) – Cross section of rotating stars, $\Omega = n0.1\Omega_c$ (where Ω_c is the breakup angular velocity) for different values of n (Figure from Collins, 1963). (b) – Variation of T_{eff} versus Θ for rotating star $\Omega = n0.1\Omega_c$. Non-rotating star model with radius of 4 R$\odot$,mass of 8 M$\odot$, and T_{eff}= 18621 K (Figure from Collins, 1963).

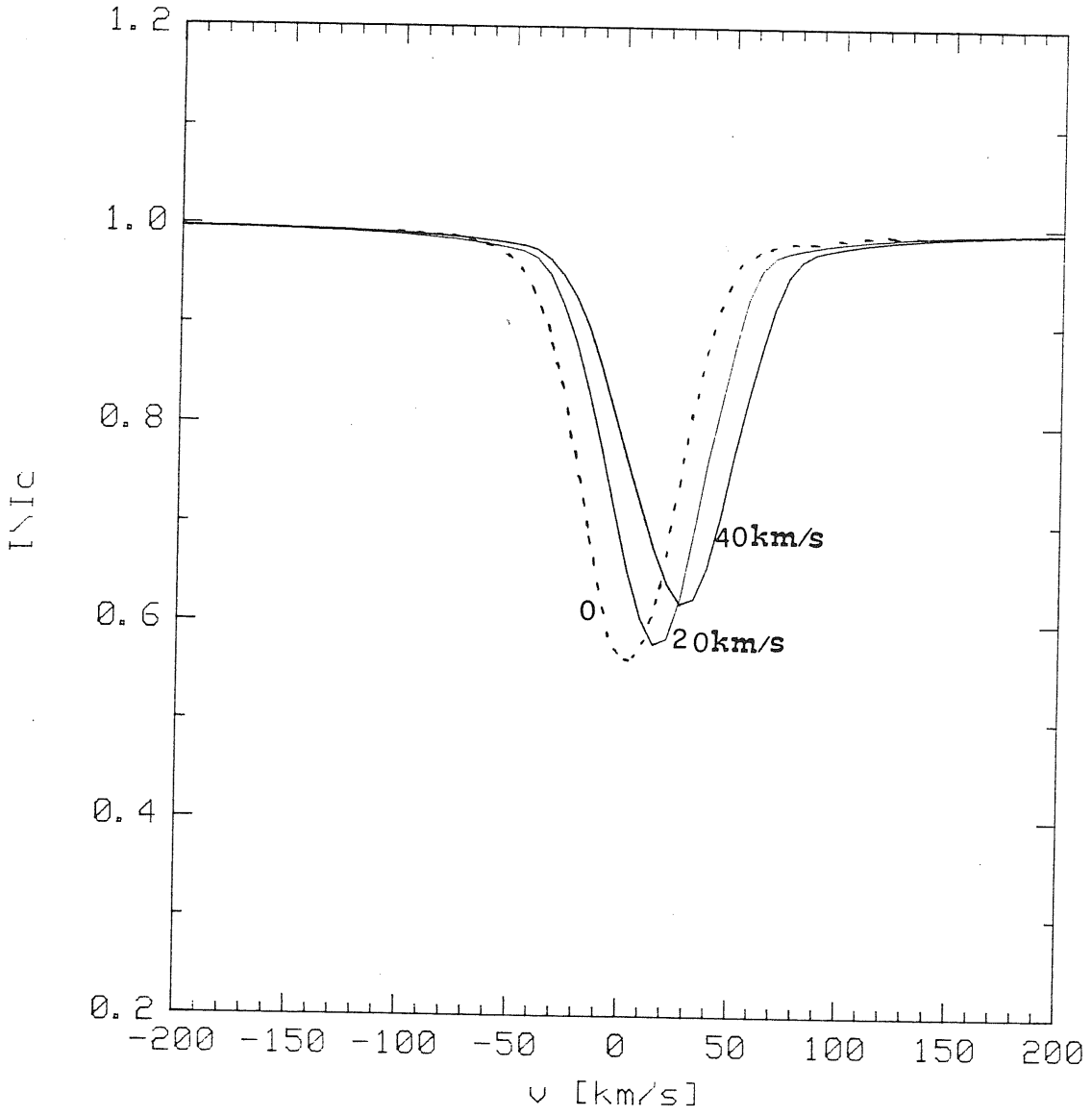

Figure 3.9– The effects on HeI-λ5876 (T_{eff}=17500 log g=4) of keeping the rotational velocity constant (V_{rot} sin i=25 km/sec) and increasing the pulsation amplitude (A=0, 20, 40 km/sec).

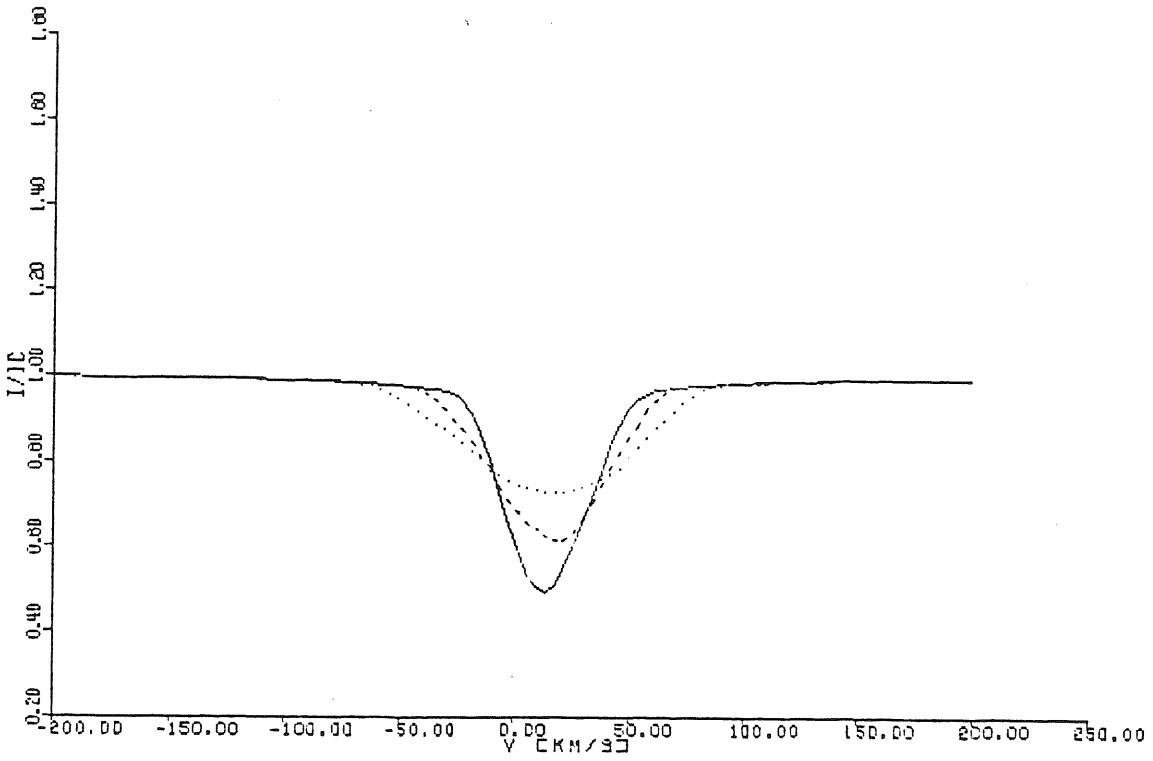

Figure 3.10 – The effects on HeI-λ 5876 (T_{eff} = 17500 log g=4) of keeping the pulsation amplitude constant and increasing the projected rotation velocity: V_{rot} sin i=10 km/sec (solid line), V_{rot} sin i=30 km/sec (dashed line), V_{rot} sin i=50 km/sec (dotted line).

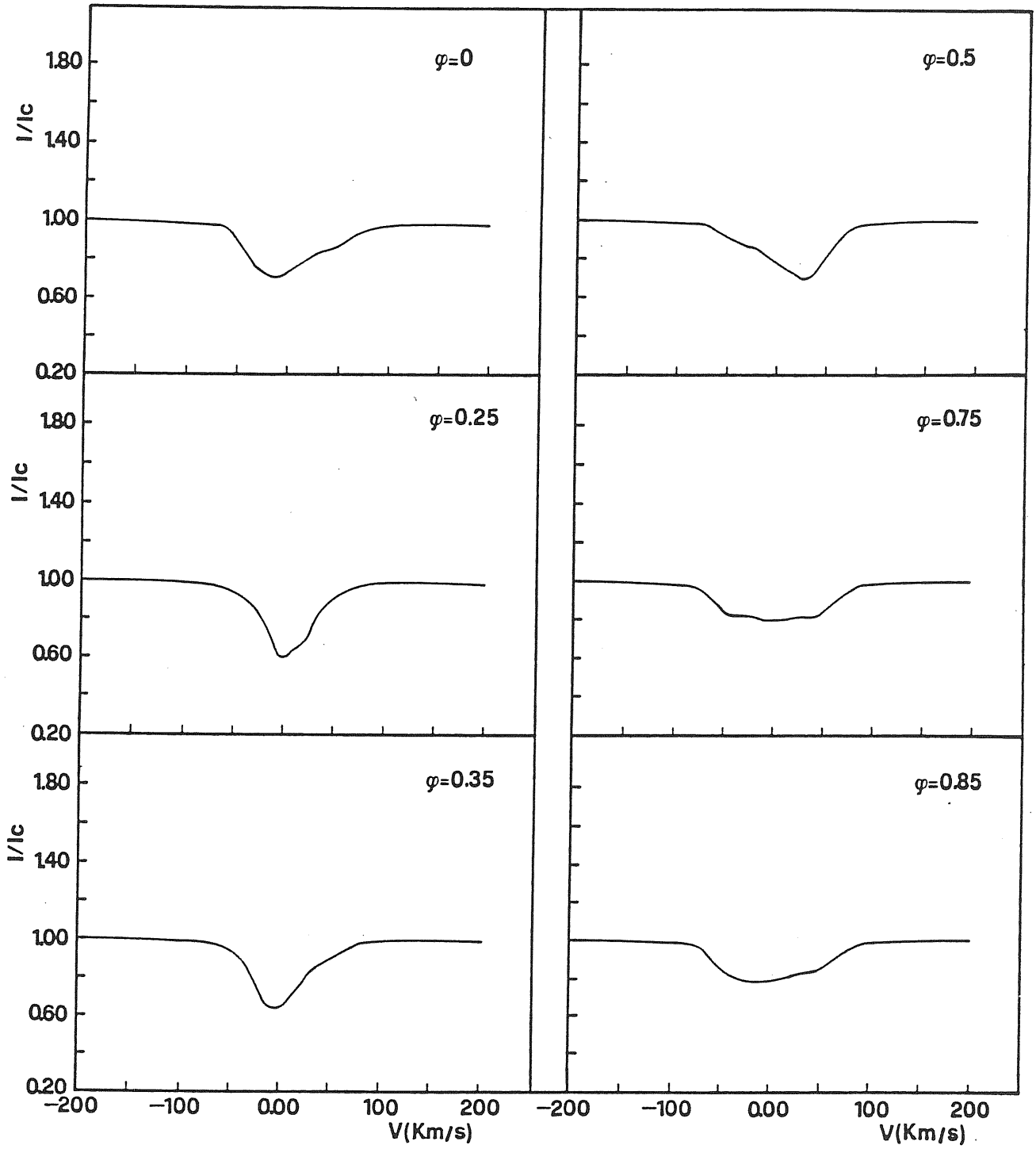

Figure 3.11 – Variation in the HeIλ-5876 line profile with phase for $l = 2$, $m = -2$, $A/V_{rot} \sin i = 0.7$, $V_{rot} \sin i = 50$km/sec, and $i = 90°$.

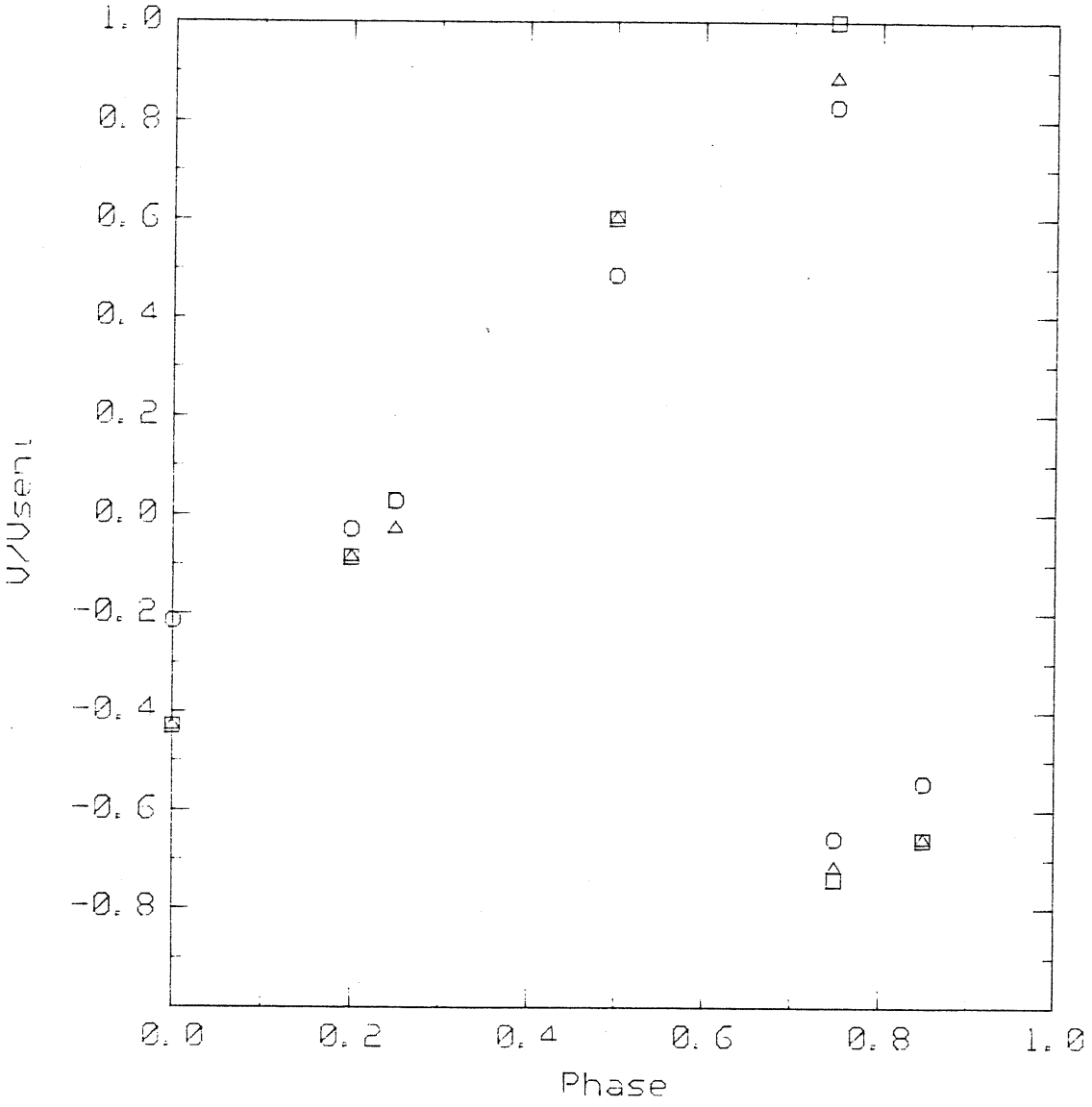

Figure 3.12 – Radial velocity curve for different values of the pulsation amplitude, ○ A=30 km/sec, □ A=60 km/sec, △ A=49 km/sec. $A/V_{rot}\sin i$. For the other parameters the same values as in Figure 3.11 are assumed.

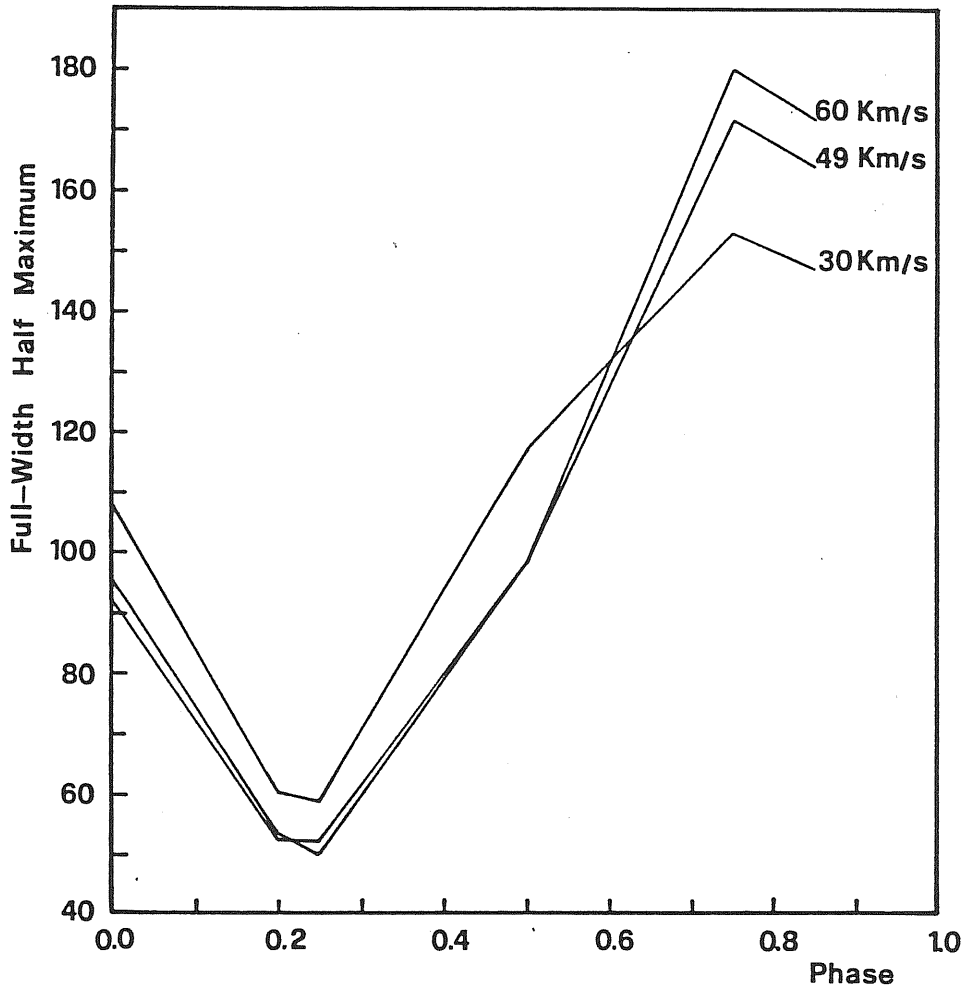

Figure 3.13– Variation in the line full width at half maximum for different values of the ratio A/V_{rot} sin i. For the other parameters the same values as in Figure 3.11 are assumed.

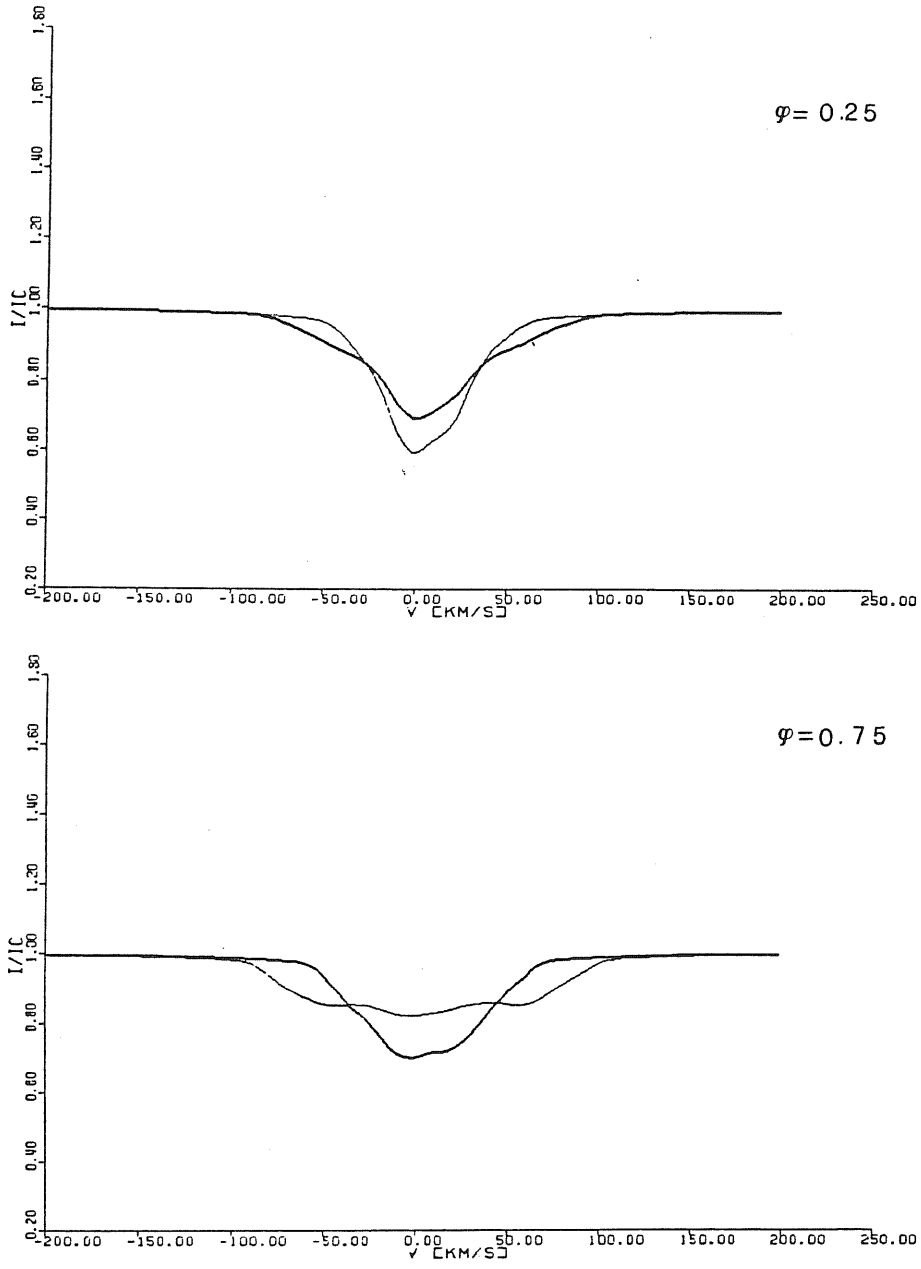

Figure 3.14 – HeIλ-5876 line profiles at ϕ=0.25 and 0.75, l=2 m=-2 mode, A/V_{rot} sin i=0.49, and k=0.1 for sin i =0.5 (thin line), and sin i = 1 (thick line).

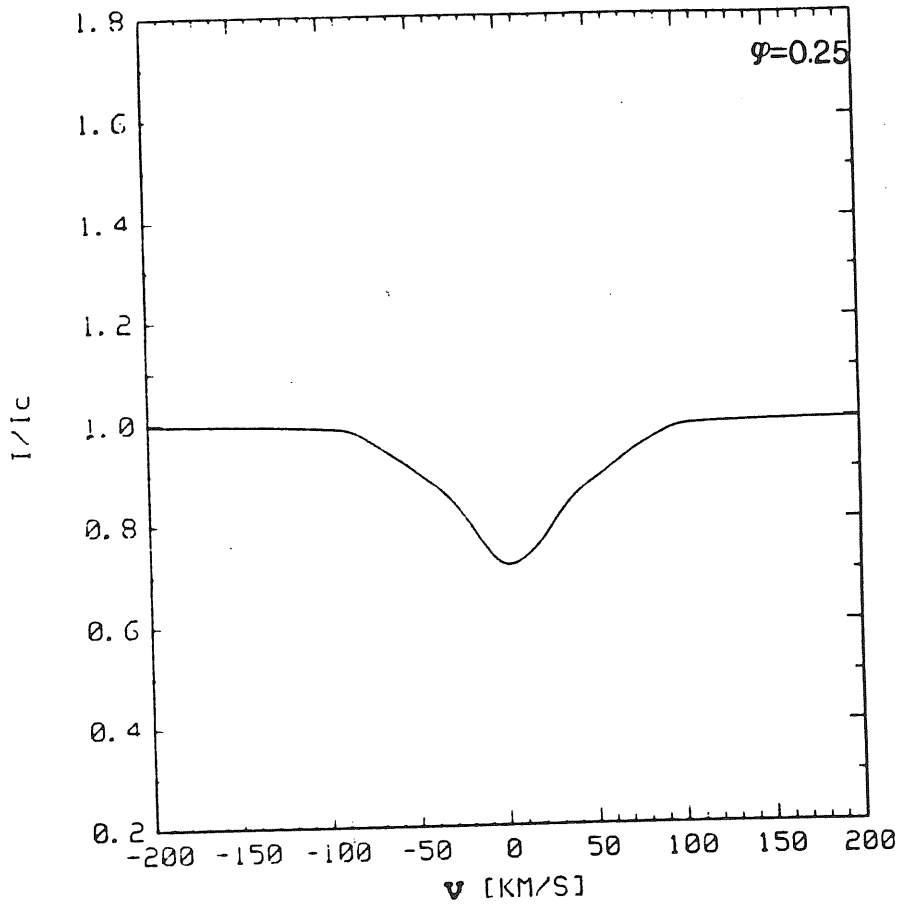
φ=0.25
1.8
1.6
1.4
1.2
1.0
0.8
0.6
0.4
0.2
I/Ic
-200
-150
-100
-50
0
50
100
150
200
V [KM/S]

Figure 3.15

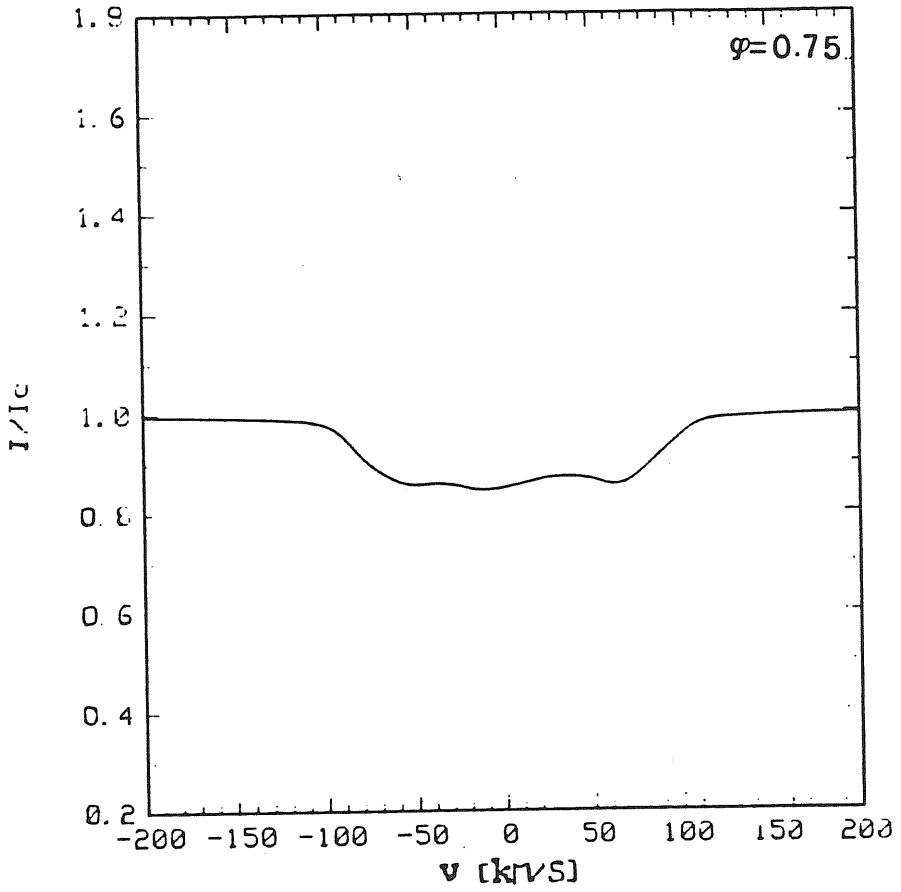

Figure 3.15 – HeIλ-5876 line profile at ϕ=0.25 and 0.75 for l=2 m=−1 mode, V_{rot} sin i=70 km/sec, i=45, A/V_{rot} sin i=0.70, and k=0.1.

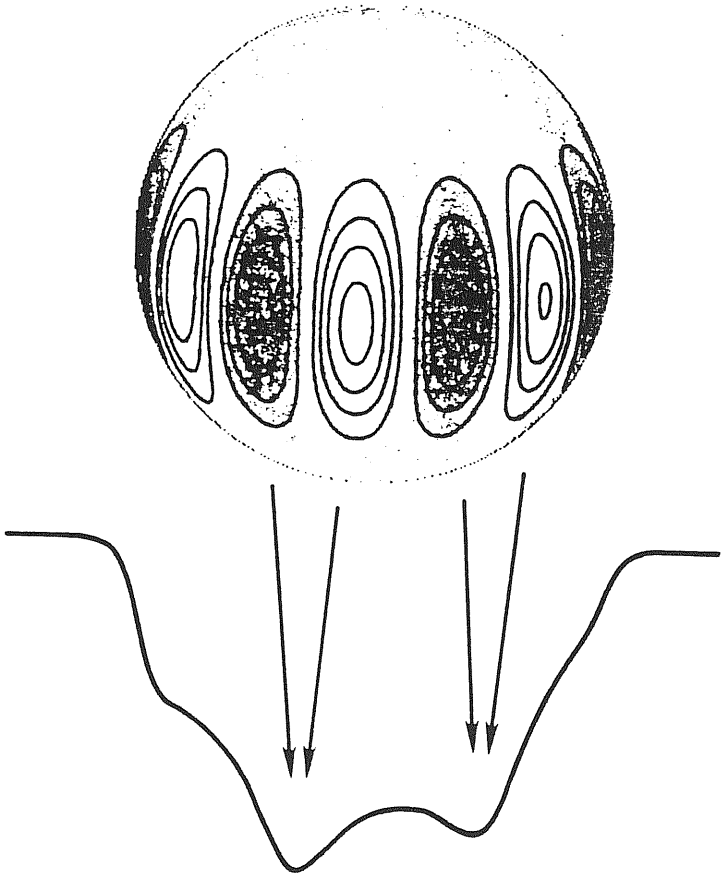

Figure 3.16 – Formation of distorsions in the line profile in a rapidly rotating non-radially oscillating star: l=8, m=−8 mode, A = 20 km/sec, k=0.1, and i=70. The width of the line profile has been scaled to match the diameter of the star. The lighter shaded zones represent material moving toward us, the darker ones, material moving away form us (Figure from Vogt and Penrod, 1983 a).

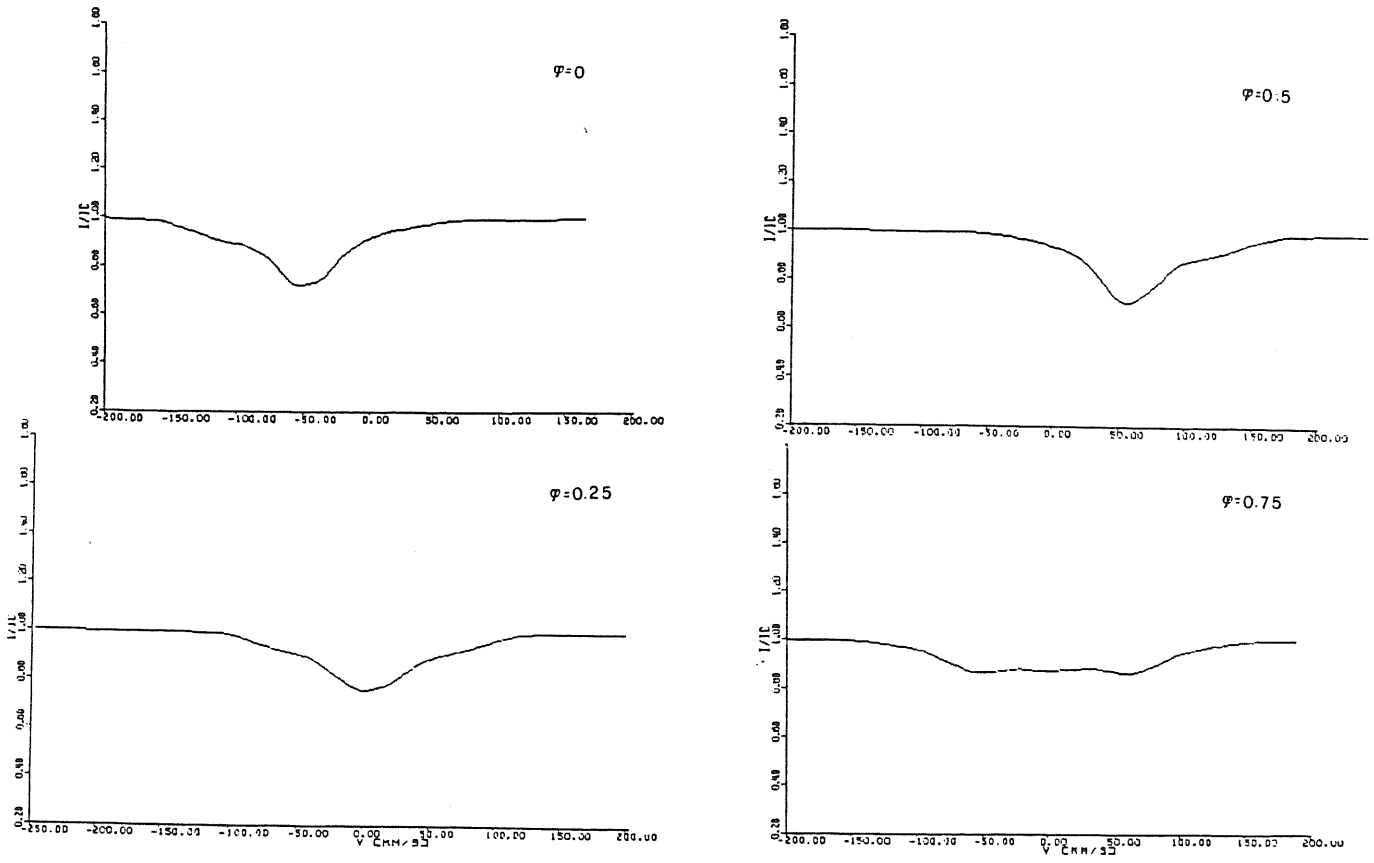

Figure 3.17 – Variation in the HeIλ-5876 line profile with phase for l=2, m=-2, A/V_{rot} sin i=0.7, V_{rot} sin i=50 km/sec, i=90, and k=2.

References

Auer, L.H., and Mihalas, D.: 1973, Ap. J. Suppl., 25, 433.

Baade, D.: 1984, Astron. Ap., 135, 101.

Barnad, A.J., Cooper, J., and Shamey, L.T.: 1969, Astr. and Ap., 1, 28.

Busse, F.H.: 1970, Ap. J., 159, 629.

Campos, A.J., Smith, M.A.: 1980, Ap. J., 238, 250.

Castelli, F.: 1987, private comunication.

Castelli, F.: 1988, Pubblicazione O.A.T., No. 141.

Chappelier, E., Le Contel, J.-M., Valtier, J.C., Gonzales, Bedolla, S., Ducatel, D., Sareyan, J.P., Geiger, J., and Antonelli, P.: 1987, Astr. Ap., 176, 255.

Collins, G.W.: 1963, Ap. J., 138, 1134.

Duval, P., and Karp, A.H.: 1978, Ap. J., 222, 220.

Furelind, I., Young A., Heyean, T., Haag, C., Crinkeaw, G.: 1987, Ap. J., 319, 264.

Griem, H.R., Barangerm M., Kolb, A.C., and Oertel, G.: 1962, Phys. Rev., 125.

Hutchings, J.B.: 1977, Dom. Ap. Obs. Victoria, 14, 59.

Kepler, S.O.: 1984, Ap. J., 286, 314.

Kubiak, M.: 1978, Acta Astron, 28, 153.

Kurucz, R.L.: 1979 a, Ap. J. Suppl., 40, 1.

Kurucz, R.L.: 1979 b, Dudley Obs. Rept. No. 14, p. 271.

Jerzykiewicz, M.: 1978, Acta Astr., 28, 465.

Ledoux, P.: 1951, Ap. J., 114, 373.

Lee, U., and Saio, H.: 1986, in "Hydrodynamics and Magnetohydrodynamic Problems in the Sun and Stars", Y. Osaki, ed., Tokyo, p. 229.

Lesh, J.R., and Aizenman, M.L.: 1978, Ann. Rev. Astr. Ap., 16, 215.

Mihalas, D.: 1972, "Non-LTE Model Atmospheres for B and O Stars", NCAR-TM/STR-76.

Osaki Y.: 1971, Publ. Astr. Soc. Japan, 23, 485.

Osaki, Y.: 1974, Ap. J., 189, 469.

Osaki, Y.: 1985, in "Seismology of the Sun and the Distant Stars", ed. D. Gough, Dordrecht: D. Reidel, p. 453.

Parson, S.B.: 1972, Ap. J., 174, 57.

Robinson, E.L., Kepler, S.O., and Nather, R.E.: 1982, Ap. J., 259, 219.

Shamey, L.J.: 1969, Ph. D. thesis, University of Colorado.

Smith, M.A.: 1977, Ap. J., 215, 574.

Smith, M.A.: 1978 a, Fourth Trieste Conf: "High-Resolution Spectrometry", ed. M. Hack (Trieste: Osser. Astr.), 356.

Smith, M.A.: 1978 b, Ap. J., 224, 927

Smith, M.A.: 1980, "Goddard Conference on Current Problems in Stellar Pulsation Instabilities, eds. J.R. Lesh, W.H. Sparks, and D. Fischel, p. 391.

Smith, M.A.: 1982, Ap. J., 254, 708.

Smith, M.A.: 1985, Ap. J., 288, 266.

Smith, M.A.: 1986, "Hydrodynamics and Magnetohydrodynamic Problems in the Sun and Stars", ed. Y. Osaki, p. 145.

Smith, M.A.: 1987, Private Comunication.

Smith, M.A., and Gray, D.F.: 1976, Pub. A.S.P., 88, 809.

Smith, M.A., and McCall, M.L.: 1978, Ap. J., 223, 221

Stamford, P.A., and Watson, R.D.: 1976, Proc. Astr. Soc. Aust., 3, 75.

Stamford, P.A., and Watson, R.D.: 1977, M.N.R.A.S., 180, 551.

Stoeckley, T.R., and Mihalas, D.: 1973,"Limb Darkening and Rotation Broadening of Neutral Helium Line Profiles in Early-Type Stars", NCAR-TN/STR-84.

Smith, M.A., Fitch, W.S., Africano, J.L., Goodrich, B.D., Halbedel, W., Palmer, L.H., and Henry, G.W.: 1984, Ap. J., 282, 226.

Veugelen, P.: 1983, Astr. Ap., 143, 458.

Vogt, S.S., and Penrod, G.D.: 1983 a, Ap. J., 275, 661.

Vogt, S.S., and Penrod, G.D.: 1983 b, " Activity in Red Dwarf Stars, I.A.U. Coll. No. 71, M. Rodono and P. Byrne eds., (Dordrecht: D. Reidel), p. 379.

von Zeipel, H.: 1924, M.N.R.A.S., 84, 665.

Waelkens, C., and Rufener, F.: 1985, Astr. Ap., 152, 6.

CHAPTER IV

A Study of Short Term Profile Variations in Be Stars: α Eri, P Car and ϵ Cap

§4.1 *Introduction*

Historically, Be stars have been defined as B stars on or near the main sequence with emission in the Balmer lines. They are characterized by hydrogen emission lines in the visible wavelength range; besides the Balmer emissions, emissions from single ionized metals may be present. Be stars are, on average, faster rotators than normal B stars of the corresponding spectral type.

The presence of emission lines is an anomaly in the system used to classify stellar spectra at visible wavelengths, and also in the classical theory of stellar atmospheres, which predicts only absorption lines. Struve (1931) attributed the origin of the emission lines in the visible spectra of Be stars to an extended envelope, confined to the equatorial region, where the gas is ionized by the ultraviolet radiation of the star. Thus the emission spectrum is a recombination spectrum. The existence of an extended atmosphere was attributed by Struve to the ejection of matter from these stars at the equator, due to rotational instability. Thus, according to Struve's model, the Be phenomenon is limited to stars which rotate at critical velocity. This model explains the diversity of the emission lines observed in Be star spectra when it is seen under different angles of inclination of the line of sight on the rotation axis. The Be stars seen equator-on are those that exhibit a shell spectrum. If the star is viewed pole-on, the photospheric absorption lines are, on the contrary, narrow, as are the emission lines which have no central reversal. If the star is viewed at an intermediate angle, the emission line exhibits a weak central reversal and a Be spectrum is observed.

Subsequent studies have demostrated that Be stars exhibit very complex phenomena, for which there is still no comprehensive theoretical understanding. An important characteristic of Be stars is their variability, which, as we have already said, ranges from very large time scales, on the order of decades, to very short ones, on the order of hours, and from large sizes, as the phase passage from Be to B-shell and to a normal B spectrum, to small sizes, as from the evidence of bumps and wiggles propagating rapidly through the line profile. Struve's model and more recent models based on his idea encounter serious difficulties in explaining the spectral variability of Be stars. Also in the high energy part of the spectrum (X-rays and far-UV) Struve-like models fail because they do not explain the presence of higly ionized regions, with temperature of the order of 10^5K, mass flow velocity exceeding the stellar escape velocity of the star surface both for pole-on stars and equator-on stars, or the variability of this mass flow. Be-star models must be rethought on an observational basis which covers the broadest wavelength range possible, from the X-ray and far-UV to IR and radio regions, it is necessary to account for the observed high velocity, superionized regions and simultaneously for the low-velocity, cool, extended Hα emitting envelope, as well as the variability of these structures.

The recent growth of interest in the short-term photometric and/or spectroscopic variablity of Be stars and its possible explanation in terms of non-radial pulsation is due, as we have already said (see Chapter I), to the possible link between non-radial pulsation and the *Be phenomenon.* Further progress in this area requires, on the theoretical side, realistic models in order to verify whether pulsation and shock can play a fundamental role in the mass loss processes in Be stars, and, on the observational side, the regular monitoring of selected Be stars, both spectroscopically and photometrically.

In this chapter the short term line profile variability in three Be stars, α Eri, P Car and ϵ Cap, is studied. The three Be stars under study are in three different phases. α Eri has lost all of its emission in Hα, and shows a normal B spectrum on the basis of the available observations. P Car shows a typical Be spectrum: Hα is in emission with a central reversal. ϵ Cap has Hα characterized by a narrow and deep absorption core bordered by emission wings, suggesting that the star is in a

Be-shell phase. We analyze the change of the HeI (λ-4471, -5876, -6678) and MgII λ-4481 lines in α Eri and in ϵ Cap, and of the HeIλ-6678 line in P Car on time scales of a few hours to a few days. The characteristic properties of the stars under study are presented in §4.2. In §4.3 we describe the data processing method. The observational results are reported in §4.4 and they are discussed in §4.5, §4.6, and §4.7.

§4.2 - *The Stars under Study*

4.2.1 - α *Eri*

α Eri (HD10144-HR472) is the brightest known Be star. The spectral type is B4Ve (Slettebak, 1982) and its projected rotation velocity ($v \sin i$) is 225 km/sec (Slettebak, 1982). The spectroscopic characteristics, derived from the fragmentary information made available during the last 25 years (see Table 4.1), show evidence of long term changes from emission to absorption in the Balmer lines. As reported by Slettebak (1982), the H α emission was already suspected in the Henry Draper Catalogue; Hα and Hβ emissions were confirmed by Andrews and Breger (1966). In 1972 Hβ was observed in absorption; in 1976 Hα was reported to be in absorption. Hα displayed emission with central reversal in 1978 (Dachs et al., 1981). In 1983 Baade (private communication to R.S.) found H α in absorption. Our observations of Hα show normal absorption lines with no trace of emission.

Buscombe and Morris (1961) reported variable radial velocity for this star with a range from 0 to 21 km/sec. Balona (1977) detected light variations in α Eri. Recently Balona et al. (1987) found a light and radial velocity period of 1.26 days, with amplitudes of 0.02 mag and 30 km/sec respectively. The light curve is of a complex shape, dominated by the fundamental and second harmonic, and appears to change with time.

4.2.2 - *P Car*

P Car (HD91465-HR4140) is a B4Ve with a projected rotation velocity, $v \sin i$ = 250 km/sec (Slettebak, 1982). The star is a known light variable (PP Car) with an amplitude of 0.1 magnitude (m=3.17 to 3.37). There is no discussion in the literature of significant changes in the Balmer emission character of the star. The V/R ratio however has displayed different values at different epochs (see Table 4.2) (Jaschek and Jaschek, 1965, Dachs et al., 1981 and Slettebak, 1982, Hanuschik, 1986). Our observed Hα profile shows two emission peaks (V/R=0.89). No HeI or metallic line emissions are observed by Jaschek and Jaschek (1965) , by Slettebak (1982) or by Hanuschik (1987). In the present study HeI λ-6678 shows a central absorption with weak emissions at the wings.

There are no published studies of radial velocity variations in P Car. P Car is a mildly active Be star, but it has not been extensively studied so far.

4.2.3 ϵ *Cap*

ϵ Cap (HD205637-HR8260) is a B3IIIe star with $\sin i$ = 250 km/sec (Slettebak, 1982). This is a Be-shell star with noticeable changes in the emission line character. The Balmer lines were in absorption in 1951 (Slettebak, 1982); from 1956 to 1975 Hα displayed a strong emission, and Hβ and Hδ were in emission with a deep absorption core (Hubert-Delplace and Hubert, 1979). The shell character became prominent in 1976 (Hα observations by Andrillat, 1983) (see also Table 4.3). Also our Hα observations show wings in emission (V$\sim$R), around a strong and sharp core.

Slettebak (1982) reported long term variations in the metallic spectrum with passage from shell profiles to normal absorption profiles. Light variations with Δm=0.02 mag and P=0.22 days are reported by Percy (1986b).

Abt and Levy (1978) did not find changes in the radial velocity on 21 spectra taken from Julian Day 2441880.963 to 2442724.651. Abt and Cadorna (1984), in a search for Be stars in binaries, report that ϵ Cap is a double system. Its duplicity was discovered by Poss (1970) using the technique of lunar occultation.

All the observations were made at ESO (La Silla) during two observing periods (2 times for 7 nights each) in 1986. They were obtained with the Coude' Echelle Spectrometer fed by the 1.4 m Coude' Auxiliary Telescope. The detector used was an unintensified 1870-diode Reticon cooled to 140 K. The resolution was set at 60000. The wavelength calibration was provided by the spectrum of a Thorium hollow cathode lamp.

Observations of Hα and HeIλ-6678 in P Car and Hα, HeIλ-4471, HeIλ-5876, HeIλ-6678 and MgIIλ-4481 in αEri and ϵ Cap were obtained. The total wavelength region covered by the Reticon was 56.5 A at Hα, 35.1 A at HeIλ-4471, 50.4 A at HeIλ-5876 and 53.5 A at HeIλ-6678. A total of 21, 24 and 18 spectra were obtained of α Eri, P Car and ϵ Cap respectively. Table 4.4 lists the dates and times of the observations and the measured radial velocities. Typical exposure times were of the order of 4 minutes for α Eri, of 16 minutes for P Car and of 40 minutes for ϵ Cap. Signal to noise ratios were of the order of 400 for α Eri, 300 for P Car and 250 for ϵ Cap. Every observation was followed by five short registrations of the fixed-pattern read-out noise of the Reticon, and the flat field of the detector was determined by using white-light provided by a mercury lamp.

The data were reduced at ESO (Garching), by using the ESO Image Handling and Processing System (IHAP). The correction for read-out noise and flat field, and the wavelength calibration were performed by using ESO IHAP. Wavelength calibration was performed by identification of ThI and ThII emission lines in the calibration spectra (Thorium atlases of D'Odorico et al., 1984). The typical standard deviation from the parabola fitted to about 10 lines is about 0.006 A for HeIλ-4471 and HeIλ-4481, 0.002 A for HeIλ-5876, 0.017 A for HeIλ-6678 and 0.009 A for Hα.

The data analysis was carried out at the Astronomical Observatory of Trieste, by using the ELSPEC interactive spectrogram processing package (Pasian et al., 1982). Normalization to the continuum was performed, using ELSPEC, by means of a cubic spline fit of a series of selected nominal continuum points. This continuum normalization was checked by visual inspection of the data on each individual

spectrum. Statistical errors produced by this method do not exceed 1% of the continuum intensity (typical errors are $< 0.5\%$). Using ELSPEC we have obtained the following quantities: equivalent widths (EW), intensities (I_0), velocity positions (v) of the maximum absorption or emission, and velocities of the violet and the red sides of the profile at half depth (vl, vr). The EW's (assumed positive in the case of absorption, negative for emission) have been obtained by direct integration. The quantities v and I_0 have been computed (a) by direct measurement on the profile or (b) by adopting a fitting procedure based on a linear combination of skewed gaussian profiles with the linear local continuum. This last procedure is an improved version of the original Frazer and Suzuki (1966) technique and has been adopted in this work (1) for evaluating the vl and vr parameters on all profiles and (2) for the optimum estimation of the v, I_0, vl and vr parameters of the broad, weak and almost featureless spectral lines observed in α Eri. This fitting procedure allows an unambiguous estimation of the errors on the parameters. The accuracy of the parameters depends on the noise level and the likelihood of the observed and computed line shapes. A convenient criterion of the goodness of fit is the mean square deviation between the observed and computed line shapes. Typical values are of the order of 0.5%.

§4.4 - *Observational Results*

4.4.1 - *The Hα Profiles*

Figures 4.1, 4.2 and 4.3 show the observed Hα profiles in α Eri, P Car and ϵ Cap. Repeated Hα measurements in the same night were achieved only for α Eri and ϵ Cap (in Figures 4.1 and 4.2 averages of the 2 measurements of these stars are shown). No changes of the Hα profiles in these two stars are detected. Atmospheric H_2O vapour absorption lines affect the Hα profiles, but it is not difficult to distinguish these narrow telluric features superimposed on the line profile.

Table 4.5 reports the Hα line profile parameters for the three program stars. Hα is an absorption profile in αEri. The Hα line in P Car is in emission with a central reversal. The ϵ Cap Hα line has the typical shape of Be-shell stars.

4.4.2 - *Absorption Line Profiles in α Eri*

Figures 4.4, 4.5 and 4.6 show the observed profiles of HeI and MgII. The radial velocity v of the HeIλ-4471, HeIλ-5876, HeIλ-6678 and MgIIλ-4481 has been measured for each profile (Table 4.4). The standard wavelengths assumed for the helium and magnesium lines are: 4471.325 A, 4481.228 A (Petrie, 1968), 5875.700 A and 6678.151 A (Wiese et al., 1966). The standard deviation of the HeIλ -5876 and HeI λ-6678 line velocities, averaged from all measurements, is more than three times the mean error on these velocities. This is consistent with Balona et al.'s (1987) measurements of radial velocity variations in α Eri. In addition, the standard deviation of the average v in the HeI λ-6678 spectra taken on J.D. 2446671 is about 8 times the mean error on v computed by the best fit, suggesting variability on time scales of the order of hours in this line. Figure 4.7 reports the measured HeIλ-6678 v, vl and vr. This HeI line displays several weak and variable features, superimposed on the broad absorption which affect the overall shape of the profile. These variable features are visible also in MgIIλ-4481 line profiles, but not in the other HeI lines.

The change in symmetry with time of all profiles was also checked by measuring vl and vr. A symmetry parameter HWL/HWR=(v-vl)/(vr-v) was introduced. In all profiles except HeIλ-6678, discussed above, no significant changes in HWL/HWR were found.

Table 4.6 gives the mean values of the EW's and the I_0's of the helium and magnesium lines, the standard deviation from the mean (when more than 2 spectra are available) and the mean errors computed by the best fit. We see that there is no evidence of significant changes in these quantities except, maybe, on the three consecutive spectra of MgIIλ-4481, where the average EW has a standard deviation which is more than 3 times the mean error and the average central depth has a

standard deviation of more than 6 times the mean error on I_0. Variations on the EW's or on the I_0's occurring within consecutive nights are also not detected.

4.4.3 - *Absorption Line Profiles in P Car*

Figure 4.8 shows a series of spectra of HeIλ-6678 taken on several consecutive nights (see Table 4.4). The lines show emission in the red and/or violet side. The absorption and the emission components of the profile are variable in intensity and equivalent widths. The absorption component of each profile contains a variable number (one to three) of features that move, with time, from negative to positive velocities, most likely across the entire line profile. The overall shape of the absorption component has variable asymmetry, which appears to be correlated with the motion of the above features. Most of the time there is a dominant component; other times all the components merge together to form a flat topped absorption core; in a few cases the central core is split into two absorption peaks of similar depth.

Figure 4.9 reports the measured radial velocity of the absorption and emission components. In order to allow for an optimal estimate of the absorptions and their errors, principally in the case of flat topped profiles, we have measured v both by direct measurement of the profile minima and by means of the best fit of the absorption component to a skewed gaussian profile. The values obtained with the two methods agree within the scatter due to the different effects of the noise in the manual and best fit approaches. The calculated standard deviation of the absorption component is always three times greater than the mean error on the v's for observations taken consecutively on the same nights. This supports the idea that HeIλ-6678 changes on time scales of the order of hours. A discontinuous radial velocity curve (two peaks in the absorption component are observed) is found on Julian days 244650+1.7086, +4.8642 and +5.6580. The discontinuity is approximately 100 km/sec.

Changes in the absorption width at half maximum (FWHM) are also detected. The FWHM reaches a maximum almost simultaneously with the appearance of

the discontinuities in the radial velocity curves. Absorption component equivalent width variations of about 10% are also detected.

4.4.4 - *Absorption Line Profiles in ϵ Cap*

Figures 4.11, 4.12 and 4.13 show the observed HeI and MgII line profiles. The lines always show two absorption peaks; there is some evidence of variable secondary features in the magnesium lines. No changes are found in the position of the two helium and magnesium line absorption peaks on time scales of the order of hours; nor are any found on vl or vr (see Figure 4.14 a-d).

Table 4.7 gives the mean values of the helium and magnesium line equivalent widths, the standard deviation from the mean (where more than 2 spectra were available) and the estimated mean error. Again there is no evidence of significant changes in these quantities. However, there is some evidence of change in the shape and strength of the two absorption peaks, which does not affect the total equivalent width. Figure 4.15 reports the ratio of the intensities of the two absorption components in the helium and magnesium lines.

§4.5 - *Short-Term Variability in α Eri and the Non-Radial Pulsation Model*

Theoretical line profiles broadened by pulsation, rotation have been generated in order to reproduce the observed HeI λ-6678 line profile variations in α Eri. We have used the line profile modeling algorithm described in Chapter III. A $T_{eff} = 17500$, $\log g = 4$ model atmosphere (Underhill et al., 1979) was calculated using the program ATLAS8, described in Kurucz (1979), and used to calculate intensity line profiles by means of the numerical code WIDTH8 (see Chapter II). 5000 grid points on the visible stellar disk are used for deriving the flux profile. This is obtained by integration across the stellar disc of the intensity profiles, corrected for Doppler motions due to non-radial pulsation and rotation.

In order to model the observed line profiles by the rotation and non-radial pulsation line-broadening algorithm, we choose the free parameters according to the criteria presented in §3.5. In summary, we first choose the projected stellar rotation velocity, the traveling-wave mode, and the ratio of horizontal to vertical pulsation velocity components. We then experiment with various values of the microturbulence, the stellar inclination, and the non-radial pulsation amplitude. When these parameters and the period are correctly chosen, the computed profiles should simply vary with the phase and fit the temporal sequence of the observed profiles. Fits are considered appropriate when all parameters but phase are held constant.

The observed α Eri line-profiles are of very high quality, but they are insufficient in number for determining a reliable period. For this reason we have assumed Balona et al.'s (1987) radial velocity and light variation period: $P = 1.26$ days. The shapes of the profiles vary during the cycle in such a way that any single profile can be used to determine the phase. The period must satisfy the profile solutions for the successive or/and previous observations with fixed pulsational amplitude and rotational velocity.

The value assumed for the projected rotation velocity of the star is $V \sin i = 225$ km/sec (Slettebak 1982). The number of bumps visible in the profiles suggests $|m| = 4$ (see §3.5). We assumeed that the modes are prograde sectorial modes ($l = -m$), after a number of trials with other modes were made. For values of l less than 4, the bumps are too far apart, while values of l greater than 4 produce too many bumps in the line profile at any given phase. No more than one mode was considered at a time. A range of microturbulence velocities from 17 to 19 km/sec is adopted in order to obtain the best fit. A pulsation amplitude $a(R) = 15$ km/sec is required for the best fit. Values of $a(R)$ contained within ± 3 do not affect the fitting. This amplitude is of the same order as that found in other Be and in the slowly rotating B stars. The fitting is obtained with an inclination angle, i, larger than 80 °. Since we cannot distinguish between inclinations of 80° or 90°, we adopt a value of 85 °. This inclination agrees well with the conclusion of Balona et al. (1987) that α Eri is seen equator on. If we assume that the mass of α Eri is 8.8

$M_\odot$ (Underhill, 1982) and the radius is 5.5 $R_\odot$ (Balona et al., 1987) we find that the ratio between the angular velocity to the breakup angular velocity of α Eri is 0.4. Figure 3.8 shows that in this case the geometrical distortion and the variation of the star due to rotation is negligible, as is the variation in effective temperature.

The value of the ratio of the horizontal to vertical oscillation velocities, k, was constrained to lie in the range 0.1-0.15 by the best fit with the observed profiles. This value agrees with the generally adopted value of 0.15 for short-period, high-mode pulsating variables, but it does not verify the theoretical relation between k and the pulsation period, P (see §3.6). Essentially because the previous is too long. The *k problem* and its possible solutions have been extensively treated in §3.6. The α Eri light variation suggests to exclude the possibility that the *Rossby modes* are involved (see §3.6).

As shown in Figure 4.16, our model with $l = -m = 4$ works well in reproducing the observed line profiles, except for the profile observed on J.D. 2446673.8857. This mode reproduces the sizes, the separations, and the shape of the observed bumps with an accuracy better than 0.5 % over the entire line profile in all the 7 observed line profiles except one. We must note that the value of the signal-to-noise ratio of this last profile is lower than that of the other ones, owing to bad weather conditions during observation.

One aspect of the observations which requires explanation is the difference in visibility of the bumps between HeIλ-6678 and the other two helium lines (HeI λ-4471 and HeIλ-5876) (see Figures 4.4 and 4.5). We measured HeIλ-5876 radial velocity variations (see §4.4.2), but the observed profiles do not show any moving superimposed feature. Concerning HeIλ-4471, we did not measure radial velocity variations', however, it has to be noted that we obtained only four profiles; and three of them differ only by 0.05 in phase.

The fact that the secondary absorption features are more or less visible in different spectral lines has been already noted by Baade (1983, 1984) and by Vogt and Penrod (1983). One possible explanation is that in the HeIλ-4471 and -5876 lines the intrinsic profiles are broader than in HeIλ-6678, because they are triplet lines and Stark broadening plays an important role in blurring out the observed

bumps.

There are no radial velocity variations in the MgIIλ-4481 lines, though bumps are visible on the observed profiles. It has to be noted that we obtained only four MgII profiles and that three of them differ only by 0.05 in phase. In order to model these profiles, we used the non-radial-pulsation line-broadening algorithm, with the same parameters as obtained by the best fit of the HeI λ-6678. The profile obtained on J.D. 2446765.846 does not agree with the calculated profiles. Concerning the other three observed profiles, we find that the theoretical profiles show an absence of an observed bump in the right wing of the line (see Figure 4.17). This "missing bump" is better modeled by a $l = 6$, $m = -6$ pulsation mode. These MgIIλ-4481 line profiles requiring higher order modes were obtained four days after the HeIλ-6678 profiles, which were fitted with a $l = -m = 4$ mode. If a variation in the non-radial pulsation mode occurred, we expect that it was also accompanied by a period variation. The observed profiles are too few and too near in phase to determine a possible new value of the period and to suggest a mode variation. We must also consider that temporary appearances and disappearances of individual bumps seem to occur, over time scales of $\sim$ 20 minutes, in the profiles of pulsating early-type stars (Smith, 1986). In addition, according to Vogt and Penrod (1983), smaller features in the observed profiles may be produced by transient modes of much higher order which, however, do not maintain any degree of coherence across the stellar disc. So we cannot fully understand this evidence of changing mode order.

In support to the reality of the $l = 4$ mode derived from the HeI lines, we report that Dziembowski (1977) has calculated theoretical light curves for non-radial modes up to l =8. The amplitude of the expected light variability due to l =4 pulsation mode is small, consistent with the small photometric variations observed by Balona et al. (1987) (see §4.2).

As we have already said (§1.4), at present there are several competing hypotheses about the cause of rapid variability besides non-radial pulsation: rotation, e.g. spots on the photosphere rotating with the star, or binarity.

The period of 1.26 days is the rotational period of α Eri, if its equatorial

velocity is 221 km/sec ($i \sim 80°$). Therefore, the rotational hypothesis can not be rejected. Balona et al. (1987) suggested that, qualitatively, a large darkspot with two smaller spots evenly spaced in longitude rotating with the star could explain the light and radial velocity variations. Migration or change in area of the spots would then be responsible for the change in the light curve with time. However, they did not construct a detailed model.

Concerning the binary hypothesis as cause of α Eri light and spectrum variability, according to Balona et al. (1987), we obtain $a_1 \sin i = 0.43$ $R_\odot$, where a_1 is the semimajor axis of the orbit of the primary star. The mass function is then 7.0 10^{-4} $M_\odot$, which gives a secondary mass of about 0.4 $M_\odot$, if the primary has mass of 8.8 $M_\odot$. Such a system would not be likely to show eclipse. and therefore binarity would not be responsible for the variability. In addition, the slight amplitude change of α Eri (see §4.2) can not be explained by a binary model.

§4.6 - *Short term variability in P Car and the Non-Radial Pulsation Model*

A search for periodicity in the changes in radial velocity and full-width hafmaximum in the HeIλ-6678 line profiles in P Car suggests a period of 0.35 $\pm$ 0.05 days with a 98% significance level. Unfortunately, the available observations are not sufficient to allow a more accurate determination of this period. Jurkevich's (1971) technique has been used for the periodicity analysis. In this technique, the search for periodicity is made by using an analysis of the *expected mean square deviations.* The period is obtained by examining the fit of the observed data sample for a range of trial periods until the best representation is obtained. This method does not require equally spaced observations. We must note that the Fourier technique for periodicity analysis is very powerful for equally spaced observations, but could be applied to irregularly spaced data by replacing actual observations with new data generated from the original set by interpolation. The effects of such a procedure are generally not known. In addition, methods such as Jurkevich's are preferred to Fourier methods in all cases in which the variations are not strictly sinusoidal.

The HeIλ-6678 line profiles in P Car show emission in the red and/or in the violet side. Assuming that the emission affects only the extreme side of the profile wings, we checked whether periodic waves induced by non-radial pulsation can reproduce the observed short-term variations of the absorption part of the profiles.

The intrinsic profiles of the HeIλ-6678 line were generated for 44 different limb angles (5000 grid points in the visible disc) by the numerical code WIDTH8 using a $T_{eff} = 17500$, $\log g = 4$ model atmosphere, computed by the program ATLAS8 (Kurucz, 1979). The value assumed for the projected rotation velocity of the star is V sin i = 250 km/sec (Slettebak, 1982). The free parameters were chosen according to the criteria presented in §3.5 (see also 4.5). We assumed the period obtained by the radial velocity variation analysis (P=0.35 days). The number of bumps visible in the profiles suggests $|m| = 6$ (see §3.4). After a number of trials with other modes, we assumed the $l = -m$ mode. Also in this case no more than one mode was considered at a time. A range of microturbulence velocity from 17 to 20 km/sec was adopted in order to obtain the best fit. A pulsation amplitude $a(R) = 18 \pm 3$km/sec and an inclination angle of more than 80° are required for the best fit. If we assume for P Car a mass of 8.8 $M_{\odot}$, appropriate for its spectral type (Underhill, 1982), and a radius of 5 $R_{\odot}$ (Underhill et al., 1979), we find the ratio of the star angular velocity to the breakup angular velocity to be 0.4. Also in this case we can neglect the geometrical distorsion of the star and the effective temperature variation due to rotation (see Figure 3.8).

The value of the ratio of the horizontal to vertical oscillation velocities, k, was constrained to lie in the range 0.1-0.15 by the fit with the observed profiles. This value verifies the theoretical relation betwee k and the pulsation period, P (see §3.6), if the previously indicated values for the mass and radius of P Car are adopted.

Many of our observed profiles (10) are best fitted by the $l = 6$, $m = -6$ mode (see Figure 4.18). This mode reproduces the shapes of the observed bumps, in many cases better than 0.5% over the entire absorption component. There are a number of cases in which the theoretical profiles show bumps in the red wings that are not observed (J.D. 244650+2.6142, +5.7448, +5.8003). In all these cases

the observed profiles are affected by strong red emissions. It is possible that the emission affects more or less extended regions of the line wings, changing the wing shape. In addition, there are some cases in which smaller features in the core of the observed profiles are present and are not predicted by the theoretical ones. As we have already said (see 4.5), according to Vogt and Penrod (1983), smaller features in the observed profiles may be produced by transient modes of much higher order respect to the $l = -m = 6$ mode. These higher order modes do not maintain any degree of coherence across the stellar disc.

Concerning the other competing hypotheses about the cause of rapid variability besides non-radial pulsation, we find that the period of 0.35 days is the rotational period of P Car, only if $i \sim 0$. In addition, this short period disproves the binary hypothesis as cause of P Car observed spectrum variability. Infact, with a radial velocity amplitude, $2K \sim 90 km/sec$, estimated from the obtained radial velocity curve of P Car, we found $a_1 \sin i \sim 0.31 R_\odot$. The mass function is then $3.210^{-3} M_\odot$, which gives a secondary mass of about $0.76 M_\odot$, if a $\sin i = 0.866$ is assumed. Finally the mass ratio gives $a_2 \sin i \sim 3.59 R_\odot$, and we found that the distance between the two stars is less than the assumed radius of P Car.

§4.7 - *The ϵ Cap Short Term Variability*

Concerning the change in the shape and strength of the observed two components of the HeI and Mg II line profiles in ϵ Cap, we do not have sufficient data to decide whether this is the result of short term variations or whether it is due to the double star nature of ϵ Cap discovered by Poss (1970). Figure 4.12 shows broad wings of the NaI D lines that could, possibly, be ascribed to the companion star.

Table 4.1

αEri HD10144-HR472

Spectral Type ->B4V e $\underline{v} \sin \underline{i}$ ->225 km/s

Balmer Lines	-1963->Weak emission in Hβ ; 1965->Broad emission in Hα and double emission in Hβ (Andrews and Breger, 1966); 1972->Normal Hβ absorption profiles (Dachs et al., 1981); 1978->Hα emission with central reversal, Hβ pure absorption partially filled in by emission (Dachs et al., 1981); 1982->Hα in emission with central reversal, Hβ in absorption (Baade, 1985); 1983-> Hα in absorption (Baade, 1985); 1986-> Hα in absorption (present study)-
Helium and Metallic Lines	-1986-> HeI and MgII in absorption (present study)-
Radial Velocity Variations	-Balona et al., 1987-> P=1.26 d, radial velocity amplitude=30 km/s-
Light Variations	-Balona, 1977-> Short period light variations- -Balona et al., 1987-> P=1.26 d, Amplitude=0.02 mag-

Table 4.2

P Car HD91465-HR4140

Spectral Type->B4Ve $\underline{v} \sin \underline{i}$->250 km/s

Balmer Lines	-1953-1963->Double emission at Hβ , V>R, narrow cores and violet emissions in Hγ and Hδ (Jashek and Jashek, 1965); 1965-> Double emission at Hβ , R>V (Jashek and Jashek ,1965); 1974-> Widely-spaced double emission at Hβ and Hζ , V>R (Slettebak, 1982); ->1976 Strong and symmetrical Hα emission (Slettebak, 1982); 1980->Double emission at Hβ , V>>R , sharp emission at Hγ and Hδ (Slettebak, 1982); 1985-> Double peaked Hα emission (Hanuschik, 1986); 1986->Double peaked Hα emission-
Helium and Metallic Lines	-1962-1963->HeI emissions (Jashek and Jashek, 1965); 1965->No emission in HeI, dubious emission in FeII 4233 and 4352 (Jashek and Jashek, 1965); 1974-> FeII double emission (Slettebak, 1982); 1985-> FeII, SiII and MgI lines in emission (Hanuschik, 1987); 1986->HeI central absorption with weak emission at the wings (present study)-
Radial Velocity Variations	-No published studies-
Light Variations	- V=0.17 (V=3.1 to 3.27)

Table 4.3

ε Cap HD205637-HR8260

Spectral Type->B4Ve $\underline{v} \sin \underline{i}$->250 km/s

Balmer Lines	-1951->Weak and sharp Hα . Sharp and deep absorption at Hβ and Hδ (Slettebak, 1982); 1956-1975->Hα strong emission and deep absorption cores in Hβ and Hδ (Hubert et al. 1979); 1978->V>R at Hα (Dachs et al., 1981); 1979->Strong and sharp absorption cores in all the Balmer lines. Weak emission in Hβ (Slettebak, 1982); 1983->Hα emission (V=R)around a deep absorption core (Andrillat, 1983); 1986->Wings in emission (V=R) around a strong and sharp core (present study)-
Helium and Metallic Lines	-1957-1958-1971->Weak absorption metallic shell spectrum (Slettebak, 1982); 1979-> No metallic shell spectrum (Slettebak, 1982); 1986-> HeI and MgII in absorption (present study)-
Radial Velocity Variations	-No radial velocity variations (Abt and Levy, 1978)-
Light Variations	-Percy, 1986b -> P=0.22d Amplitude=0.02mag

Table 4.4 - Journal of Observations.

Star	Profile	Date(D-M-Y)	U T (H-M)	Julian Day	v (km/sec)
αEri					
	HeI6678	29-8-86	5-45	2446671.7427	60.0
	HeI6678	29-8-86	6-55	2446671.7913	34.2
	HeI6678	29-8-86	8-21	2446671.8510	20.9
	HeI6678	29-8-86	9-24	2446671.8947	47.6
	HeI6678	29-8-86	9-38	2446671.9045	44.7
	HeI5876	30-8-86	8-05	2446672.8399	-03.8
	HeI5876	30-8-86	9-29	2446672.8982	-03.9
	HeI5876	30-8-86	9-42	2446672.9072	14.6
	HeI5876	31-8-86	6-10	2446673.7600	28.3
	HeI5876	31-8-86	8-16	2446673.8475	28.5
	HeI5876	31-8-86	8-33	2446673.8593	21.4
	HeI6678	31-8-86	9-11	2446673.8857	-68.3
	HeI6678	31-8-86	9-58	2446673.9184	-16.5
	HeI5876	1-9-86	8-03	2446674.8385	8.6
	HeI5876	1-9-86	9-33	2446674.9010	6.1
	Hα	1-9-86	6-03	2446674.7552	16.9
	Hα	1-9-86	7-23	2446674.8107	16.9
	HeI/MgII 4471/81	2-9-86	8-14	2446675.8461	25.8 /32.9 (*)
	HeI/MgII 4471/81	3-9-86	2-10	2446676.5934	24.2 /36.9
	HeI/MgII 4471/81	3-9-86	4-01	2446676.6704	13.3 /26.0
	HeI/MgII 4471/81	3-9-86	4-14	2446676.6795	11.1 /13.3
P Car					
	HeI6678	12-3-86	3-56	2446501.6662	36.2
	HeI6678	12-3-86	4-57	2446501.7086	30.9
	HeI6678	13-3-86	2-41	2446502.6142	91.2
	HeI6678	13-3-86	4-50	2446502.7037	-29.1, 75.7 (**)
	Hα	14-3-86	3-17	2446503.7079	-44.0, 50.7
	HeI6678	15-3-86	5-53	2446504.6309	72.0
	HeI6678	15-3-86	8-41	2446504.8642	-32.5, 72.1
	HeI6678	16-3-86	1-26	2446505.5621	-27.5
	HeI6678	16-3-86	3-02	2446505.6288	- 6.7
	HeI6678	16-3-86	3-44	2446505.6580	3.1
	HeI6678	16-3-86	4-11	2446505.6767	28.8
	HeI6678	16-3-86	5-49	2446505.7448	75.4
	HeI6678	16-3-86	6-28	2446505.7719	-32.8, 63.1
	HeI6678	16-3-86	7-09	2446505.8003	48.0
	HeI6678	16-3-86	7-38	2446505.8205	53.2
	HeI6678	17-3-86	3-16	2446506.6386	14.4
	HeI6678	17-3-86	3-41	2446506.6559	23.5
	HeI6678	17-3-86	4-04	2446506.6719	14.8
	HeI6678	17-3-86	4-27	2446506.6879	38.4
	HeI6678	17-3-86	6-34	2446506.7761	57.9
	HeI6678	17-3-86	8-12	2446506.8441	65.7
	HeI6678	18-3-86	3-04	2446507.6303	6.3
	HeI6678	18-3-86	3-47	2446507.6601	6.1
	HeI6678	18-3-86	7-02	2446507.7955	44.2
ε Cap					
	HeI6678	28-8-86	0-17	2446670.5167	-22.9, 37.7
	HeI6678	28-8-86	1-25	2446670.5640	-20.2, 58.3
	HeI6678	28-8-86	3-02	2446670.6313	-25.0, 48.2
	HeI6678	28-8-86	3-45	2446670.6612	-21.5, 41.0
	HeI6678	28-8-86	6-41	2446670.7834	-23.8, 35.1
	HeI6678	28-8-86	7-20	2446670.8105	-13.2, 33.2
	HeI6678	28-8-86	8-20	2446670.8522	-23.9, 35.0
	HeI6678	29-8-86	3-12	2446671.6383	-27.5, 35.0
	HeI6678	29-8-86	3-59	2446671.6709	-34.7, 31.4
	HeI5876	31-8-86	4-07	2446673.6764	- 7.1, 63.5
	HeI5876	31-8-86	6-37	2446673.7806	7.7, 65.2
	Hα	1-9-86	4-17	2446674.6834	-179.8, 0.0, 191.5
	Hα	1-9-86	5-15	2446674.7237	-179.0, 0.0, 192.9
	HeI/MgII 4471/81	2-9-86	2-10	2446675.5952	-50.1, 71.4/-35.0, 57.8
	HeI/MgII 4471/81	2-9-86	4-18	2446675.6841	-39.6, 71.2/-29.5, 58.9
	HeI/MgII 4471/81	2-9-86	7-14	2446675.8063	-49.7, 49.2/-39.8, 36.1
	HeI/MgII 4471/81	2-9-86	18-44	2446676.2855	-55.8, 69.6/-41.9, 45.9
	HeI/MgII 4471/81	3-9-86	0-55	2446676.5431	-47.5, 45.1/-23.2, 49.6

Notes: (*) The radial velocities of the HeIλ-4471 and MgIIλ-4481 lines are separated by '/'.
(**) The radial velocities of different components (see text) in the same line are separated by ','.

Table 4.5 - Parameters for Hα profiles.

Star	J.D. 2444	EW (A)(*) Err EW	v (km/s) Err v	vl (km/s) Err vl	vr (km/s) Err vr	I_0 Err I_0	V/R(**)
αEri	6674	2.55 0.03	16.9 0.8	-212.3 2.6	236.0 2.6	0.239 0.001	
P Car	6503	-24.52 0.24	-44.0 50.7 4.1 3.5	-145.1 5.8	198.8 2.1	-2.60 -2.95 0.02 0.02	0.88
εCap	6674	-1.32 0.91 -1.51 0.02 0.02 0.02	-179.4 -0.0 192.2 4.5 2.3 4.0			0.306 0.540 0.324 0.002 0.003 0.002	0.95

Table 4.6 - Equivalent widths and depths of helium and Magnesium lines in α Eri.

	Equivalent Width				Depth			
	HeI4471	MgII4481	HeI5876	HeI6678	HeI4471	MgII4481	HeI5876	HeI6678
Date	2-9-86	2-9-86	30-8-86	29-8-86	2-9-86	2-9-86	30-8-86	29-8-86
Mean	0.854	0.423	0.614	0.475	0.150	0.066	0.089	0.060
Sigma			0.012	0.007			0.002	0.001
Mean Error	0.025	0.010	0.015	0.013	0.002	0.001	0.001	0.001
Date	3-9-86	3-9-86	31-8-86	31-8-86	3-9-86	3-9-86	31-8-86	31-8-86
Mean	0.853	0.416	0.658	0.425	0.157	0.062	0.090	0.057
Sigma	0.050	0.049	0.008		0.005	0.006	0.002	
Mean Error	0.025	0.010	0.013	0.020	0.005	0.001	0.001	0.001
Date			1-9-86				1-9-86	
Mean			0.649				0.090	
Sigma								
Mean Error			0.017				0.001	

Table 4.7 - Equivalent widths of helium and magnesium lines in ϵ Cap.

	Equivalent Width			
	HeI4471	MgII4481	HeI5876	HeI6678
Date	2-9-86	2-9-86	30-8-86	28-8-86
Mean	1.181	0.296	1.080	1.097
Sigma	0.040	0.007		0.044
Mean Error	0.015	0.039	0.015	0.015
Date	3-9-86	3-9-86		29-8-86
Mean	1.100	0.284		1.145
Sigma				
Mean Error	0.011	0.007		0.009

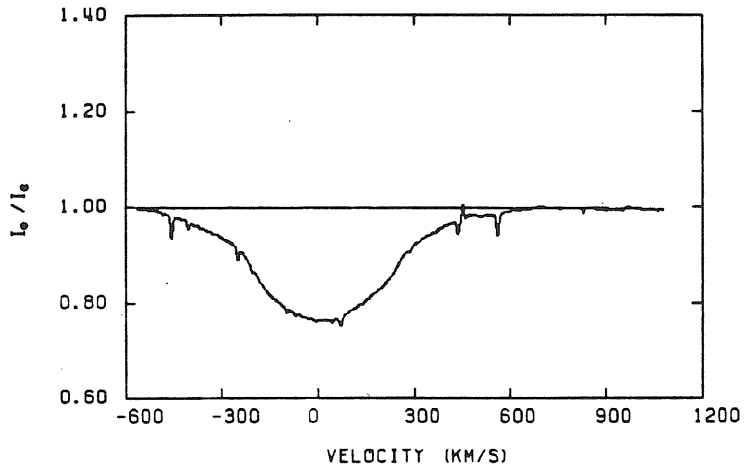

Figure 4.1 – The Hα profile in α Eri. This is an average of two profiles taken on J.D. 2446674. Narrow absorption features are telluric lines. midinsert

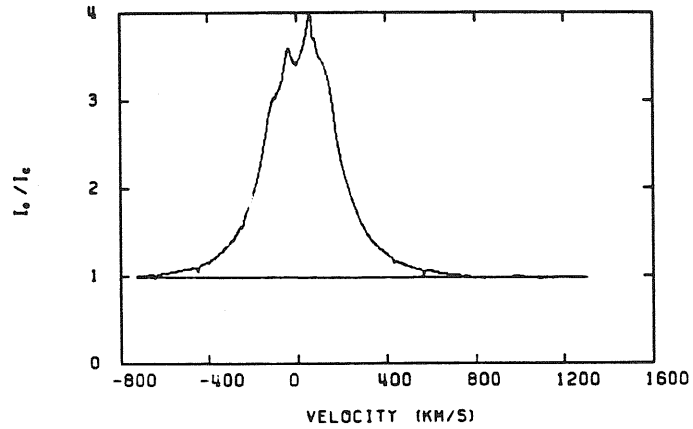

Figure 4.2 – The Hα profile in P Car taken on J.D. 2446503. Narrow absorption features are telluric lines.

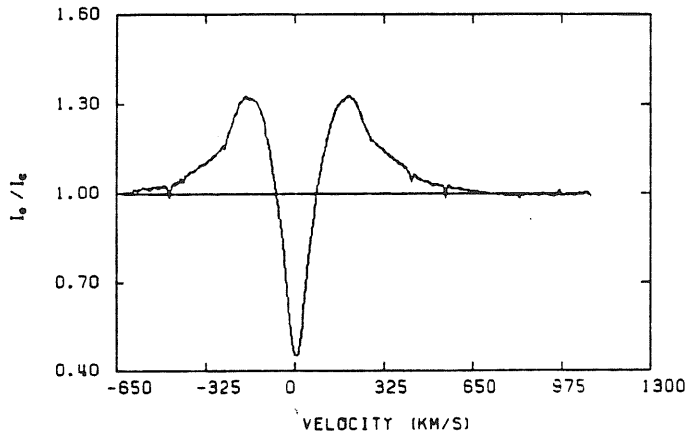

Figure 4.3 – The Hα profile in ϵ Cap. This is an average of two profiles taken on J.D. 2446674. Narrow absorption features are telluric lines.

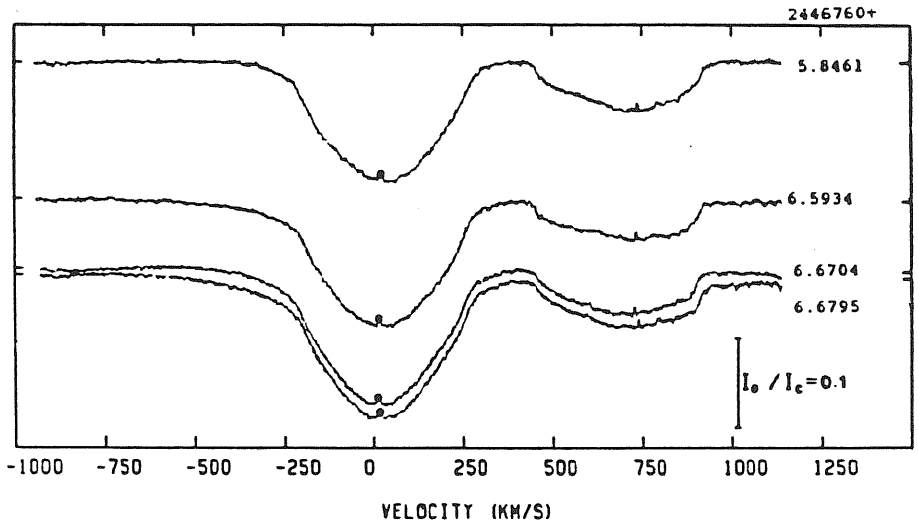

Figure 4.4 – Series of 1 (top) and 3 (bottom) spectra of HeIλ-4471 and MgIIλ-4481 in α Eri, observed during two consecutive nights. The abscissae are velocities relative to the HeIλ-4471 line. In this velocity scale the zero point for MgIIλ-4481 is at 664.43 km/s. The ordinates are intensities relative to the continuum intensity. The time of observation (with an arbitrary day as zero point) is given on the right.

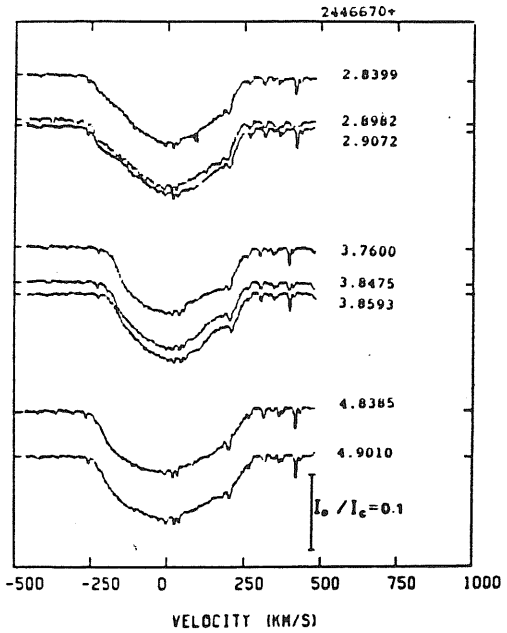

Figure 4.5 – Series of 3, 3 and 2 spectra of HeIλ-5876 in α Eri observed on three consecutive nights. The time of observation (with an arbitrary day as zero point) is given on the right. Narrow absorption features are telluric lines.

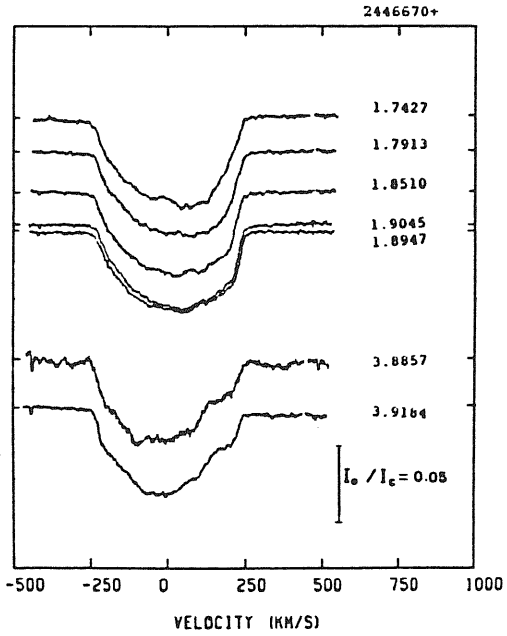

Figure 4.6 – Series of 5 and 2 spectra of HeIλ-6678 in α Eri observed on two different nights. The time of observation (with an arbitrary day as zero point) is given on the right.

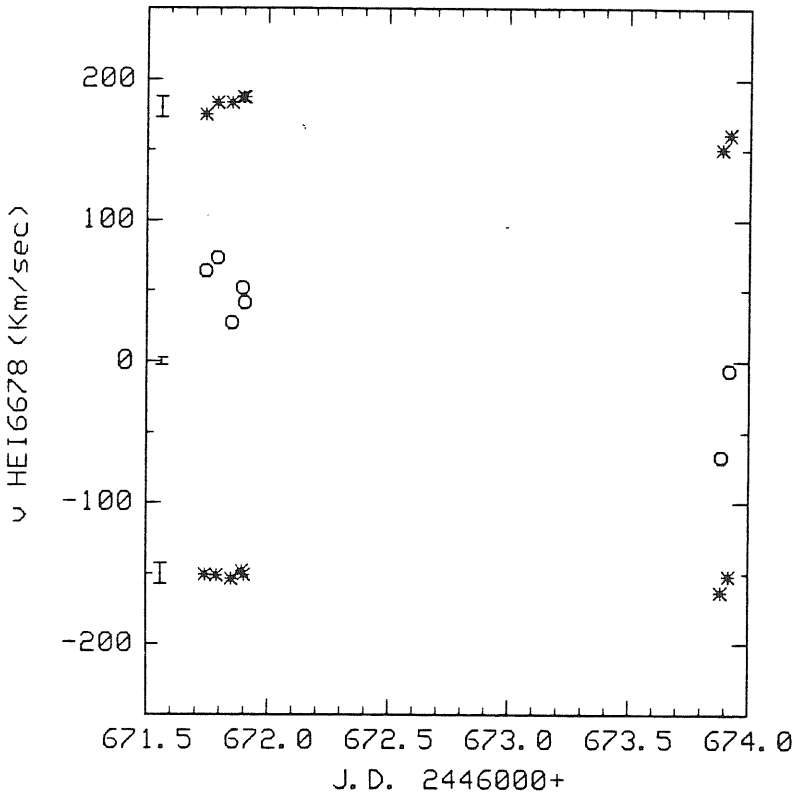

Figure 4.7 – Velocity position of the centre [o] and wings at half depth [*] of the HeIλ-6678 lines in α Eri versus J. D. The vertical bars on the right indicate the mean error on the velocities, which was computed by the best fit.

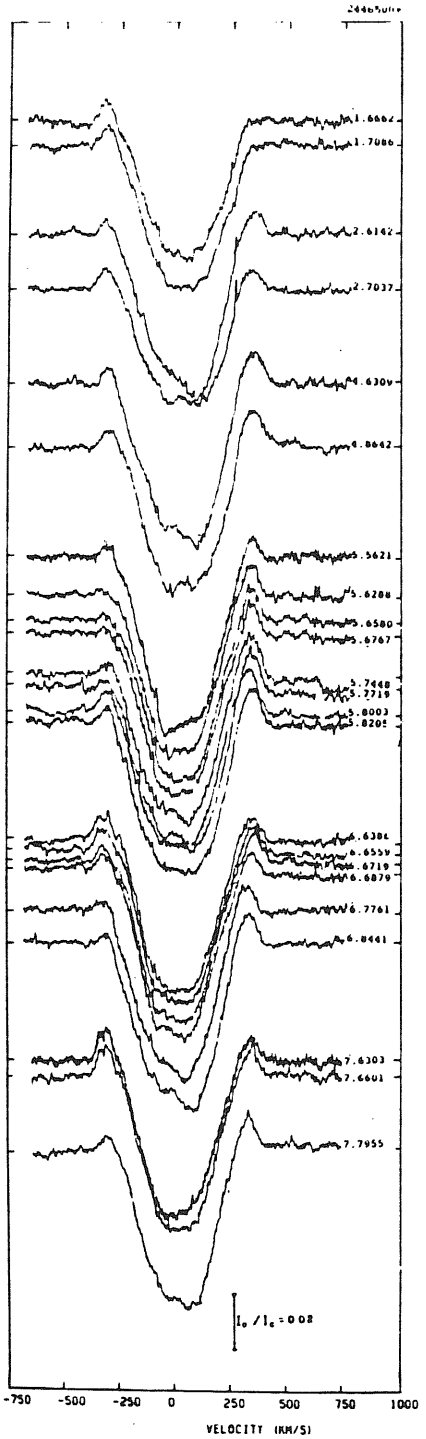

Figure 4.8 – Series of 2, 2, 2, 8, 6, and 3 spectra of HeIλ-6678 in P Car observed on consecutive nights. The time of observations (in days arbitrary zero point) is given on the right.

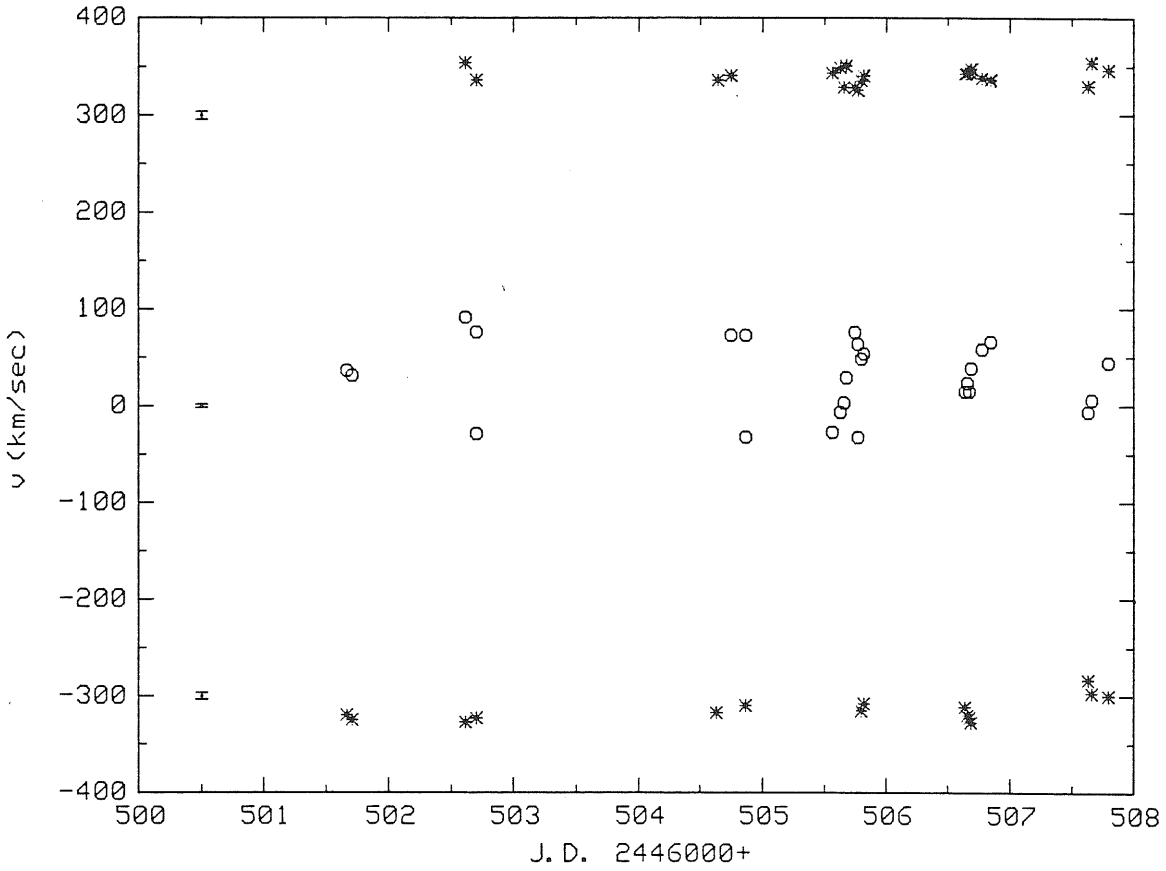

Figure 4.9 – Radial velocities of the absorption [o] and emission [*] components of the HeIλ-6678 line profiles in P Car. Only emissions with I_o/Ic larger than 3σ of the continuum have been measured.

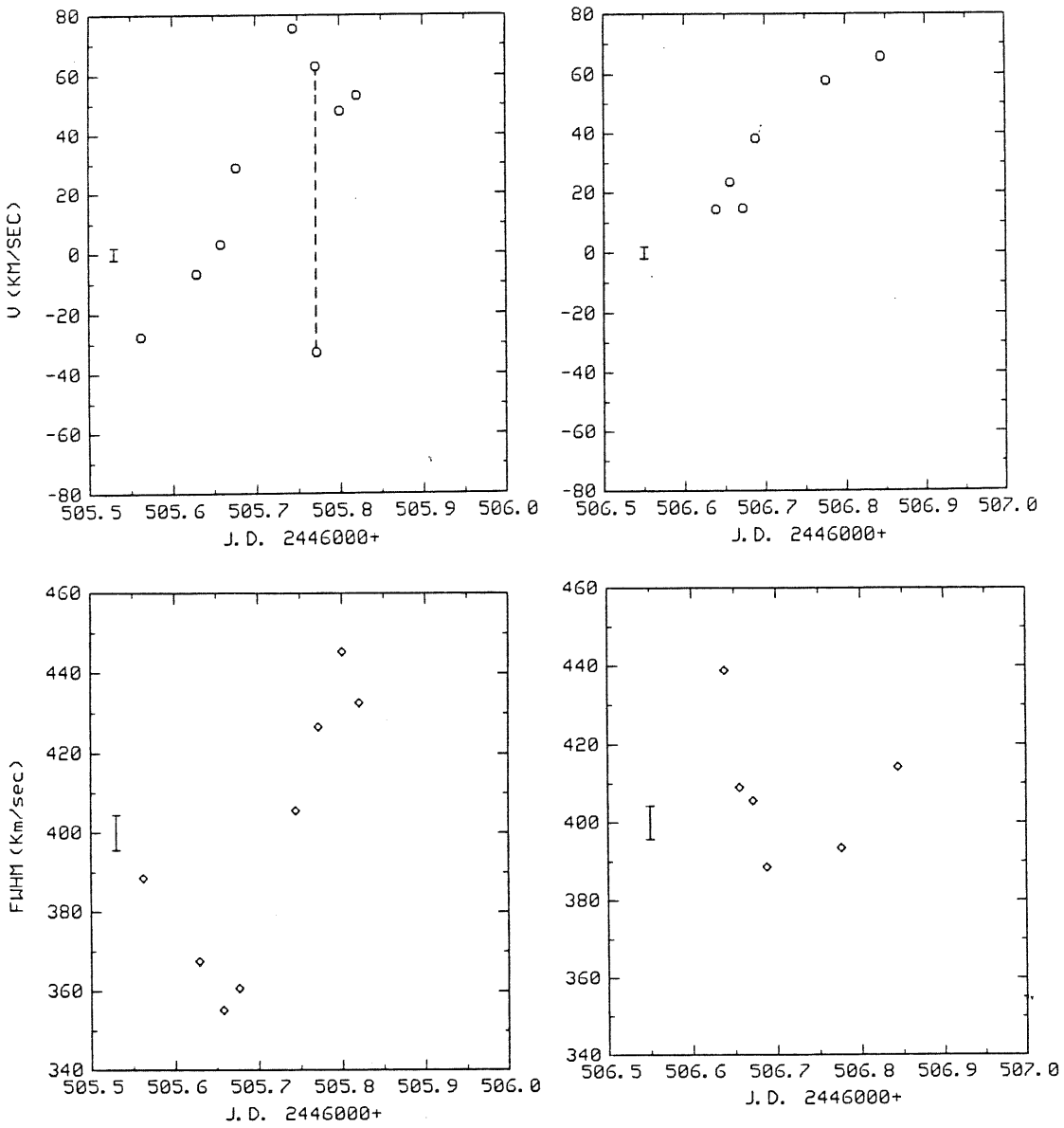

Figure 4.10 – Radial velocities and FWHMs of the HeIλ-6678 absorption components in P Car at J.D. 2446505 and J.D. 2446506. The vertical bars on the right indicate the mean estimated error.

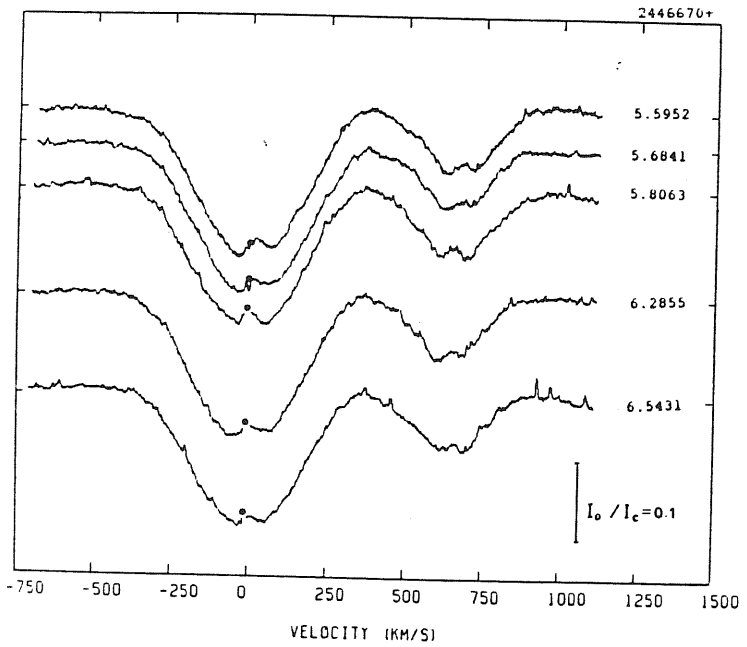

Figure 4.11 – A series of 3 (top) and 2 (below) spectra of HeIλ-4471 and MgIIλ-4481 in ϵ Cap, observed on two consecutive nights. The time of observation (with an arbitrary day as zero point) is given on the right. The same remark as in Figure 4.4 applies to the abscissa axis.

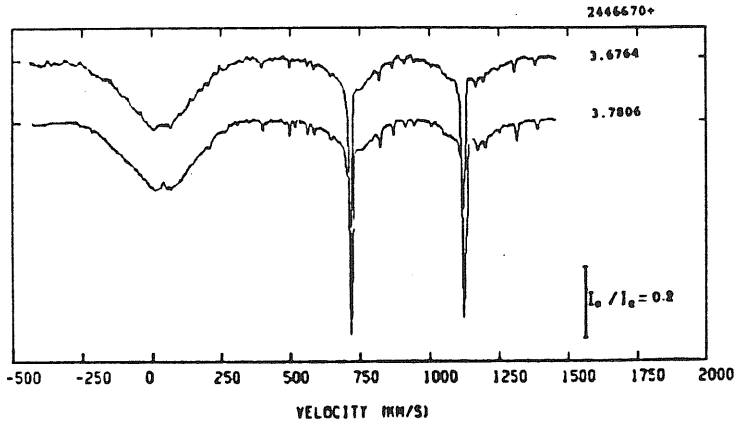

Figure 4.12 – A set of 2 spectra of HeIλ-5876 and NaI D lines in ϵ Cap, observed on the same night. The time of observation is given on the right. The broad wings of the sodium lines could possibly be ascribed to the companion star detected by Poss (1970). Weak and narrow absorption features are telluric lines.

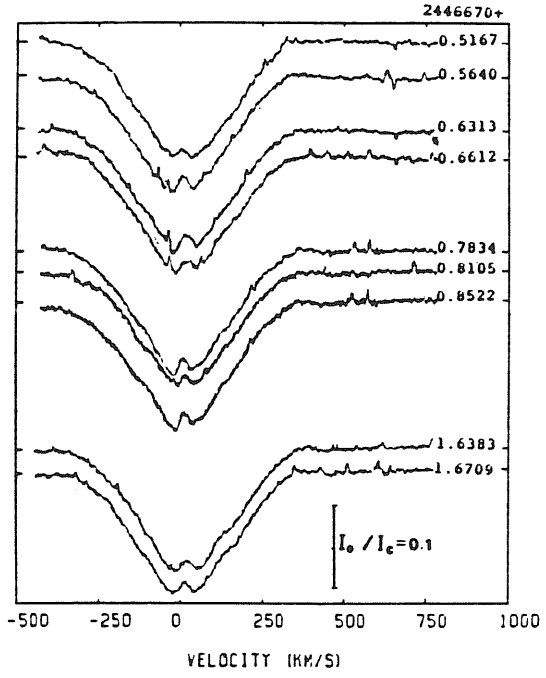

Figure 4.13 – A series of 7 and 2 spectra of HeIλ-6678 in ϵ Cap, observed on two consecutive nights. The time of observation is given on the right.

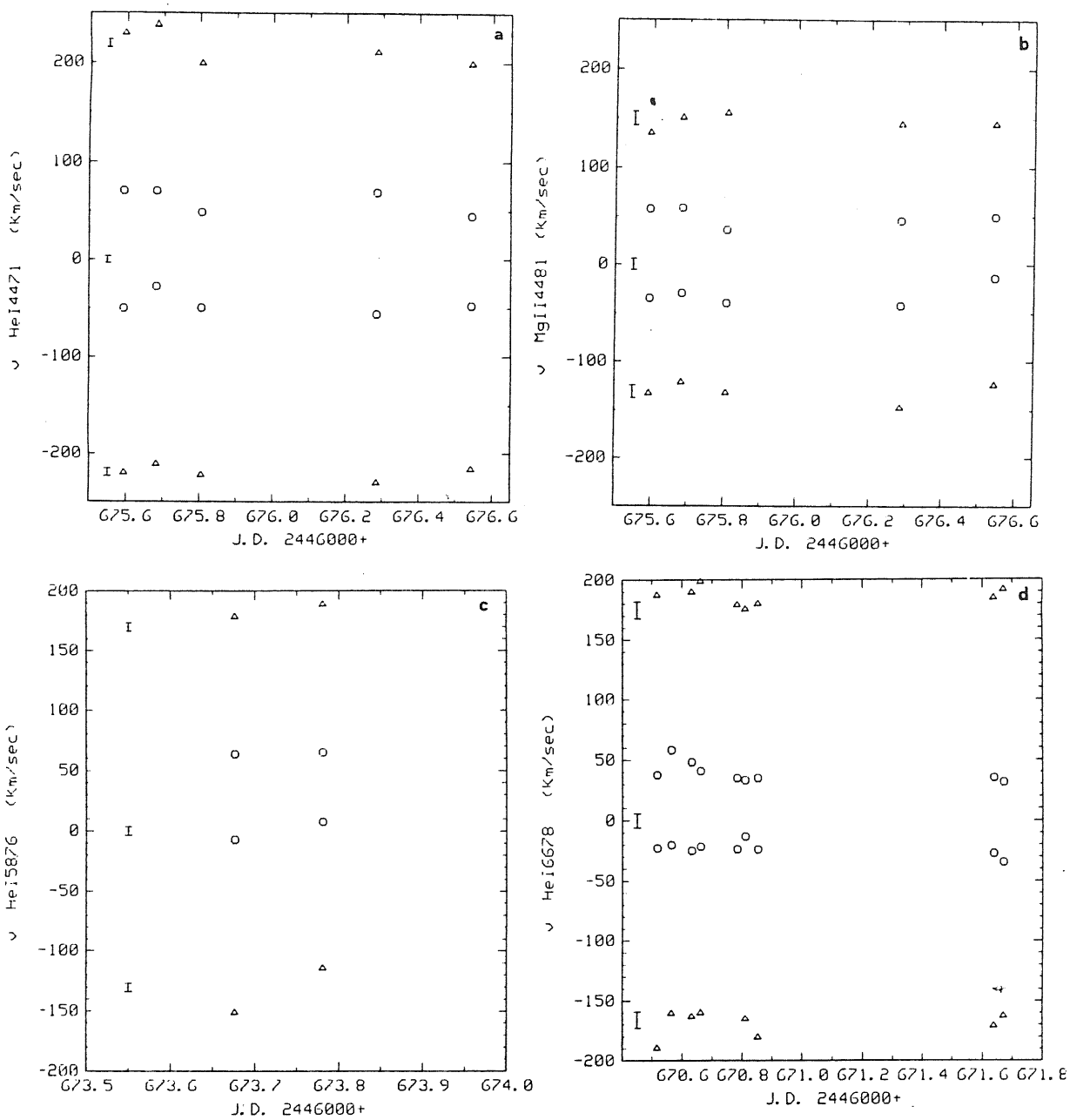

Figure 4.14 a-d – Centre (o) and wing (△) velocity positions of the two absorption components of the HeIλ-4471 (a), MgIIλ-4481 (b), HeIλ-5876 (c) and HeIλ-6678 (d) in ϵ Cap versus J.D.. The vertical bars on the right indicate the mean estimated error.

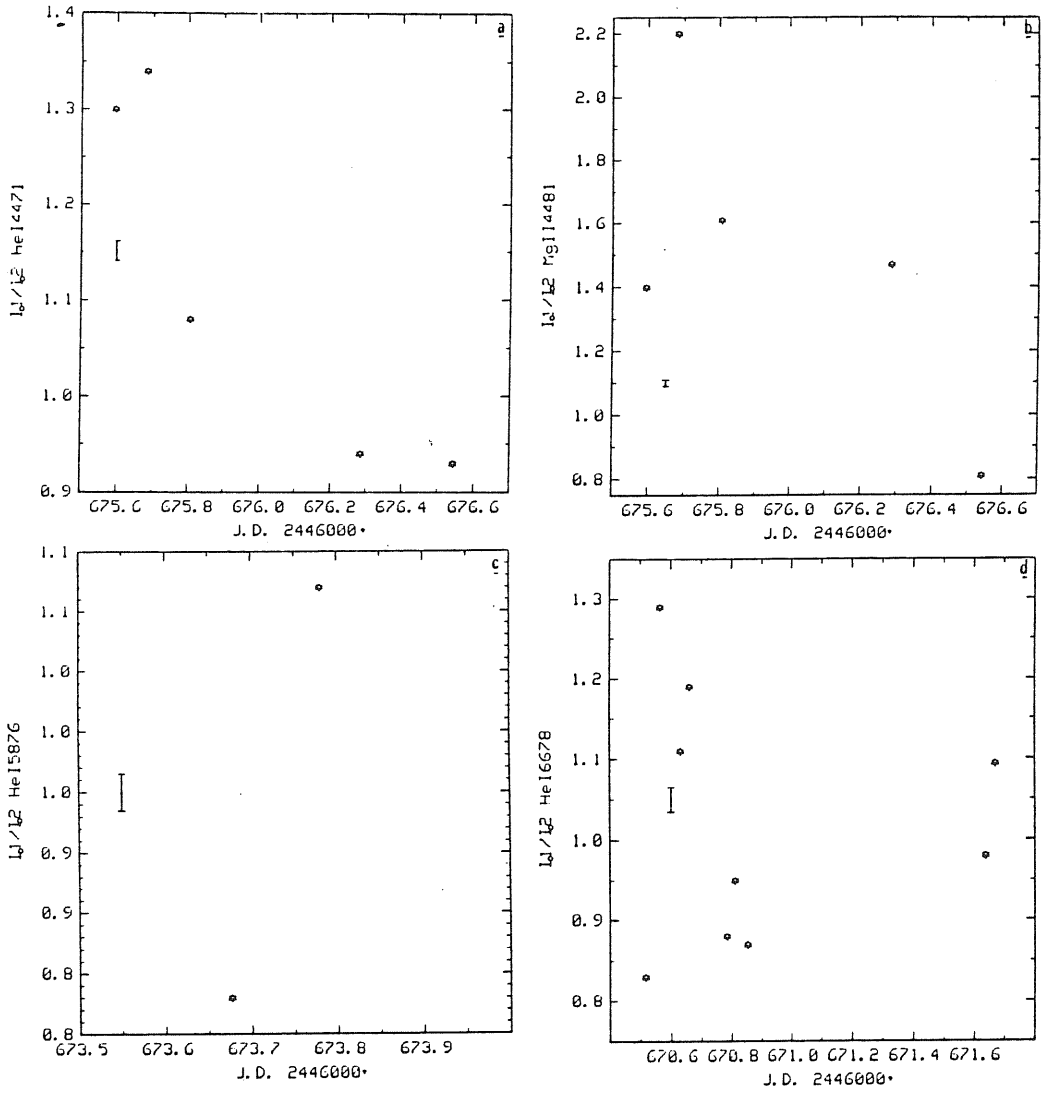

Figure 4.15 a-d – Ratio I_0/I_c of the two absorption components of the HeI λ -4471 (a), MgII λ -4481 (b), HeI λ -5876 (c) and HeI λ -6678 (d) in ϵ Cap versus J.D.. The vertical bars on the right indicate the mean error on the velocities which has been computed by the

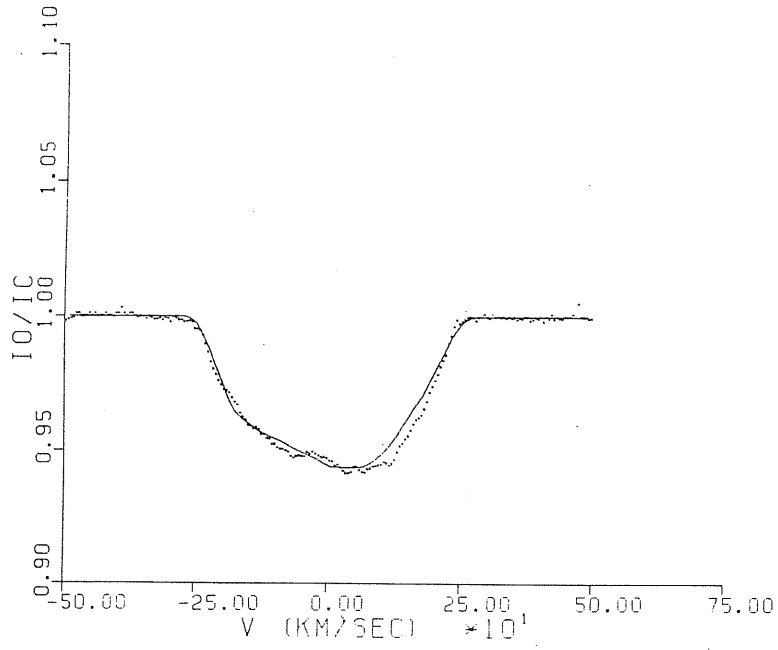

J.D. 2446671.7427

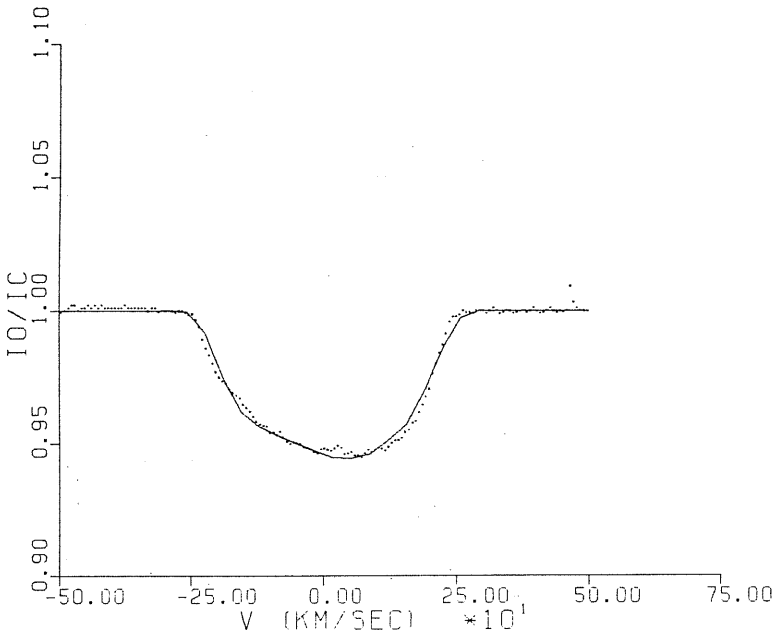

J.D. 2446671.7913

Figure 4.16

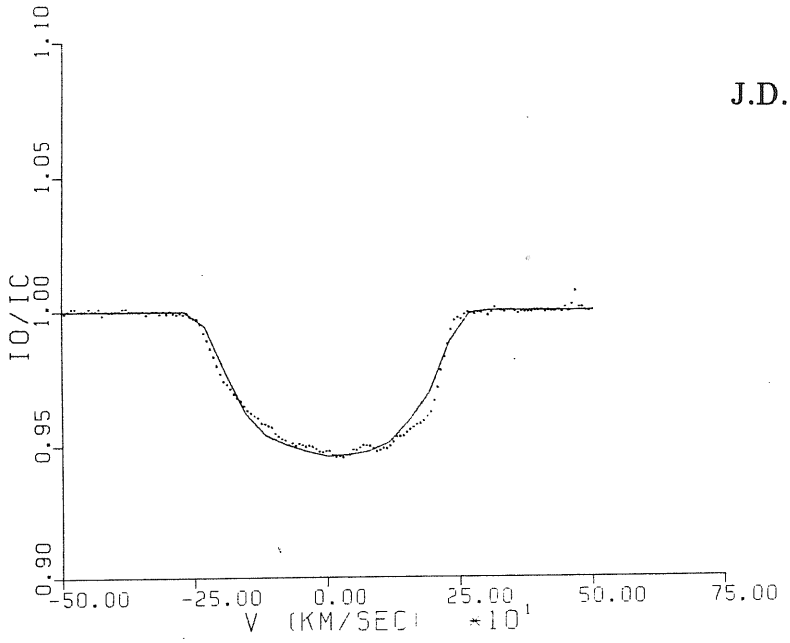
J.D. 2446671.8510
IO/IC
1.10
1.05
1.00
0.95
0.90
-50.00
-25.00
0.00
25.00
50.00
75.00
V (KM/SEC) *10¹

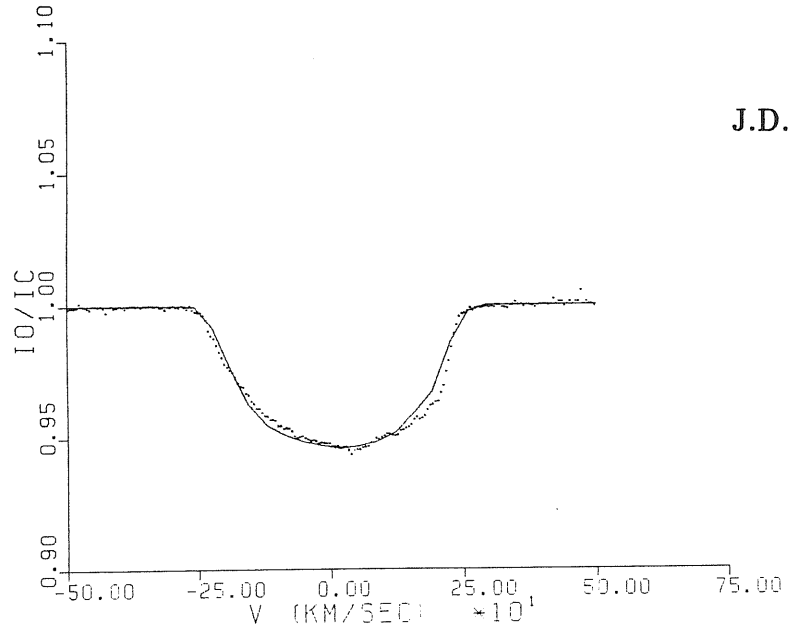
J.D. 2446671.9045
IO/IC
1.10
1.05
1.00
0.95
0.90
-50.00
-25.00
0.00
25.00
50.00
75.00
V (KM/SEC) *10¹

Figure 4.16

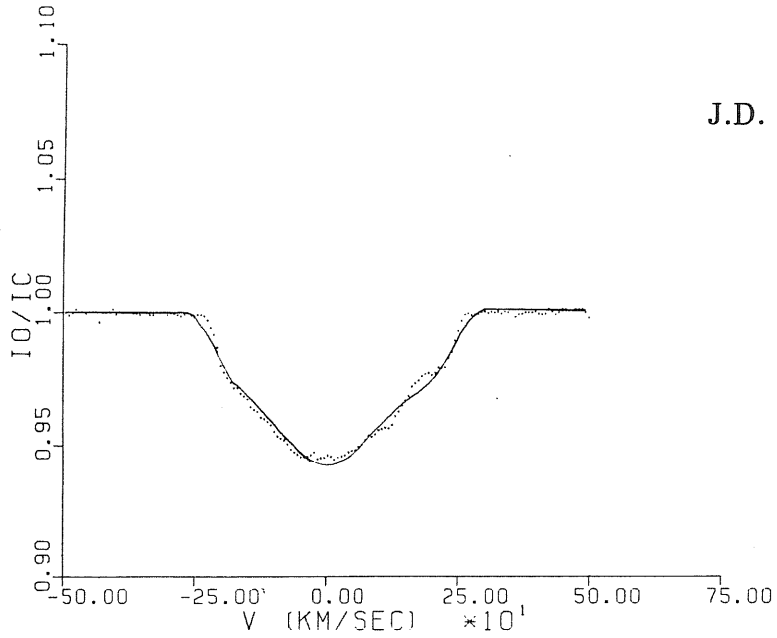

Figure 4.16 – Best fits of the non-radial pulsation model ($l = -m = 4$) to the observed HeIλ-6678 line profiles in α Eri. The theoretical profiles are shown as solid lines. The J.D. of the observations are given on the right.

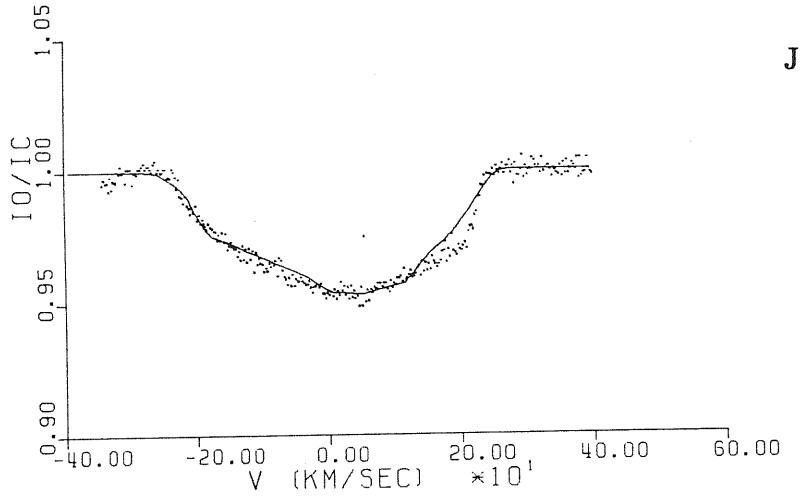

Figure 4.17 – Fit of the non-radial pulsation model to an observed MgII λ-4481 line profile in α Eri. The theoretical profile (solid lines) utilize the $l = -m = 4$ velocity field and indicate the absence of the observed bump in the right wing of the line. The J.D. of the observation is given on the right.

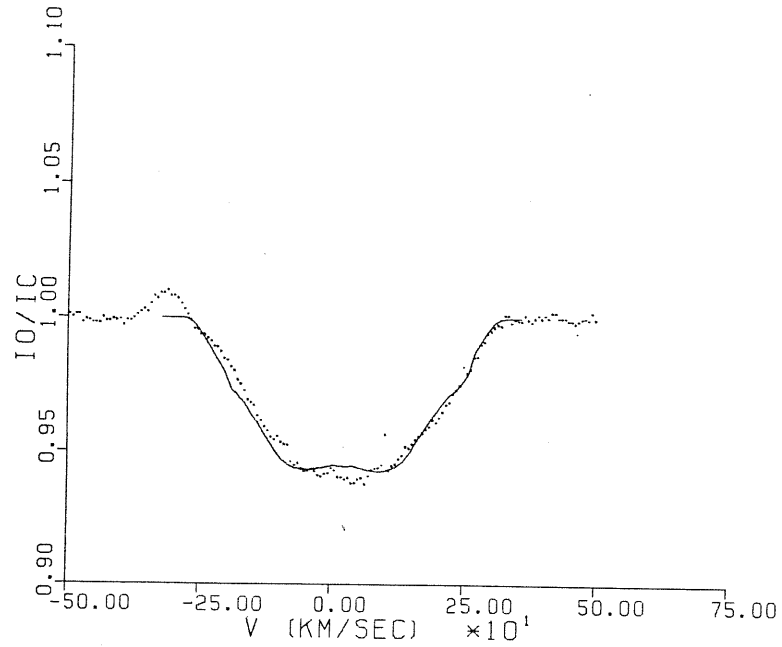
J.D. 2446501.6662
IO/IC
1.10
1.05
1.00
0.95
0.90
-50.00
-25.00
0.00
25.00
50.00
75.00
V (KM/SEC) *10¹

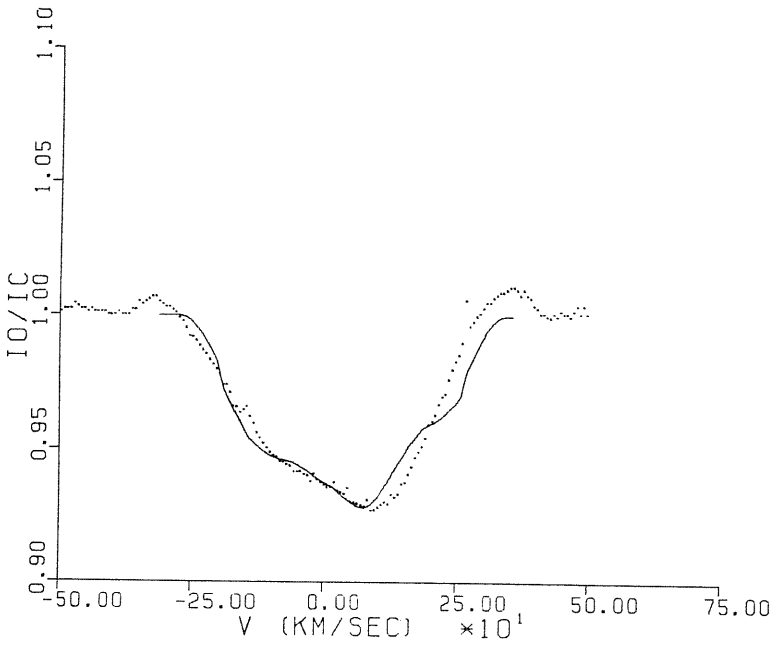
J.D. 2446502.6142
IO/IC
1.10
1.05
1.00
0.95
0.90
-50.00
-25.00
0.00
25.00
50.00
75.00
V (KM/SEC) *10¹

Figure 4.18

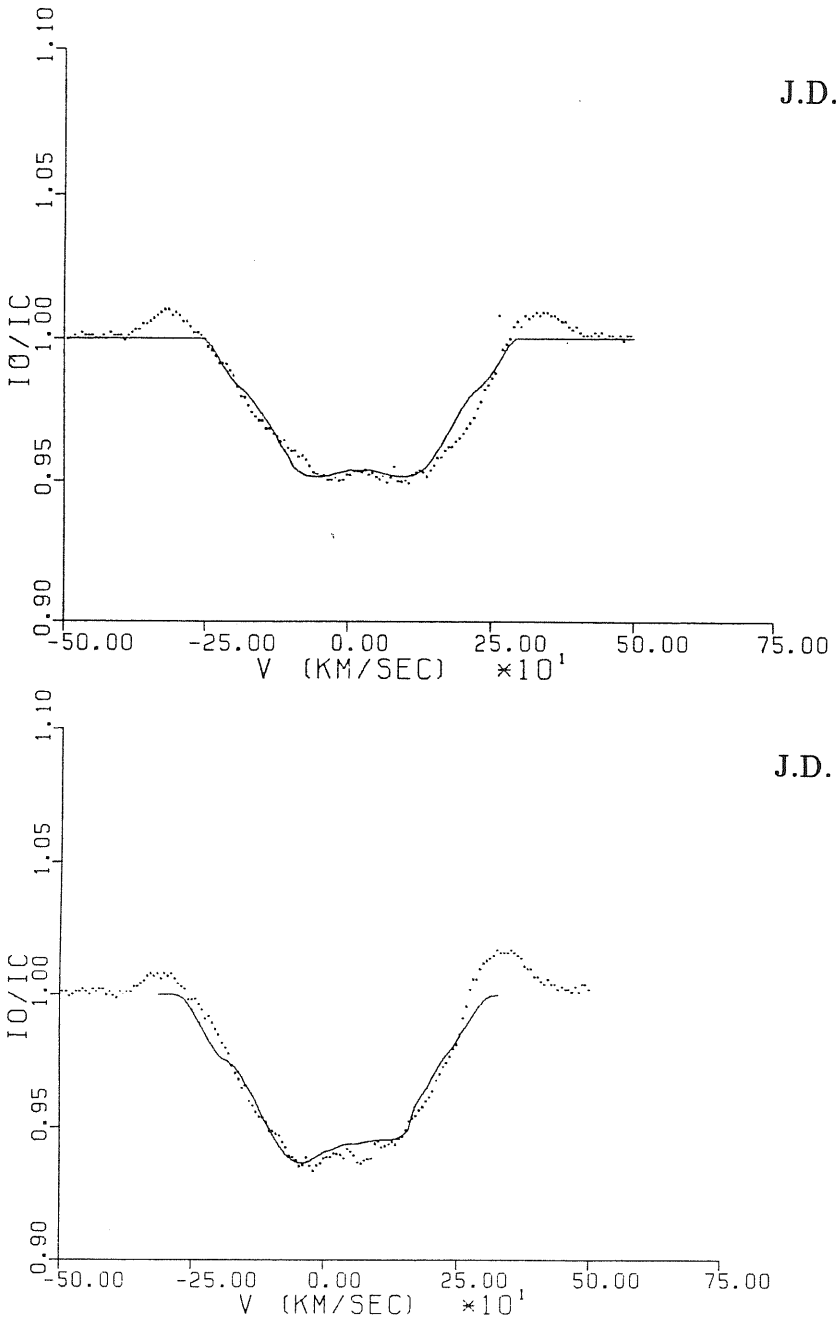
J.D. 2446502.7037
I0/IC
1.10
1.05
1.00
0.95
0.90
-50.00
-25.00
0.00
25.00
50.00
75.00
V (KM/SEC) *10¹
J.D. 2446504.8642
IO/IC
1.10
1.05
1.00
0.95
0.90
-50.00
-25.00
0.00
25.00
50.00
75.00
V (KM/SEC) *10¹

Figure 4.18

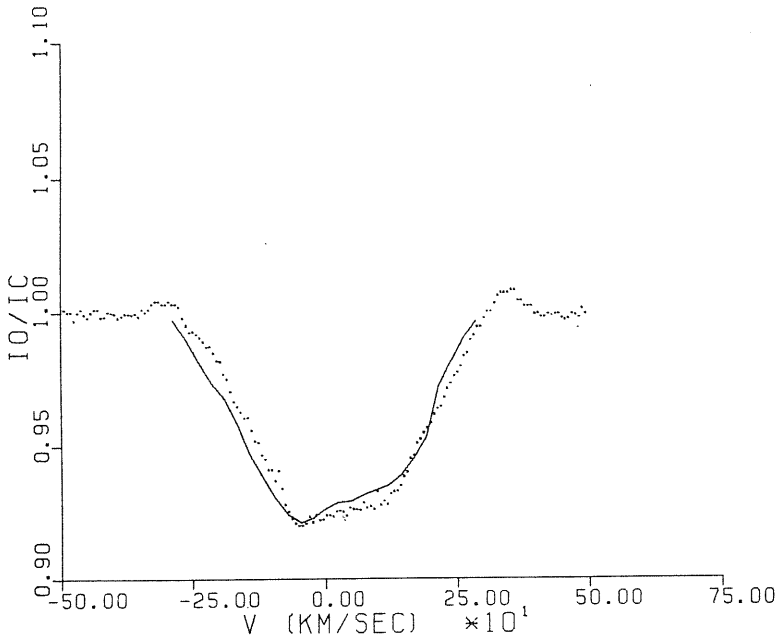
J.D. 2446505.5621
IO/IC
1.10
1.05
1.00
0.95
0.90
-50.00
-25.00
0.00
25.00
50.00
75.00
V (KM/SEC) *10¹

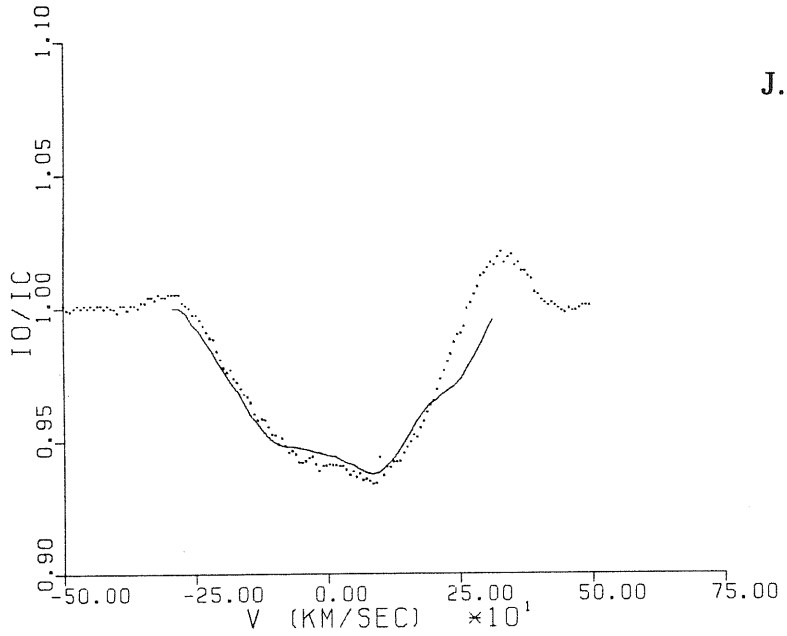
J.D. 2446505.7448
IO/IC
1.10
1.05
1.00
0.95
0.90
-50.00
-25.00
0.00
25.00
50.00
75.00
V (KM/SEC) *10¹

Figure 4.18

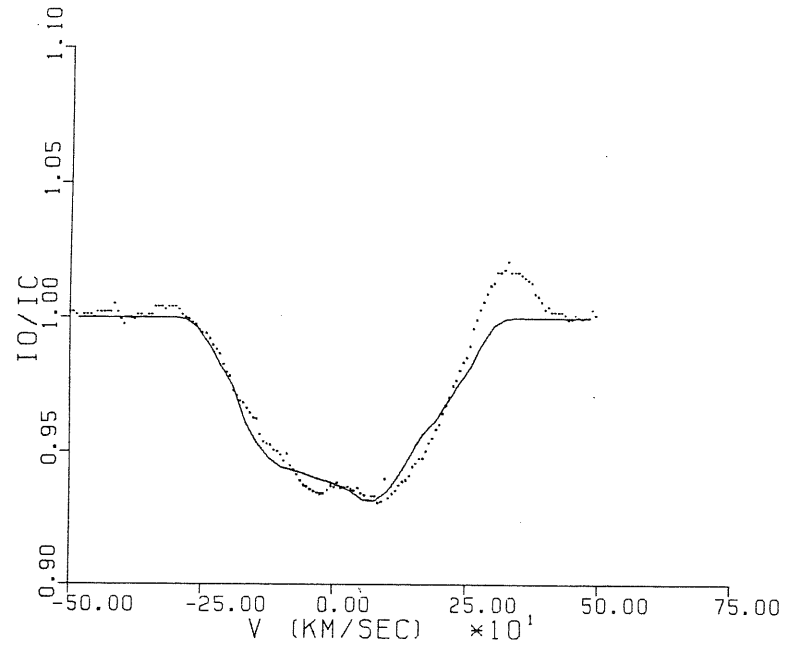

J.D. 2446505.7719

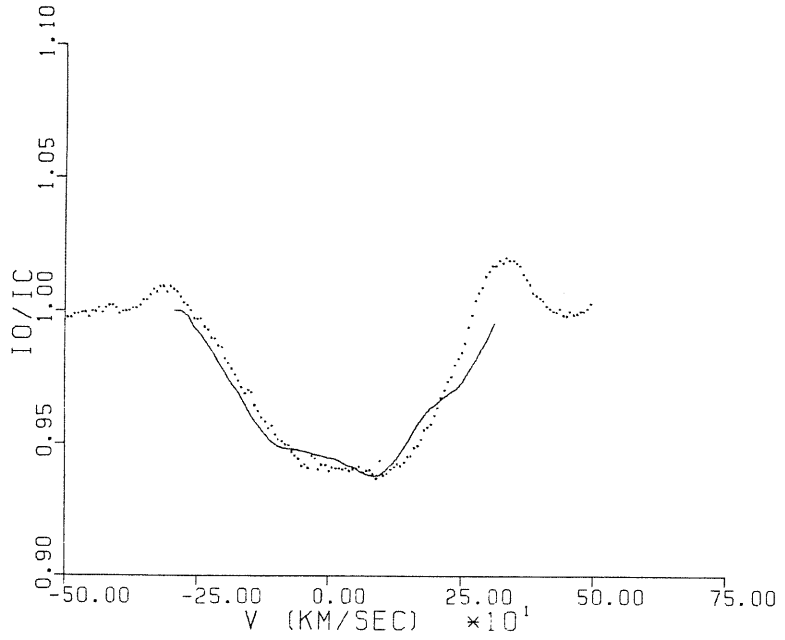

J.D. 2446505.8003

Figure 4.18

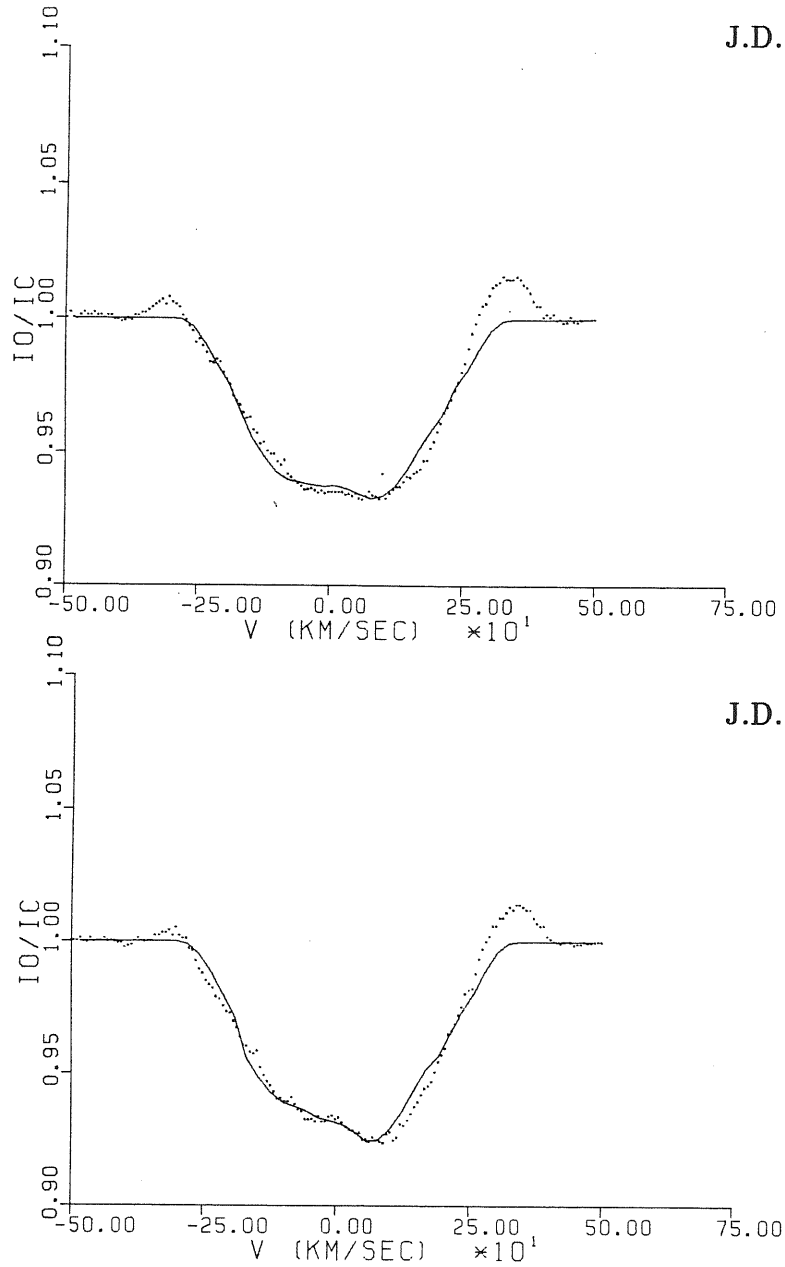

Figure 4.18 – Representative fits of the non-radial pulsation model ($l = -m = 6$) to a number of observed HeIλ-6678 line profiles in P Car. The J.D. of the observations are given on the right.

References

Abt, H.A. and Levy, S.G.: 1878, Astrophys. J. Suppl. Ser., 36, 241.

Abt, H.A. and Cadorna O.: 1984, Astrophys. J., 285, 190.

Andrews, P.J.,and Breger, M.: 1966, Observatory, 86, 108.

Andrillat, Y.: 1983, Astron. Astrophys. Suppl. Ser., 53, 319.

Baade, D.: 1983, The Messanger, 34, 28.

Baade, D.: 1984, Astr. Ap., 134, 105.

Balona, L.A.: 1977, Mem. R. Astr. Soc., 84, 101.

Balona, L.A.,Egelbrecht, C. A. and Marang, F.: 1987, Mon. Not. R. Astr. Soc., 227, 123.

Buscombe, W., and Morris, P.M.: 1961, Mon. Not. R. Astr. Soc., 123, 233.

Dachs J., Eichendorf, W., Schleicher H., Schmidt-Kaler, T., Stift, M., Tug, H.: 1981, Astron. Astrophys. Suppl. Ser., 43, 427.

D' Odorico, S., la Dous, C., Ponz, D., Tanne', J.L.: 1984, ESO Scientific Report N. 2.

Dziembowski, W.: 1977, Acta Astr., 27, 203.

Frazer, R.D.B., Suzuki, F.: 1966, in "Spectral Analysis: Methods and Techniques", ed. J.A. Blackburn (Dekker, New York), p. 171.

Hanuschik, R.W.: 1986, Astron. Astrophys., 166, 185.

Hanuschik, R.W.: 1987, Astron. Astrophys., 173, 299.

Hubert-Delplace, A-M, Hubert H.: 1979, "An Atlas of Be Stars" (Paris Meudon Observatory).

Jaschek, C., and Jaschek, M.: 1965, Pub. A. S. P., 77, 376.

Jurkevich, I.: 1971 Astrophys. Space Sci., 13, 155.

Pasian, F., Rusconi, L., Sedmak, G.: 1982, Publ. Oss. Astron. Trieste, N. 807.

Penrod, G.D.: 1986, Pub. A. S. P., 98, 35.

Percy, J.R.: 1986b, "Highlights in Astronomy", J.P. Swings (eds), 265.

Petrie, R.M.: 1968, Publ. Dom. Astrophys. Obs., 12, 1.

Poss, H.L.: 1970, Highlights Astronomy, vol. 2, 692.

Slettebak, A.: 1982, Astrophys. J. Suppl. Ser., 50, 55.

Slettebak, A., Collins, G.W., Boyce, P.B., White, N.M., and Parkinson, T.D.: 1975, Ap. J. Suppl, 29, 137.

Smith, M.A.: 1986, "Hydrodynamic and Magnetohydrodynamic Problems in the Sun and Stars" ed. Y. Osaki, Univ. of Tokio press, 145.

Smith, M.A.: 1988, "Pulsation and Mass Loss in Stars", ed.s R. Stalio, L.A. Willson, Reidel, Dortrecht, in press.

Struve, O.: 1931, Ap. J., 73, 94.

Underhill, A.: 1982, in "The B stars with and without Emission Lines", NASA SP-456, Doazan, V., Underhill, a., eds., p. 36.

Underhill, A.B., Divan, L., Prevot-Bunnichon, M.-L., and Doazan, V.: 1979, M.N.R. A.S., 189, 601.

Vogt, S.V., Penrod, G.D.: 1983, Ap. J., 275, 661.

Wiese, W.L., Smith, H.W., Glennon, B.M.: 1966, "National Boreau of Standards 4", Vol. I, Washington, D.C..

CHAPTER V

Analysis of Ultraviolet Spectra of a β Cephei Star: ν Eri

§5.1 *Introduction*

There has been considerable new observational data on the line profile of variable B stars, but the instability mechanism that drives the variability of these stars is still unknown. The key to understanding it seems to lie with the β Cephei variables, mostly because the periodic variability of these stars is generally interpreted as the result of predominant radial oscillations, and the radial mode are easier to interpret theoretically. The possible driving mechanisms for β Cephei pulsations, that have been appeared in the literature, have been recently reviewed by Osaki (1987). He concludes that each of the considered mechanisms has serious flaws. Progress in this field can be obtained by a complete and reliable description of the physical processes in the radiating layers resulting from the pulsation.

We have already presented the general properties of this class of pulsating stars (see §1.4). In this section we only summarize some β Cephei characteristics that will be considered in this chapter.

The light curves of the β Cephei stars do not generally display simple sinusoidal patterns; in addition, these patterns may be different at different wavelengths. The radial velocity curves display a similar complexity as the light curves. There is also evidence that line profiles and intensity changes cannot be interpreted uniquely in terms of the pulsation induced velocity fields. Modern analyses of the data suggest that radiative transfer effects must be taken into account in order to describe the pulsation (Furelind et al. 1987).

The β Cephei radiate most of their energy in the far ultraviolet, peaking shortward of about 1200 A, and have effective temperatures from approximately 20,000

to 27,000 K. UV light variations are observed with amplitudes ranging from about 2 to 8 times the values in the visible. Such amplitudes increase as one goes to shorter wavelengths. Thus the larger amplitude at short wavelengths is well suited to the confirmation of suspected variables whose light variation is marginal at visible wavelengths. In addition, The UV side of the spectrum, and especially the region longward the Lyman discontinuity (from 912 Å to approximately 2000 Å), is important because it provides a rather sensitive indicator of photospheric temperature changes. The same spectral region also contains lines of the Lyman series of hydrogen and the resonance lines of CII-III-IV, NIII-V and other important ionic species. Some of these resonance lines are wind lines which seem to be stronger in β Cephei stars to not pulsating stars of the same spectral type (Cassinelli and Lamers 1987).

In this chapter a set of Voyager ultraviolet spectrometer observations (500-1700 Å) of the large amplitude β Cephei variable ν Eri (HD 29248) is analysed. The observations cover 6 pulsation cycles. In the following section (§5.2) we present the characteristics of the star under study. In §5.3 we describe the observations and the data analysis procedures. In §5.4 we investigate the variations in light, temperature, gravity and radius, and in CIII equivalent widths of ν Eri during the pulsation cycle. In §5.5 we discuss the pulsation related variability also on the light of previous similar analysis of another β Cephei star, BW Vul, by Barry et al. (1984).

§5.2 - *The Star under Study*

ν Eri (B2III, Lesh and Aizenman, 1978) has been the subject of numerous ground-based spectroscopic and photometric studies. It has among the largest amplitudes (second in light, third in radial velocities) among the β Cephei variables. It is of particular interest for its complicated period structure. A long series of radial velocity observations (Struve et al. 1952; Struve and Abhyankar, 1955) of ν Eri

were analyzed in terms of simple beat phenomena and led to the determination of 2 periods P_2=0.1735089 days and P_1=0.1779 days with velocity amplitudes 24.5 km/s and 8.15 km/s, respectively. A period analysis of the same data, by Saito (1976) and Kubiak (1980 a), suggests that the secondary oscillation P_1 is actually a triplet of closely spaced frequencies. Walker (1952), using photometric data obtained over an interval of 29 days, confirmed the spectroscopic period P_2 with an amplitude of 0.114 mag, but found a slightly larger value of the secondary period (with amplitude of 0.067 mag) which produces a beat modulation with a period of 8.7 days, different from the 6.98 days beat period determined from spectroscopic observations. According to Kubiak (1980 b) this discrepancy can be understood in view of triplet structure of the secondary oscillation that has different amplitude ratios of the components in the the radial velocity and light curves. An analysis of the radial velocity and light curves by de Jager (1953) showed that at the principal light maximum (maximum T_{eff}) the star has minimum radius; this anti-phase behavior is consistent with the observed 1/4 period lag between the light and the radial velocity curves which in turn is consistent with a predominance of adiabatic oscillation. The times of best observed maxima of the light curve corresponding to the two periodicities, P_2 and P_1, are given by Watson (1971).

An analysis of 31 high resolution Reticon observations of the Si III 4567 line (Smith, 1983) showed that the observed profile variations are fully compatible with the four periods reported by Kubiak (1980 a,b) and that line wing profile variations are caused by moving shell which arise from atmospheric shocks. Smith found that only radial modes with the period of 0.1735089 can mimic the observed radial velocity variations and showed that the triplet modes are identified with $l = 2$ and $m = -2, -1$ and 0.

Observations of ν Eri in the ultraviolet have been limited. TD-1A observations (Beeckmans and Burger 1977, Burger et al. 1980 a, b) showed that the maximum magnitude difference ranges from 0.19 at 1550 Å to 0.12 at 2820 Å. TD-1A spectra of ν Eri and other β Cephei stars were investigated by Lamers et al. (1972), Beeckmans and Burger (1977) and Zorec et al. (1983) with the purpose of detecting differences with the spectra of normal stars of the same spectral type; no differences were found.

Copernicus studies of ν Eri have been limited to discussion of radial velocity and line profile variations exhibited by the photospheric and other atmospheric features (Lesh, 1978). Fischel and Sparks have obtained a series of SWP, high resolution IUE spectra that cover one pulsation period of the star. The result of the analysis of these spectra has not yet been published.

§5.3 - *Observations*

This section presents the observed UV fluxes of ν Eri obtained with the ultraviolet spectrometers (UVS) on the Voyager 1 spacecraft during a 27 hour observing period beginning on 9 March 1981 and the measured equivalent widths of an absorption feature near 985 A which is formed mostly by a blend of the CIII 977 Å, HI Lyγ at 972 Å, and NIII 990 Å.

The Voyager UVS (Broadfoot et al. 1977) are objective grating instruments sensitive in the 500-1700 Å spectral region. The reciprocal dispersion is 9.26 Å per detector channel, yielding an effective resolution of ~15 Å (about two channels). The Voyager UVS calibration has been discussed by Holberg et al. (1982) and by Polidan and Holberg (1985). During observing periods, the Voyager scan platform is fixed in the direction of the target, while the spacecraft limit cycle motions move the field of view (FOV) of the spectrometer on and off the target to obtain both source and background signals. In the dispersion direction a transit of a point source through the FOV produces a well-determined gaussian-like response having an angular half-width of 0.097 degrees. In the cross-dispersive direction, the instrument response is rectangular with a 0.86 degrees full width.

ν Eri was observed with Voyager 1 from March 9, 1981 at 22^h19^m UT to March 11, 1981 at 1^h17^m UT (JD 2444673.425 to 2444674.547). A total of 15,496 spectra were obtained with an integration time of 3.84 seconds per spectrum. The individual spectra were combined into 15.36 s averages and the sky background removed. An aspect solution was then performed on the entire data set in order to

locate the star in the FOV. These data were then binned on the nominal position of the star in the FOV and corrected for all instrumental effects. The final spectra, used in this investigation, included only the data obtained within ± 0.035 degrees of star's position in the FOV. During the analysis of the data each successive transit of ν Eri through the FOV (approximately 35 separate transits in total) were treated as independent observations. The spectra obtained within a single transit were averaged to improve signal-to-noise. In cases of slow transits of the FOV the data was subdivided in order to avoid a significant phase smoothing of the data from the variable. In this study the maximum temporal window allowed was 20.21 minutes (1 observation) which equates to a maximum phase averaging of 0.081. Typical value of phase averages are less than 0.02. Concerning the photometric errors we note that for a relatively bright source like ν Eri, the photon statistics associated with the measurement of fluxes are small compared to external errors. The external errors are, in general, systematic rather than random errors. Specifically, they affect the flux level and not the flux distribution. These external errors are dominated by the accuracy of the aspect solution and can be evaluated through analysis of stellar transit though the FOV and the pointing information. Typically the error bars are 2% in the region below 1200 Å and range from 4 to 10 % in the 1200 - 1700 Å region.

Table 5.1 presents the journal of observations; in column one through seven we list the Julian date of the middle of the observation interval, the corresponding phase, the phase averaging for each spectrum, the integrated flux average for the spectral region between 950 and 1150 Å, F_{1050}, and their 1 sigma error, the integrated flux average for the spectral region between 1350 and 1550 A, F_{1450}, and their 1 sigma error.

Figure 5.1 illustrates the Voyager spectra of ν Eri taken at the minimum light (average of the spectra indicated by *m* in Table 5.1) and maximum light (average of the spectra indicated by *M*). The principal spectral features which are detectable at the Voyager UVS resolution are: a feature near 985 Å mostly due to a blend of the CIII 977 Å, HI Lyγ at 972 Å, and NIII 990 Å resonance lines; a feature near 1030 Å due to a blend of the HI Lyβ line at 1026 Å and the CIII 1037 Å resonance lines; the

Si IV resonance doublet near 1400 Å. The identification of the main components of the 985 Å and 1030 Å line has been made by using Rogerson's (1985) Copernicus ultraviolet spectral atlas of γ Peg, a B2 IV β Cephei star very similar to ν Eri.

We have measured the equivalent widths (EW's) of the 985 A feature only because it is the most clearly detectable among all these features. Since the true continuum cannot be easily discerned at the Voyager resolution our procedure was to measure the EW's with respect to a pseudo-continuum. It was obtained by joining with a straight line two points at the right and at the left of the line center where the wings merge into a smooth curve which fits the upper envelope of the spectral energy distribution. These points were taken at 956.16 Å and at 1002.46 Å. In Table 5.2 we list the measured EW's for each spectrum as a function of time. The measurements errors depend mostly upon the internal consistency with which we fix the pseudo-continuum for each spectrum. By taking into account the RMS noise of the data we find that typical uncertainties are of the order of 9%. Perhaps a better evaluation of the uncertainty of each individual measurement can be obtained by using the dispersion about an empirically fitted curve through all measurements as a function of phase. This procedure, which has been described in section 5.4.3, gives a characteristic uncertainty of 7% which is smaller than the uncertainty derived with the individual lines and suggests that the observed variation of EW's with phase is real.

§5.4 - *Analysis*

5.4.1 - *Light Curves*

Both the F_{1050} and the F_{1450} fluxes reported in Table 5.1 indicate a periodic variability. Since the observations cover only slightly more than a one day interval the spectral resolution in the Fourier domain is only about 1 cycle/day. We, therefore, cannot detect multi periodicities with $1/\Delta P$ larger than 1 cycle/day. This

means that with the available data set we cannot determine the two periods reported in the literature. A search for periodicity of the F_{1050} fluxes using Jurkevich (1971) technique suggests a period of 0.174±0.005 days with a 99% significance level. The analysis of the F_{1450} fluxes using the same technique gives a period of 0.171±0.008 days with a 96% significance level. These periods are fully consistent with the P_2 period or with a weighted combination of the P_2 and P_1 periods. As we have already said (§4.5), Jurkevich's method is based on a sequence of fits of the observed data sample for a range of trial periods until the best representation is obtained. A Fourier transform analysis, adapted for non-equally spaced data (Deeming, 1975), was also made (care of E. Antonello) in order to double check the previous results. The periods obtained are consistent with those derived with the previous method.

In order to derive a phase diagram we have assumed that the pulsation of ν Eri occurs in a purely radial mode (Smith, 1983) and that the observed (from visual observations) non-radial modes are of sufficiently small amplitude that they are undetectable in our observations. The phase diagrams of ν Eri as derived from the F_{1050} and F_{1450} fluxes have been calculated and are presented in Figure 5.2; the diagrams were obtained by using the period of 0.1735089 days reported in the literature.

We fitted a sine curve through the observed points, by using the method of least squares, at λ=1050 and λ=1450. The root mean square error of the fits, σ_{fit}, is 2.6 % for F_{1050} and 4% for the F_{1450} points. It is known that the quantity σ_{fit} will, in general, contains a systematic component due to difference between the actual and assumed fitting function. We believe that the poor fitting is due to the assumption of simple sinusoidal patterns for fitting the ultraviolet ν Eri light curves. The sine curve does not reproduce the behaviour of the data at the maximum and minimum of light, confirming that the light curves of the β Cephei stars do not generelly display simple sinusoidal patterns (§5.1). From the fitting of the phase diagrams with a 6^{th} order polynomial we obtain that the standard deviations of the fits are 1.7% and 2.6% respectively for the F_{1050} and F_{1450} curves respectively. The polynomial curves are given in Figure 5.2, it appears that the scatter remains

larger during the maximum light phase. There is an effect of increasing amplitude of maximum light with time while the minima remain constant. This effect is seen more clearly in Figure 5.3 where we have plotted the F_{1050} data versus time of observation and fitted the data with a sequence of (6^{th} order polynomial) phase diagram curves.

The Julian date corresponding to the maximum phase t_0 is JD=2444673.600 $\pm$ 0.005. In order to check for the long term changes in the period we have compared our data with the ephemerides determined by Watson (1971) from visual photometry. The phase difference between Watson's and our t_0's after 23719 cycles is $\Delta\phi = 0.13$; this corresponds to a phase difference per cycle of about 5×10^{-6}, i.e. of 9×10^{-7} days which is much smaller than our estimated error in t_0.

As a further point we note that the phase curve is broader at minimum than at maximum; this effect is also present in de Jager (1953)'s visual light curve.

5.4.2 - *Stellar Parameters*

The maximum and minimum spectra of Figure 5.1 have been corrected for interstellar reddening by adopting the extinction curve of Longo et al. (1988) and E(B-V)=0.02 (Bohlin et al. 1983). As a working hypothesis we have assumed that the spectral energy distribution of ν Eri can be mimicked at any phase by a proper "standard" LTE model. Thus we have compared, by means of an automatic least square fitting procedure fully described in Morossi and Malagnini (1985), the Voyager spectra represented in Figure 5.1 and dereddend as described above with those predicted by Kurucz's (1979) models. The goal was to get an estimate of the magnitude of the temperature, gravity and angular diameter variations between maximum and minimum phases. The Voyager data have been reduced at the same resolution of the models and resampled to get directly comparable observed and theoretical values at the same wavelengths. We have weighted the observed values taking into account the photometric uncertainties and, for each spectrum, we have determined the tern, T_{eff}, log g and ϕ, associated with the model which best reproduces the

observations. ϕ is the apparent angular diameter of the star. The fitted parameters are reported in Table 5.3 together with the corresponding uncertainties and the relevant information about the fitting procedure. We note that the root mean square error of the fits is about three times the average photometric error. The poor fitting indicates either (1) a low accuracy of Kurucz's models in the wavelength region in study or (2) a too small wavelength range to be adequately fitted with the above procedure or (3) a failure of the initial assumption that static LTE models can be used to fit the spectral energy distributions of the dynamic atmosphere of a β Cephei star. Concerning the first point we note that Longo et al. (1988) have extensively discussed the relatively good adequacy of Kurucz's models in fitting the UV spectral energy distributions of main sequence stars about spectral type B0 but have pointed out some failure by the models in fully taking into account the line blanketing. As for the second point we refer again to the work of Longo et al. who demonstrate that in the wavelength range that we are fitting the spectral energy distribution of B stars is very sensitive to small changes in effective temperature. Therefore we expect that Morossi and Malagnini's fitting procedure works well at these wavelengths.

The above-mentioned problem prevent us in claiming the soundness of the T_{eff}, log g and ϕ values that we have obtained; nevertheless the relative variations of these parameters can be taken with more confidence. In fact, the change in the stellar parameters between maximum and minimum phase is too small for producing an observable difference in the line blanketing. Thus, if line blanketing is the main cause of error in the fitting procedure, it would affect the absolute values of the fitting parameters but not their relative values. In addition it is probably reasonable, in fitting the dynamical atmosphere with a static model, to treat the atmosphere, in a differential sense, as being formed in conditions approximating a static situation. Thus the relative values of the parameters could be maintained.

Uncertainties in reddening correction, which is very small, is not a cause of concern in the fitting procedure, especially in view of the differential approach that we are discussing.

5.4.3 - *Equivalent Widths*

Figure 5.4 compares the measured equivalent widths (EW's) of the 985 A feature (Table 5.2), plotted against pulsation phase, with the F_{1050} curve. The EW's variation that is found, ranging between ~5.9 and ~7.9 Å, recapitulates the form of the light curve with a 1/2 period phase lag. The maximum strength is achieved in the phase range from ~0.2 to ~0.5 where the star atmosphere is at its maximum expansion and minimum temperature. Vice versa the 985 Å feature has minimum strength in correspondence with light maximum, i.e. maximum atmosphere contraction and temperature.

A 6^{th} order polynomial fit ot the EW's data is also presented in Figure 5.4 ($\sigma_{fit} = 45\%$); it shows a broad maximum indicating that during the expansion phase and at the beginning of the contraction phase the EW's of the line change very little and a slightly narrower minimum.

As it has been discussed in section 5.3, the 985 Å feature is prevalently formed by the following resonance lines: CIII 977 Å, HI Lyγ at 972 Å, NIII 990 Å. In addition many other excited lines are present but their contribution is less important even if, in overall, they could affect the total equivalent width of the blend. We refer again to the Copernicus ultraviolet atlas of γ Peg (Rogerson 1985) for the line identification.

The line opacities (i.e. the effective number of absorbers) of the resonance lines are quite sensitive to the variation of the atmospheric temperature and pressure, as can be seen from the EW's calculations presented in Table 5.4. These calculations, which have been performed only with the goal of finding the main contribution of the blend, cannot give a direct comparison with the observations owing to the insufficient resolution of our data which forbids us to detect the complete line profiles, but only the highest points of them . For these calculations we have assumed that all lines form in conditions which approximate a static, LTE case and used WIDTH8 code, available at the Astronet node of Trieste (Castelli, 1987) in conjunction with Kurucz's (1979) LTE, line blanketed model atmospheres. No interstellar contributions and stellar wind components of the three lines have

been taken into account. The equivalent width of the interstellar component of Lyγ is estimated to be 4.5 Å on the basis of the interstellar neutral hydrogen column density, $N_{HI} = 2.8\,10^{20}$ obtained by Bohlin et al. (1983). The interstellar contributions of CIII and NIII are assumed to be negligible. There is probably no effect in the EW's of the wind components because they are scattering lines with zero net EW (emission plus absorption).

CIII appears to be the dominant stellar feature of the blend under a range of T_{eff} and gravity which corresponds to typical velues of early-B main sequence and giant stars. The observed increase in EW's at minimum light, i.e. at high values of T_{eff} and gravity, and the decrease in EW's at low values of T_{eff} and gravity are consistent with the model predictions.

§5.5 - *Discussion*

In this final section we attempt to depict the physical processes occurring in the UV radiating regions of ν Eri as they could be inferred from the low resolution, 912 - 1700 A spectrophotometric observations discussed before. We base our analysis upon the F_{1050} and F_{1450} light curves, the relative values of the stellar parameters at maximum and minimum light, and the CIII 977 Å EW's curve. We also make a parallel comparison with the results of the other β Cephei star, BW Vul, obtained by Barry et al. (1984) using Voyager observations.

As it has been discussed in section 5.4.1 the F_{1050} and F_{1450} light curves of ν Eri (a) are consistent with the previously determined P_2 period of the star as well as with a weighted combination of the P_2 and P_1 periods, (b) do not exhibit any evidence of long term changes of period, (c) do exhibit an effect of increasing maximum light with time and of constant minima, (d) display a broad minimum and a relatively narrow maximum in accordance with optically determined light curves.

The variable intensity at maximum light deserves some further discussion.

There are several reports in the literature about changes in the visual light curves of β Cephei stars; we refer to the paper by Sterken et al. (1987) for information on the relevant cases. More specifically Sterken et al. comment on the large scattering which has been measured during the stillstand phase of BW Vul (Sterken et al. 1986) and conclude that the variable shape of the observed stillstand is often a consequence of the observational undersampling which could be responsible for odd stillstand shapes. In the same 1987 paper, Sterken et al. compare the ultraviolet phase curve of BW Vul (adapted from Barry et al. 1984) with the visual and infrared curves. They point out that, at UV wavelengths, the light amplitude is larger and that the stillstand is barely visible. The original F_{1050} curve of Barry et al. (1984) displays, at stillstand, a larger than average dispersion of data points.

Our ν Eri UV light curves (6 cycles) show a distinctive, constant increase of the maximum flux with time: at 1050 Å it amounts to 0.01 mag/cycle. This is not an effect due to a stillstand which could be masked by data undersampling; in fact, there is no specific reference to a stillstand phase at optical wavelengths and our data at maximum have relatively high temporal resolution. Neither this is an effect due to the modulation of the P_2 and P_1 periods discussed in section 5.2 because we observe constant minima. It is likely that a correct interpretation of the UV light curve must consider the inherent non linearity of the pulsation or, at least, take into account some combined dynamical and radiative transfer effect which is capable of making the UV fluxes, at the end of the contraction phase and at the beginning of the expansion, variable. Similar arguments apply for interpreting the asymmetric shape of the light curve which favors a slightly longer temporal extension of the minimum with respect to the maximum phase.

In section 5.4.2 we have analyzed the UV spectral energy distributions of ν Eri at the phases of maximum and minimum light. In both cases we have averaged the spectra over 4 peaks of the light curve. Low and high maxima have not been considered separately.

Morossi and Malagnini (1985) automatic fitting procedure leads to large error bars in the derived parameters (T_{eff}, gravity and angular diameter); this is ascribed principally to the inadequacy of the adopted grid of model atmospheres -the static,

LTE, line-blanketed model of Kurucz (1979)- in representing the dynamical atmosphere of a pulsating star. A comparison of the maximum and minimum spectra of ν Eri with the Voyager spectra of the non pulsating stars of similar spectral type ϵ CMa, B2II, and κ Cen, B2IV, confirms the above point: there is a remarkable difference in spectral shape between the comparison stars and ν Eri at the two studied phases. This is illustrated in Figure 5.5 where the dereddened fluxes, log F_λ/F_V, versus log wavelength are presented. F_V has been derived from the V magnitude using the relation V=-2.5 log(F_V)+21.017. The adopted unreddened V magnitude of ν Eri at maximum is assumed to be V_0=3.84 and at minimum is V_0=3.96. These values were computed from a mean observed magnitude of V=3.96 and a peak to peak amplitude of ΔV=0.11 (Lesh and Aizenman 1978) and dereddened according to the relation $A_V/E(B-V)$=3.1. The Voyager spectra of the comparison stars have been analysed before in Longo et al. (1988); we refer to that paper for the relevant information on those stars. The dereddened V magnitudes of ϵ CMa and κ Cen are 1.47 mag and 3.00 mag respectively.

The above arguments suggest that we must rather rely on relative comparisons than on absolute ones.

The relative changes in stellar parameters, T_{eff}, gravity and angular diameter (see Table 5.3), determined by fitting with Morossi and Malagnini (1985) procedure the dereddened maximum and minimum spectra of ν Eri, show that the pulsation affects mostly the star temperature. We find a temperature difference between maximum and minimum of ΔT_{eff}=1200 K, the change in gravity of 0.2 in the log and the change in angular diameter is small. This is a different situation than in BW Vul, the B2IV star which has extreme β Cephei characteristics. BW Vul has been studied by Barry et al. (1984) from Voyager UVS spectra covering two pulsation cycles. From their analysis, which has been performed in a similar way as ours, we abstract the results presented in Table 5.5 and compare them with the results of the present study. The relative parameters listed in Table 5.5 confirms the fact that BW Vul has stronger β Cephei characteristics than ν Eri.

An additional way of testing the validity of the relative approach is presented in Figure 5.6, where we compare the magnitude difference between the theoretical

spectra at maximum and minimum EW, in the wavelength range 912 - 7000 Å with the magnitude difference of the spectra of Figure 5.1, after dereddening. In the plot we also indicate the light amplitudes in the V band and the maximum magnitude differences at 2820 Å and 1550 Å reported in the literature (see section 5.2). It is seen that the models provide a reasonable representation of the observed relation betwen amplitude and wavelength, as well as a reasonable fitting of the relative (maximum/minimum) fluxes.

As it has been discussed in section 5.4.3, the resonance line of CIII is the dominant stellar feature forming the blend at 985 Å. The EW's of CIII vary in accordance to the adopted period with a 1/2 period phase lag. This is an effect of both temperature and pressure changes with phase. The CIII strength decreases when the light increases, the star is contracting and increasing its atmospheric temperature. This last effect favors higher ionization stages, that is ionization of CII in CIII. However, the pressure is increasing, and offsets the thermal effects, since our static models indicate that the ionization of carbon is quite sensitive to pressure in these atmosphere (see Table 5.4). The observed trend of the variations in the strength of the CIII lines seems to be in favor of ionization changes with the pulsation phase.

TABLE5.1. - Journal of observations*

J.D. 2444600+	Phase	△Ph.	F_{1050}	δF_{1050}	F_{1450}	δF_{1450}
73.5097	0.059	0.009	0.3031	0.0006	0.2555	0.0019
73.5396m	0.231	0.055	0.2709	0.0005	0.2397	0.0018
73.5702	0.408	0.026	0.3002	0.0015	0.2396	0.0037
73.6208M	0.699	0.009	0.4534	0.0030	0.3146	0.0070
73.6319M	0.763	0.004	0.4385	0.0046	0.3172	0.0107
73.6843	0.065	0.081	0.2785	0.0018	0.2208	0.0044
73.7269m	0.311	0.009	0.2645	0.0024	0.2354	0.0064
73.8974m	0.294	0.026	0.2642	0.0032	0.2180	0.0010
73.9070	0.349	0.025	0.2711	0.0014	0.2137	0.0035
73.9182	0.413	0.013	0.2835	0.0005	0.2187	0.0014
73.9234	0.443	0.008	0.3034	0.0029	0.2535	0.0074
73.9493	0.593	0.017	0.3847	0.0005	0.2568	0.0013
73.9558	0.630	0.020	0.4416	0.0005	0.3119	0.0013
73.9659M	0.688	0.018	0.4849	0.0022	0.3230	0.0050
73.9736M	0.733	0.008	0.4671	0.0038	0.2914	0.0077
73.9831M	0.787	0.003	0.4694	0.0056	0.3270	0.0131
74.3190M	0.723	0.009	0.5010	0.0034	0.3665	0.0080
74.3347	0.814	0.003	0.4617	0.0056	0.3422	0.0135
74.3518	0.912	0.005	0.3885	0.0038	0.2615	0.0086
74.3648	0.987	0.008	0.3435	0.0034	0.2824	0.0088
74.3719	0.028	0.012	0.3278	0.0005	0.2636	0.0016
74.3869	0.115	0.012	0.3035	0.0005	0.2574	0.0016
74.4119m	0.259	0.023	0.2701	0.0007	0.2399	0.0022
74.4237m	0.327	0.037	0.2797	0.0004	0.2386	0.0013
74.4516	0.488	0.012	0.3266	0.0021	0.2841	0.0056
74.4722	0.606	0.004	0.4113	0.0010	0.3644	0.0033
74.4737	0.615	0.005	0.4232	0.0010	0.3225	0.0029
74.4785	0.643	0.008	0.4487	0.0032	0.3093	0.0074
74.4960M	0.744	0.015	0.5113	0.0025	0.3872	0.0060
74.5010M	0.772	0.014	0.5112	0.0025	0.3753	0.0060
74.5190	0.876	0.026	0.4373	0.0018	0.3330	0.0045
74.5256	0.914	0.014	0.4080	0.0007	0.3158	0.0022
74.5496	0.052	0.014	0.3372	0.0021	0.2725	0.0054
74.5695	0.167	0.037	0.2868	0.0005	0.2485	0.0015

(*) F_{1050} and F_{1450} are expressed in 10^{-8} erg cm^{-2} s^{-1} $Å^{-1}$

TABLE5.2 - Equivalent widths of the 985 Å feature			
J.D. 2444600 +	EW (Å)	J.D. 2444600 +	EW (Å)
73.5097	7.0	74.3347	6.0
73.5396	7.4	74.3518	6.9
73.5702	7.9	74.3648	6.4
73.6208	6.5	74.3719	7.1
73.6319	6.6	74.3869	6.9
73.6843	7.1	74.4119	7.2
73.7269	6.9	74.4237	7.1
73.8974	7.4	74.4516	6.9
73.9070	7.5	74.4722	7.8
73.9182	7.8	74.4737	6.6
73.9234	7.2	74.4785	7.0
73.9493	7.5	74.4960	6.6
73.9558	6.5	74.5010	5.9
73.9659	6.4	74.5190	6.8
73.9736	6.4	74.5256	7.0
73.9831	5.0	74.5496	6.5
74.3190	6.1	74.5695	7.5

TABLE5.3 - Model atmosphere fit*				
	T_{eff} (°K)	log g (CGS)	ϕ (marcsec)	σ_{fit}
Minimum	19700 ±1300	3.3 ±0.5	0.30 ±0.06	2.6%
Maximum	20900 ±1100	3.5 ±0.4	0.29 ±0.05	2.2%

* The parameters listed in the line labeled minimum refer to an average of the spectra indicated with m in Table 1; those given in the line labeled maximum refer to an average of the spectra indicated with M. In the fitting procedure the following data are not taken into account: fluxes at 920 and 940 Å, because of the undersampling of Kurucz models at those wavelenghts; fluxes at 1187, 1210, 1229, and 1254 Å, because of large uncertainties in the Voyager calibration around Ly α.

TABLE5.4 - Equivalent width computations.				
log g	T_{eff} (°K)	C III 977.026 Å EW(Å)	Lyγ 972.537 Å EW(Å)	N III 990.98 Å EW(Å)
3.0	18000 20000 22500	22.21 23.52 22.62	3.23 2.00 1.23	5.59 6.40 6.86
3.5	18000 20000 22500	16.73 17.96 18.00	4.24 2.82 1.74	4.40 4.88 5.00
4.0	18000 20000 22500	12.85 13.97 14.38	5.65 3.87 2.53	3.14 3.72 4.14

TABLE 5.5

		ν Eri	BW Vul
T_{eff}	*max*	20900 ± 1300	22600 ± 200
	min	19700 ± 1100	18400 ± 250
ΔT_{eff}		1200	4200
$\log g$	*max*	3.5± 0.4	3.5
	min	3.3± 0.5	3.5
$\Delta \log g$		0.2	
$\frac{L_{max}}{L_{min}}$		1.18	2.59
$\frac{R_{max}}{R_{min}}$		1.02	1.09

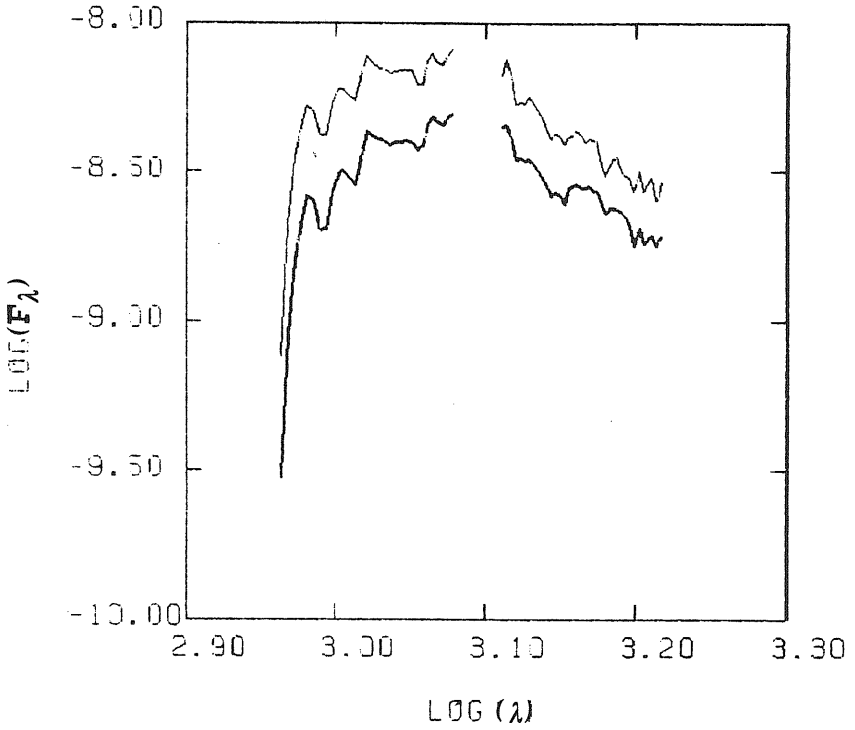

Figure 5.1 - Voyager spectra of ν Eri at maximum and at minimum of the light.

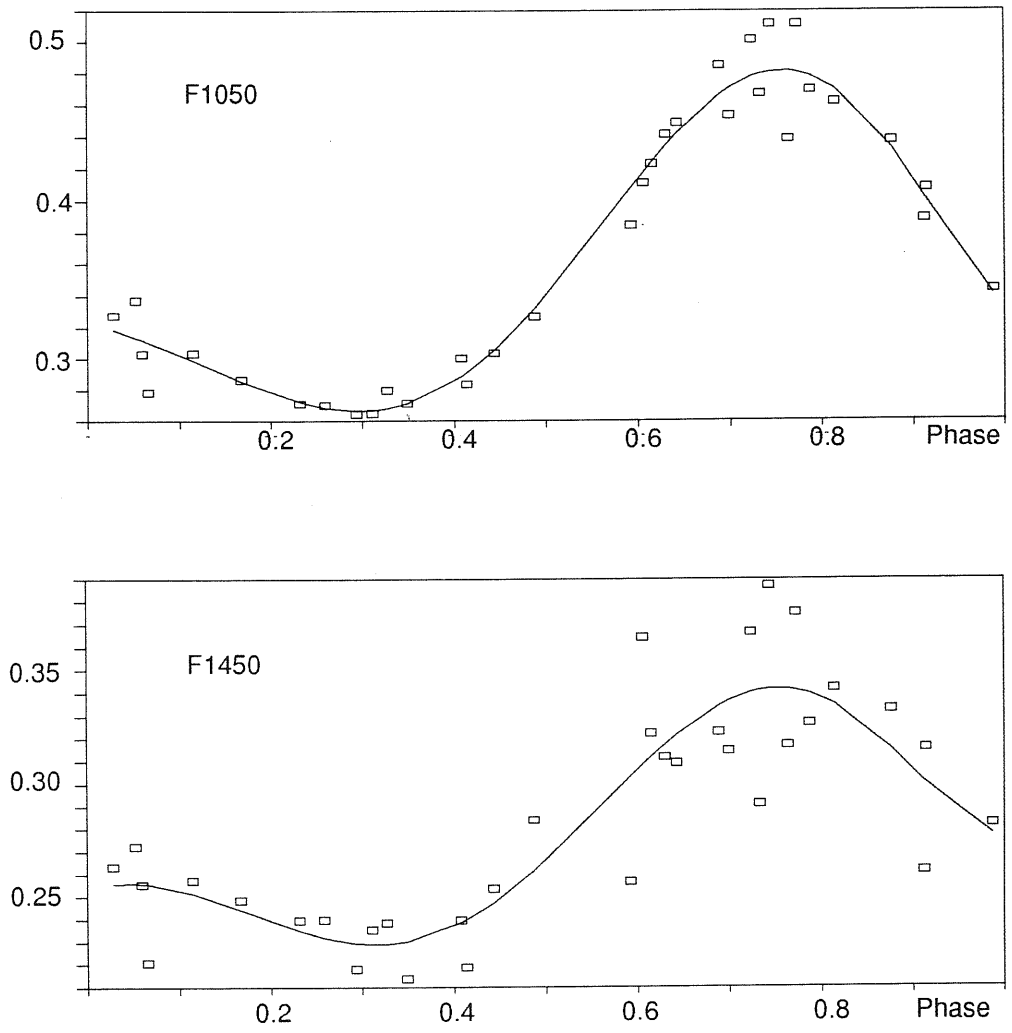

Figure 5.2 - Light curves for ν Eri at effective wavelengths 1050 Å and 1450 Å. The solid lines represent a 6^{th} order polynomial fit .

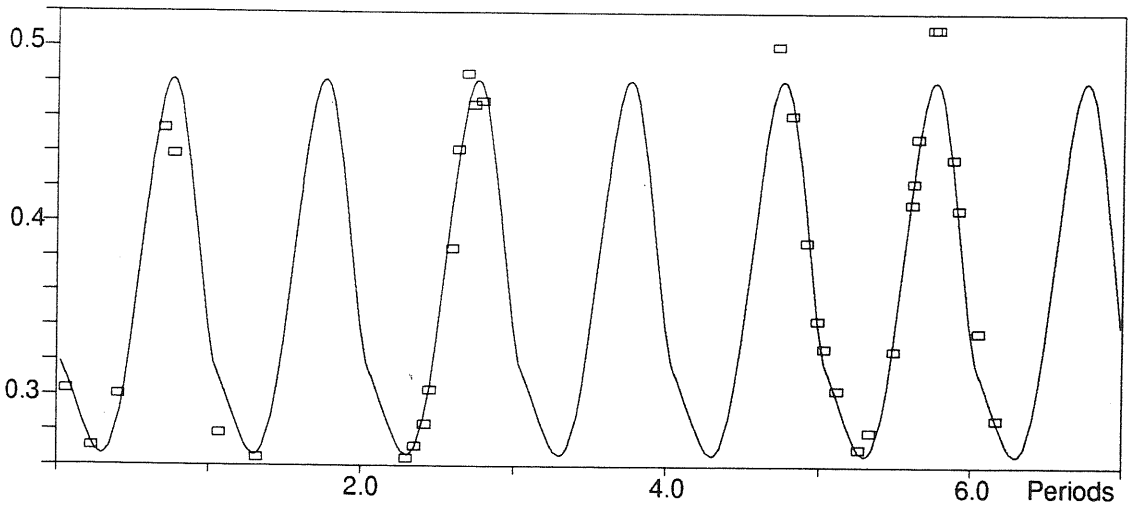

Figure 5.3 - F_{1050} data versus time of observation. The solid line represents a sequence of 6^{th} order polynomial fits.

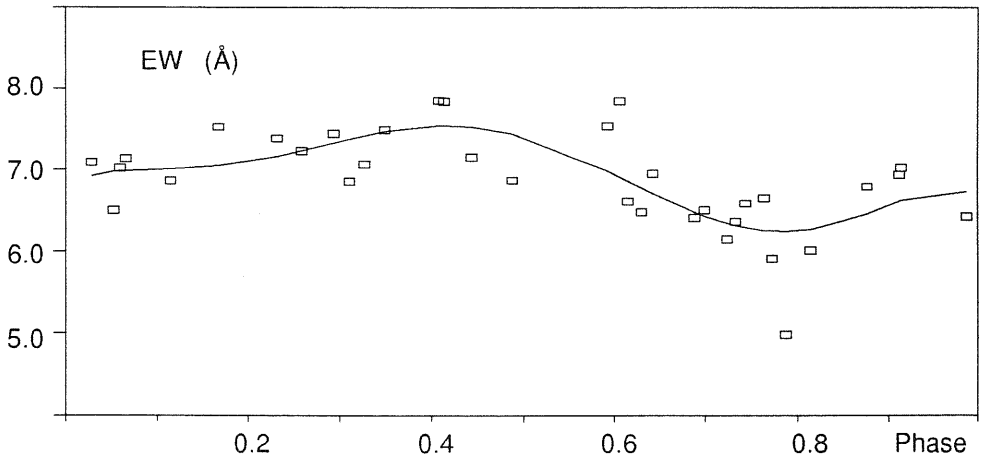

Figure 5.4 - EW of the 955 Å feature versus the pulsation phase. The solid line represents a 6^th order polynomial fit .

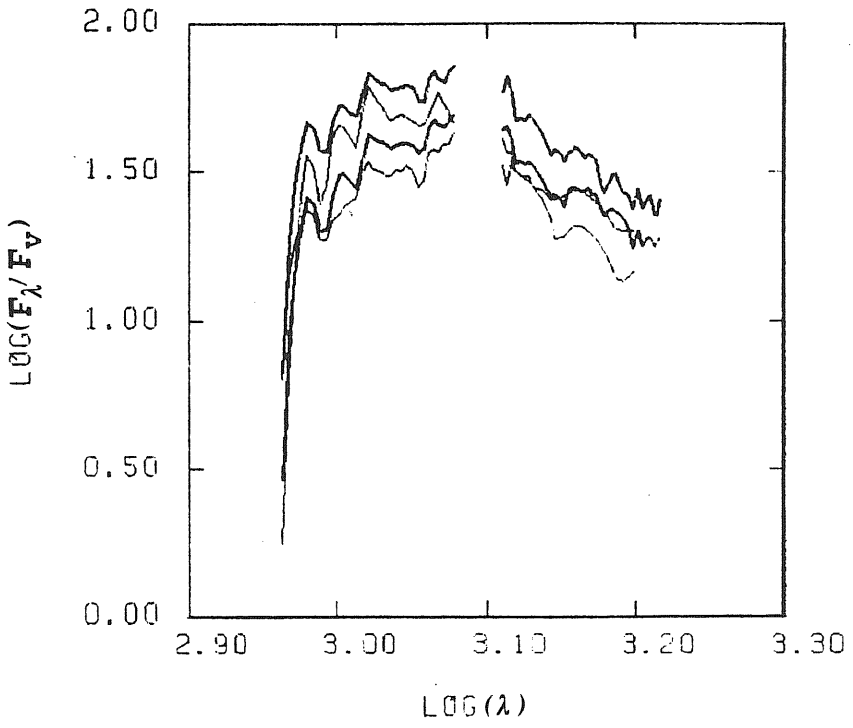

Figure 5.5 - The dereddened Voyager spectrum of ν Eri at minimum and maximum light (thick lines) compared with the Voyager spectra of the non-pulsating stars ϵ CMa (B2II) and κ Cen (B2IV).

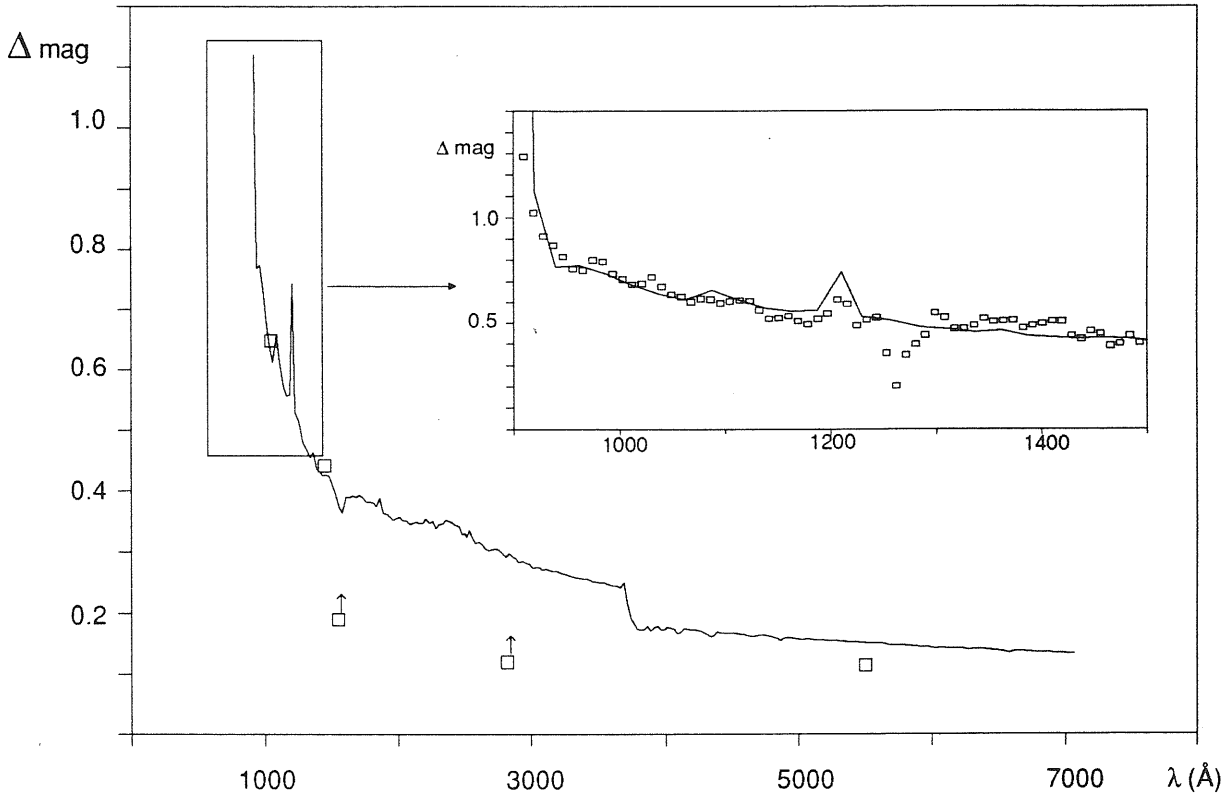

Figure 5.6 - Comparison between the theoretical and observed magnitude differences as a function of the wavelength. The light amplitude in the V band and the maximum magnitude differences observed at 2820 and 1550 Å (Burger et al. 1980 a, b) are also indicated.

References

Barry D.C., Holberg, J.B., Forrester, W.T., Polidan, R.S., 1984, Ap. J., **281**, 766.

Beckmans, F., and Burger, M. 1977, Astr. Ap., **61**, 815.

Bohlin, R.C. 1986, Ap. J., **308**, 1001.

Bohlin, R.C., Hill, J.K., Jenkins, E.B., Savage, B.D., Snow, T.P., Spitzer, L., York, D.G., 1983, Ap. J. Suppl., **51**, 277.

Broadfoot, A.L., et al. 1977, Space Sci. Rev., **21**, 183.

Broadfoot, A.L., et al. 1981, J. Geophys. Res.,**86**, 8259.

Burger, M., Beeckmans, F., Kamperman, T.M. 1980a, Astron. Suppl. Ser., **39**, 301.

Burger, M., De Jager, C., Kamperman, T.M., Neven, L. 1980 b, Astron. Ap., **90**, 170.

Burger, M., De Jager, C., van den Aord, H.H.J., and Saito, N. 1982, Astron. Ap., **107**, 320.

Castelli, F., 1987, Private comunication.

Cassinelli J.P., Lamers, H.J.G.L.M., 1987, in " Exploring the Universe with IUE Satellite", Y. Kondo editor in chief, Reidel Dordrecht, p. 139.

Deeming, T.J. 1975, Ap. Space Sci., **36**, 137.

De Jager, C. 1953, Bull. Astr. Inst. NL, **12**, 88.

Drilling, J.S., Holberg, J.B., and Schoenberner, D. 1984, Ap. J., **283**, L67.

Furenlid, I. 1984, Ap. J., **281**, 766.

Furenlid, I., Young, A., Meylan, T., Haag, C., Crinklaw, G. 1987, Ap. J., **319**, 264.

Holberg, J.B., Forrester, W.T., Shemansky, D.E., and Barry, D.C. 1982, Ap. J., **257**, 656.

Jurkevich, I. 1971, Ap. Space Sci., **13**, 154.

Kubiak, M. 1980 a, Acta Astr., **30**, 41.

Kubiak, M. 1980 b, Acta Astr., **30**, 219.

Kurucz, R.L.: 1979, Ap. J. Suppl., **40**, 1.

Lamers, H.J.G.L.M., Faraggiana, R., Burger, M. 1972, Astr. Ap. Suppl., **38**, 227.

Lesh, J.R. 1978, Ap. J., **219**, 247.

Lesh, J.R. 1981, "Proceedings of the Workshop on Pulsating B stars", Ed.s C. Sterken and J.M. Le Contel, Nice Observatory, p. 157.

Lesh, J.R., and Aizenman, M.L. 1978, Ann. Rev. Astr. Ap., **16**, 215.

Longo, R., Stalio, R., Polidan, R.S., Rossi, L. 1988, Ap. J., in press.

Morossi, C., and Malagnini, M.L.: 1985, Astron. Ap. Suppl. Ser., **60**, 365.

Osaki, S.P. 1987, in "Instabilities in Early-Type stars ", H.J.G.L.M. Lamers and W.H. de Loore eds., Reidel Publishing Company, p. 39.

Polidan, R.S., Stalio, R., and Peters, G.J. 1988, Ap. J., in preparation

Polidan, R.S., and Holberg, J.B.: 1985, in " Calibration of Fundamental Stellar Quantities", p. 101.

Rogerson, J.B. 1985, Ap. J. Suppl., **57**, 751.

Saito, K. 1976,in "Multiple Periodic Variable Stars", ed. W.R. Fitch, (Akademiai Kiado, Budapest), p. 47.

Smith, M.A. 1983, Ap. J., **265**, 338.

Sterken, C., Young, A., and Furenlid, I.: 1987, Astron. Ap., **177**, 154.

Sterken, C. et al. :1986, Astron. Ap. Suppl. ser., **66**, 11.

Struve, O., McNamara, D.H., Kraft, R.P., Kung, S.M., Williams, A.D. 1952, Astr. J., **116**, 391.

Struve, O., Abhyankar, K.D. 1955, Ap. J., **122**, 409.

Walker, M. F. 1952, Ap. J., **116**, 391.

Watson, R.D. 1971, Ap. J., **170**, 345.

Young, A., Furenlid, I., and Snowden, M.S. 1981, Ap. J., 245, 998.

Zorec, J., Briot, D., and Divan, L. 1983, Astron. Ap., **126**, 205.

This work represents a contribution to the study of non-radial pulsation in early-type stars.

A model has been developed in order to predict line profiles broadened by rotation and radial or non-radial pulsation. The approach adopted is an improved version of that used by Osaki (1971), Smith (1977) and Vogt and Penrod (1983). A comparison with results published by these authors, however, does not show considerable differences. The method used by us permits to take into account the presence of envelopes or shells surrounding the star, to simulate non-spherical bodies quite well, to consider temperature and gravity changes as a function of the stellar surface, and to simulate the effects of eclipses of one star by another.

By using our modeling we have studied the short term variability in three Be stars, α Eri, P Car, and ϵ Cap. The three stars under study are in three different phases. α Eri has lost of its emission in Hα, and shows a normal B spectrum. P Car shows a typical Be spectrum. ϵ Cap has Hα characterized by a narrow and deep absorption core bordered by emission wings suggesting that the star is in a Be-shell phase. The non-radial pulsation models provide reasonably good fits of many of the observed spectra in two of the stars under study, α Eri and P Car, suggesting that non-radial pulsations are likely to occur. The pulsation periods, modes and amplitudes are indicated. Competing hypotheses concerning the cause of the observed rapid variability, besides non-radial pulsation (e.g. rotation of an inhomogeneous surface brightness distribution, and binarity), are checked and disproved.

The strength of non-radial pulsation hypotheses is that it is physically plausible, it can explain a large number of observations of short term line-profile and light variations in early-type. In addition, it provides the possibility of understanding unexplained observations showing that the winds from hot stars exhibit a time-variable three-dimensional structure, and among the B stars Be stars are those with the highest and most variable mass loss rates. However, there are some weaknesses

in modelling the line-profile variations observed in the early-type stars with non-radial pulsations. There are several free parameters in the modelling and it is not always clear whether the derived parameters are unique. Modelling is done in the framework of spherical harmonics, which may not be a good assumption in the case of rapidly rotating stars, as the Be stars generally are. Sometimes there is disagreement between the observed and the theoretical values of the ratio of horizontal to vertical oscillation velocities, the so called *k problem.* In addition, features due to pulsation can mask features due to shocks propagating through the atmosphere and vice versa.

Further progress in this area requires, on the observational side, high quality spectroscopic observations, possibly concentrated on a small number of targets. We have tried to use this approach on this thesis. Coordinate spectroscopic and photometric observations may be very useful, because some modes (sectorial and Rossby for istance) can produce similar line profile variations, but quite different photometric variations. Ultraviolet observations would also be necessary in order to study the physical and dynamical properties of the star wind during the pulsation cycle. On the theoretical side, realistic models must be constructed to verify that pulsation and induced-pulsation shock waves can actually drive mass loss in Be stars. In addition, the instability mechanism that drives the variability of early-type stars is still unknown.

The key to understanding the mechanism which drives and sustains the oscillations observed at the surface of early-type stars seem to lie with β Cephei variables. Progress in this field can be obtained by a complete and reliable description of the physical processes in the radiating layers resulting from the pulsation. The β Cephei stars radiate most of their energy in the far ultraviolet, but only a few ultraviolet observations covering the whole pulsation cycle of a β Cephei star, exist so far. We have analyzed Voyager ultraviolet spectrometer (500-1700 A), low resolution, observations covering about 6 pulsation cycles of the large amplitude β Cephei variable, ν Eri.

Our ν Eri ultraviolet light curves show an asymmetric shape, which favors a slightly longer temporal extension of the minimum with respect to the maximum.

In addition, there is evidence of a costant increase of the maximum flux with time. A correct interpretation of the observed light curves must take into account combined dynamical and radiative transfer effects. Model energy distributions fitted to the observations at maximum and minimum light suggest that we must rather rely on relative comparison than absolute ones. The relative changes in effective temperature is 1200 K and in gravity is 0.2, in the log. Observed variations in the strength of the CIII 977 Å resonance line are a consequence of changing ionization fractions during the pulsation cycle.

Acknowledgements

Special thanks to prof. Roberto Stalio for his advice and supervision.

I would also like to thank Fiorella Castelli, Ron Polidan, Carlo Morossi, Luciano Lampi, Elio Antonello, Roberto Krasna and Ali Babar for their help during the preparation of this work.

I have benefitted from fruitful and stimulating discussions with Lee Anne Willson, Bruno Cester, Myron Smith and John Miller.

Support from the International School for Advanced Studies during my Ph.D. studies is gratefully aknowledged, as well as the hospitality by the Astronomical Observatory and the Department of Astronomy of Trieste.

The computations were carried out on the VAX 11/750 of the ASTRONET Pole of Trieste.